ENVIRONMENTALLY FRIENDLY CONCRETE PAVING BLOCKS FOR PHOTODEGRADATION OF AIR POLLUTANTS

JUN CHEN

Ph.D

The Hong Kong Polytechnic University

2010

The Hong Kong Polytechnic University

Department of Civil and Structural Engineering

ENVIRONMENTALLY FRIENDLY CONCRETE PAVING BLOCKS FOR PHOTODEGRADATION OF AIR POLLUTANTS

by

JUN CHEN

A thesis submitted in partial fulfillment of the

requirements for the degree of Doctor of Philosophy

February 2010

CERTIFICATE OF ORIGINALITY

I hereby declare that this thesis is my own work and that, to the best of my knowledge and belief, it reproduces no material previously published or written nor material that has been accepted for the award of any other degree or diploma, except where due acknowledgement has been made in the text.

_____ (Signed)

Jun Chen (Name of the student)

DEDICATION

In appreciation of the love and support given by my family, this dissertation is dedicated to my wonderful parents, 陈维新 and 韩健香, who have raised me to be the person I am today. You have been with me every step of the way, sharing every cherishing memories of my life. Thank you for the unconditional love, guidance, and support that you have always given me. I also want to dedicate this dissertation to my wife 戴娈, who has always been a great source of motivation and inspiration. I could not have made it through without you by my side. I love you!

ABSTRACT

Heterogeneous photocatalysis has been intensively studied in recent decades because it only requires photonic energy to activate the chemical conversion contrasting with conventional catalysis which needs heat for thermo-activation. Over the years, the theories for photochemical phenomenon including photo-induced redox reaction and super-hydrophilic conversion of TiO_2 have been established. The progress in academic research significantly promotes its practical applications in the field of photocatalytic construction and building materials. TiO_2 modified building materials are most popular because TiO_2 has a high activity and it is traditionally used as a white pigment. The major applications of TiO_2 based photocatalytic building materials include environmental pollution remediation, self-cleaning and self-disinfecting. The advantage of using solar light and rainwater as driving force for pollution treatment has opened a new domain for environmentally friendly building materials.

Incorporation of nano-photocatalysts into cementitious materials is an important development for large scale applications. The aim of this project is to make the "cross over" of solid waste recycling and photocatalytic technology feasible and to apply such technology in urban air pollution treatment. A systematic study on assessing the pollutant degradation effectiveness by concrete surface layers that incorporate TiO_2 and recycled glass cullets was conducted. Recycled glass cullets,

derived from crushed waste beverage bottles, were used to replace sand in preparing the concrete surface layers. The photocatalytic activity of the samples was determined by photocatalytic NO_x conversion test in the laboratory. Factors which may affect the pollutant removal performance of the concrete layers, such as glass color, aggregate size and curing age, were investigated. The results showed a significant enhancement of the photocatalytic activity due to the use of glass cullets as aggregates in the concrete layers. The samples fabricated with clear glass cullets exhibited threefold of NO_x removal efficiency compared to the samples fabricated with river sand. The light transmittance property of glass was postulated to account for the efficiency improvement, which was confirmed by a separate simulation study. It was also found that the influence of the size of glass cullets was not evident because the shape and size of the aggregates may be changed by the high compaction pressure during the fabrication process. In addition, the photocatalytic activity of the concrete surface layers decreased with curing age, showing a loss of 20% NO_x removal after 56 days curing.

To further explore of the mechanisms, the photocatalytic NO_x conversion by TiO_2 blended cement pastes was used as a standard process to evaluate the internal factors which may influence the depollution performance. The chemical composition and microstructure of the TiO_2 modified cement pastes were characterized and analyzed. The active photocatalytic sites related to the surface area of TiO_2 are the key factor in determining the photocatalytic activity. Ordinary Portland cement pastes showed lower photocatalytic activity than white cement pastes probably due to the influence of minor metallic components. X-ray diffraction and TG analysis demonstrated that TiO_2 was chemically stable in the hydrated cement matrix. The decreasing trend of

NO_x removal ability with the increase of curing age was confirmed again. This could be attributed to the cement hydration products which filled up capillary pores forming diffusion barriers to both reactants and photons. It was also proved that surface carbonation could reduce the NO_x removal efficiency after the hydration of cement.

On the other hand, as a new functional construction material, the basic properties of the photocatalytic cement-based material must be identified. Therefore, the side effects of adding nano-TiO_2 on inherent properties of hardened cements were also examined. Two types of nano-TiO_2 with different particle sizes were blended into cement pastes and mortars. Their effects on hydration and physical properties of cements were investigated. The admixture of nano-TiO_2 powders significantly accelerated the hydration rate and promoted the degree of hydration at early ages. It was demonstrated that the distribution of TiO_2 in cement pastes was not homogeneous. The total porosity of paste sample decreased and the pore size distribution was also altered. The acceleration of hydration rate and the change of microstructure affected the physical and mechanical properties of the cement-based materials. The initial and final setting time was shortened and more water was required to maintain a standard consistence due to the addition of nano-TiO_2. The compressive strength of the mortar was enhanced, especially at early ages. It is concluded that nano-TiO_2 may act as “a catalyst” in cement hydration reactions.

The effectiveness of using photocatalytic paving blocks to remove common air pollutants such as NO_x has been well demonstrated at laboratory level. To evaluate the performance of the photocatalytic paving blocks used in complex ambient air

conditions, two field trials were conducted. One was carried out at the campus of The Hong Kong Polytechnic University, and another one was carried out at three primary schools in different districts of Hong Kong. It was found that the NO_x removal efficiency of the paving blocks decreased with time. Washing the block surface with detergent or polishing the surface can regenerate the pollution removal ability. The statistic analysis of the monitoring data showed that 7.2 % NO_x was reduced at ground level compared with the NO_x concentration in breathing zone in one year monitoring period. Compared with the air quality monitoring method, the sampling box method is more accurate in demonstrating the NO_x removal performance. It is suggested that the photocatalytic blocks should be washed periodically and applied in heavily polluted areas to maximize their pollutant removal function.

PUBLICATIONS ARISING FROM THE THESIS

Chen, J. and Poon, C.S. Photocatalytic construction and building materials: from fundamentals to applications. *Building and Environment* **2009**, 44 (9), 1899-1906.

Chen, J. and Poon, C.S. Photocatalytic activity of titanium dioxide modified concrete materials – Influence of utilizing recycled glass cullets as aggregates. *Journal of Environmental Management* **2009**, 90 (11), 3436-3442.

Chen, J. and Poon, C.S. Photocatalytic cementitious materials: influence of the microstructure of cement paste on photocatalytic pollution degradation. *Environmental Science and Technology* **2009**, 43 (23), 8948-8952.

Chen, J., Kou, S.C. and Poon C.S. Hydration and properties of nano-TiO_2 blended cement composites. *Submitted to Cement and Concrete Composites, under review.*

ACKNOWLEDGEMENTS

Firstly I would like to thank my supervisor, Professor Chi-sun Poon, for his great support and guidance during my PhD study. He believed in my ability and gave me a lot of room to develop, making me feel confident of challenging research problems occurred in this project. I may not achieve the research objectives on time without his patience and encouragement. Thank you so much for a memorable experience. Secondly, many thanks to Dr Shi-cong Kou for helping me conduct many laboratory tests. His invaluable suggestions for both experimental set-up and results discussion are appreciated.

I also wish to express my sincere thanks to our laboratory technicians, Mr. W. F. Tam and Mr. K. H. Wong, for their assistance and hard work in equipment maintenance. The help from final year student Miss Y. Y. Tsang, Miss Y. T. Chow and Miss R. Smith and the financial support from the Hong Kong Polytechnic University is acknowledged. Thanks are given to all staff members in the Department of Civil and Structural Engineering, for creating a comfortable and friendly work environment. Good luck to each of you in your future endeavors.

Finally, I must say I owe my family too much in the past years. Special thanks are given to my whole family for their firm support and enormous love.

Contents

List of Figures

List of Tables

ABBREVIATIONS

TiO_2	Titanium Dioxide
NO_x	Nitrogen Oxides
NO	Nitric Oxide
NO_2	Nitrogen Dioxide
UV	Ultraviolet
RH	Relative Humidity
PCO	Photocatalytic Oxidation
VOCs	Volatile Organic Compounds
$^{\cdot}OH$	Hydroxyl Radical
TCE	Trichloroethylene
PCE	Perchloroethylene
VC	Vinyl Chloride
BETX	Benzene, Toluene, Ethylbenzene, O-xylene
C_3S	Tricalcium Silicate
C_2S	Dicalcium Silicate
C_3A	Tricalcium Aluminate
C_4AF	Tetracalcium Aluminoferrite
$C\bar{S}H_2$	Calcium Sulfate Dihydrate
CSH	Calcium Silicate Hydrate
CH	Calcium Hydroxide

AFt	Ion Substituted Ettringite
AFm	Mono-sulphoaluminate
OPC	Ordinary Portland Cement
WC	White Cement
ASR	Alkali-Silica Reaction
XRD	X-Ray Diffraction
TGA	Thermal Gravimetric Analysis
MIP	Mercury Intrusion Porosimetry
EDX	Energy Dispersive X-ray
SEM	Scanning Electron Microscope
w/b	Water to binder ratio
w/c	Water to cement ratio

Chapter 1 Introduction

1.1 Background

Hong Kong faces serious urban air pollution problems due to its dense population and fast economic growth. With a large population of seven million there is a high demand for transportation and power to support the daily life of the inhabitants. The high traffic volume results in a high air pollutant concentration at street level throughout densely populated and congested areas, which may cause health problems for the population as well as detrimental effects on the environment. The air pollution issue can also lead, ultimately, to economic loss for Hong Kong both from increase in demand of health services and from reduced attraction of investment and skilled labour beyond the region.

Different solutions have been made and proposed to combat the problem of air pollution in Hong Kong. These measures include the July 2006 Action Blue Sky Campaign and the November 2007 vehicle idling ban. Cleaner vehicles have also been introduced but due to the sheer scale of the traffic and the street canyon effect in Hong Kong other methods need to be sought to combat the problem. In the past decade, the removal of trace levels of inorganic and organic contaminants in air through photocatalytic process has received much attention as this technology is potentially suitable for air purification in office buildings, homes, cars and aircrafts [Zhao and Yang, 2003]. Coating photocatalyst modified cementitious materials onto

the external surface of buildings or roads may be a good supplement to conventional technologies to treat the gaseous exhaust emission. These materials also have other functions such as self-cleaning and self-disinfecting.

The use of photocatalysts, particularly titanium dioxide (TiO_2), together with building materials started from the early 1990s in Japan [Fujishima and Zhang, 2006]. The versatile function of TiO_2, which can both serve as photocatalytic materials and coating materials, has facilitated its application in exterior construction materials and interior furnishing materials, such as cement mortar, exterior tiles, paving blocks, glass and PVC fabric. Under irradiation of solar light, gaseous pollutants can be converted to harmless forms on the surface of construction materials and eventually washed away by rain. The whole removal process of pollutants is driven by natural energy alone.

Although the potential for a wider use of photocatalytic construction and building materials in urban air pollution mitigation is huge and promising, the durability and efficiency of these materials still need improvement. The loss of photocatalytic activity due to the immobilization of TiO_2 on solid supports is significant [Rachel et al., 2002]. Therefore, there is a need to further study the mechanisms of air pollution removal by photocatalysts that are incorporated in construction and building materials.

1.2 Objectives

The aim of this study is to make the "cross over" of waste recycling and photocatalytic technology feasible and applying such a technology in urban air pollution treatment. To maximum the air pollutant removal efficiency of photocatalytic paving blocks made of recycled glass, it is necessary to understand the interaction between photocatalysts and construction materials. In addition, for potential large applications, the long term air pollutant removal performance in real harsh environment must be verified. As a result, the objectives of this study are:

- ▲ Investigate the potential of enhancing the photocatalytic air pollution removal efficiency by using recycled glass as parent materials for photocatalytic paving blocks.
- ▲ Identify the factors affecting the air pollution removal performance of the blocks, including glass cullet size, glass color and curing age.
- ▲ Examine the microstructure of hardened photocatalytic cement pastes and its influence on photocatalytic pollution degradation.
- ▲ Study the impact of adding nano-TiO_2 on the properties and hydration of cement-based materials.
- ▲ Develop monitoring frameworks and testing protocols for the measurement of air pollutant removal efficiency of the photocatalytic blocks.
- ▲ Evaluate the long term air pollution removal performance of the photocatalytic paving blocks in real environment.

1.3 Scope of Thesis

To fulfill the objectives of this study, the following planned research sub-projects were carried out.

- ▲ Photocatalytic activity of TiO_2 modified concrete materials – influence of utilizing recycled glass cullets as aggregates.
- ▲ The influence of the microstructure of cement paste on photocatalytic pollution degradation.
- ▲ Hydration and properties of nano-TiO_2 blended cements.
- ▲ Evaluation of the air pollutants removal performance of photocatalytic paving blocks in ambient air environment.

The designs, methodologies, experiment results, discussions and conclusions of these projects are sorted and reorganized to eight chapters in this thesis.

The present chapter covers the background, objectives and scope of the research project.

Chapter 2 reviews the mechanisms of photocatalysis, the principles and kinetics of photocatalytic decomposition of air pollutants, and the influence of operation parameters on photocatalytic reaction, such as temperature, humidity, light intensity, pollutant concentration and residence time. A brief review of cement-based materials is also presented. Finally, the mechanisms and applications of photocatalytic construction and building are summarized according to the classification of

photocatalytic air purification, self-cleaning effect and anti-bacterial effect.

Chapter 3 describes the experimental methods of this project. The materials, preparation methods for photocatalytic cement-based materials, experimental set-up for photocatalytic NO_x degradation test and testing protocols are presented in this chapter. Experimental details for the determination of properties of photocatalytic cement-based materials are also given. The final part of this chapter shows two monitoring methods adopted for the evaluation of NO_x removal efficiency by photocatalytic paving blocks in the field trials.

Chapter 4 shows the results of the experimental study on assessing the feasibility of utilizing recycled glass cullets as aggregates in photocatalytic concrete surface layers. The influence of glass color, aggregate size and curing age on photocatalytic pollutant degradation are also discussed.

Chapter 5 reports the results of the study conducted to examine the microstructure of photocatalytic cement pastes and the effect of this structure on its pollution degradation ability. Factors which may influence the depollution performance including TiO_2 type, chemical composition alteration in cement hydration, microstructure of hardened cement paste and carbonation level are systematically analysed based on experimental results.

Chapter 6 focuses on the hydration and properties of nano-TiO_2 blended cements. The change of hydration reaction rate and the degree of hydration is shown. The nano-particle distribution and the porosity change of the cement/TiO_2 composite are

also presented. The effects of nano-TiO_2 admixtures on cement properties, such as standard consistence, setting time and compressive strength are discussed.

Chapter 7 presents the field trial monitoring results using two different sampling methods. The results of durability tests and statistical analyses are illustrated.

Chapter 8 summarizes the general conclusions obtained from the experimental studies and data analyses. The recommendations and suggestions for future research in air pollution mitigation using photocatalytic cement-based materials are proposed.

Chapter 2 Literature Review

2.1 Photocatalysis

2.1.1 Background

It has been recognized for quite a long time that titania-based exterior paints tend to undergo “chalking” in strong sunlight. This means that a non-adherent, white powdery substance tends to form on the surface, similar to the chalk on a blackboard. This effect was recognized to result from the actual removal of part of the organic component in the paint, leaving the titania itself exposed [Fujishima et al., 2008]. With this observation, Goodeve and Kitchener (1938), at University College, London, carried out a study on the photocatalytic decomposition of a dye on titania powder in air, including absorption spectra and determination of quantum yields. They proposed that titania acts as a catalyst to accelerate the photochemical oxidation and also studied a number of other oxides and speculated on the precise mechanism. At that time, the term “photocatalysis” was still the subject of some debate. It was not clearly defined and it was only known that solar energy was required for certain chemical conversions such as natural photosynthesis in biogenic forms [Parmon, 1997]. It was also argued that the idea of a photo-catalyzed reaction is fundamentally incorrect, since it implies that light is acting as a catalyst in the reaction, whereas it always acts as a reactant which is consumed in the chemical process [Mills and Hunte, 1997].

In 1972, Fujishima and Honda first discovered water photo-splitting phenomena in a TiO_2 anode photochemical cell. They exposed an n-type TiO_2 semiconductor electrode, which was connected through an electrical load to a platinum black counter electrode, to near-UV light. When the surface of the TiO_2 electrode was irradiated, photocurrent flowed from the platinum counter electrode to the TiO_2 electrode through the external circuit. Oxygen evolution occurred at the TiO_2 electrode and the hydrogen evolution occurred at the platinum electrode. This work promoted extensive research in semiconductor photo-electrochemistry during the 1970s and 1980s, which greatly assisted the development of photocatalysis [Fujishima et al., 2000]. In 1977, Frank and Bard investigated the decomposition of cyanide in water by heterogeneous photocatalysis, which proved that TiO_2 is excellent for photocatalytic breaking down of organic compounds. Since then, there has been increasing interest of using photocatalysis in the field of environmental purification.

Photocatalysis is defined by Fujishima et al. (2008) as “the catalysis of a photochemical reaction at a solid surface”. In reality the term “photocatalysis” in wide spread use means that “acceleration of a photoreaction by the presence of a catalyst” [Kisch, 1989]. The term “photoreaction” is sometimes elaborated as a “photo-induced” or "photo-activated" reaction. Heterogeneous photocatalysis involves photoreactions which occur at the surface of a catalyst. If the initial photo-excitation process occurs in an adsorbate molecule, which then interacts with the ground state of the catalyst substrate, the process is referred to as a "'catalyzed photoreaction"; if, on the other hand, the initial photo-excitation takes place in the catalyst substrate and the photo-excited catalyst then interacts with the ground state

adsorbate molecule, the process is a "sensitized photoreaction". In most cases, heterogeneous photocatalysis refers to semiconductor photocatalysis or semiconductor-sensitized photoreactions [Mills and Hunte, 1997].

2.1.2 Mechanisms

2.1.2.1 Band theory of solids

The electronic properties in solids can be described by the quantum theory of the electronic energy band structure. The electrons of a single isolated atom occupy atomic orbitals, which form a discrete set of energy levels. If several atoms are brought together into a molecule, their atomic orbitals split, as in a coupled oscillation. This produces a number of molecular orbitals proportional to the number of atoms. When a large number of atoms are brought together to form a solid, the number of orbitals becomes exceedingly large, and the difference in energy between them becomes very small, so the levels may be considered to form continuous bands of energy rather than the discrete energy levels of the atoms in isolation. However, the electronic wave functions of constituent atoms overlap, and the application of the Pauli Exclusion Principle leads to the splitting of the discrete energy levels of the isolated atoms into bands of allowed electron levels separated by so called forbidden bands or gaps [Yacobi, 2003].

The bands of possible electron energy levels in a solid are called allowed energy bands. The energy gap separates the highest filled (or valence) band and the lowest empty (or conduction) band. The allowed energy bands sometimes overlap and sometimes are separated by forbidden bands. The presence of a forbidden band immediately above the occupied allowed states is the principal difference in the

electronic structures of a metal and a semiconductor or insulator. As shown by Fig. 2.1, in the latter two substances there is a gap between the valence band and the conduction band. The presence of a gap means that the electrons cannot easily be accelerated into higher energy states. However, the energy gap in the case of a semiconductor is relatively narrow, so that the electrons from the top of the valence band can be excited across the gap by thermal or optical means. In insulators, the energy gap is so much greater that the probability of excitation of an electron from the valence band to the conduction band is very low. In a metal there is no gap between occupied and unoccupied states [Tyagi, 1991.; Yacobi, 2003].

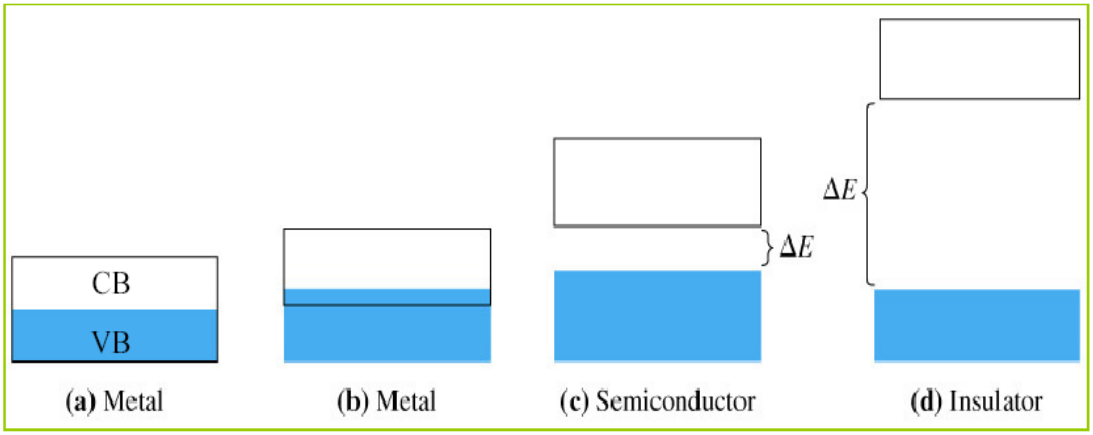

Figure 2.1 Diagram of the electronic band structure of metals, semiconductors, and insulators

2.1.2.2 Photoactivation of semiconductors

Semiconductors, such as TiO_2, ZnO, CdS, GaP, SiC, WO_3, ZnS and CdSe have been found to show certain photocatalytic activities. The activation of the semiconductor photocatalyst and corresponding photocatalytic reactions at the semiconductor surface can be described by the following six steps as indicated in Fig. 2.2 [Mills and

Lee, 2002]:

(a) Adsorption of photons having an energy matches or greater than its band gap energy of the semiconductor;

(b) Promotion of an electron e^- from the valence band to the conduction band, with the concomitant generation of a hole h^+ in the valence band;

(c) e^- and h^+ diffuse and migrate to the surface where they can react;

(d) Recombination of the electron-hole pairs;

(e) Stabilization of e^- and h^+ at the surface to form a trapped electron and a trapped hole respectively;

(f) Reduction of a suitable electron accepter and oxidation of a suitable electron donor.

Among above reaction steps, the absorption of light (step (a)) and subsequent redox reactions at the surface (step (f)) are the key process in photocatalysis. Step (c) and (e) sometimes occur too fast to be observed in the reaction [Kaneko and Okura, 2002].

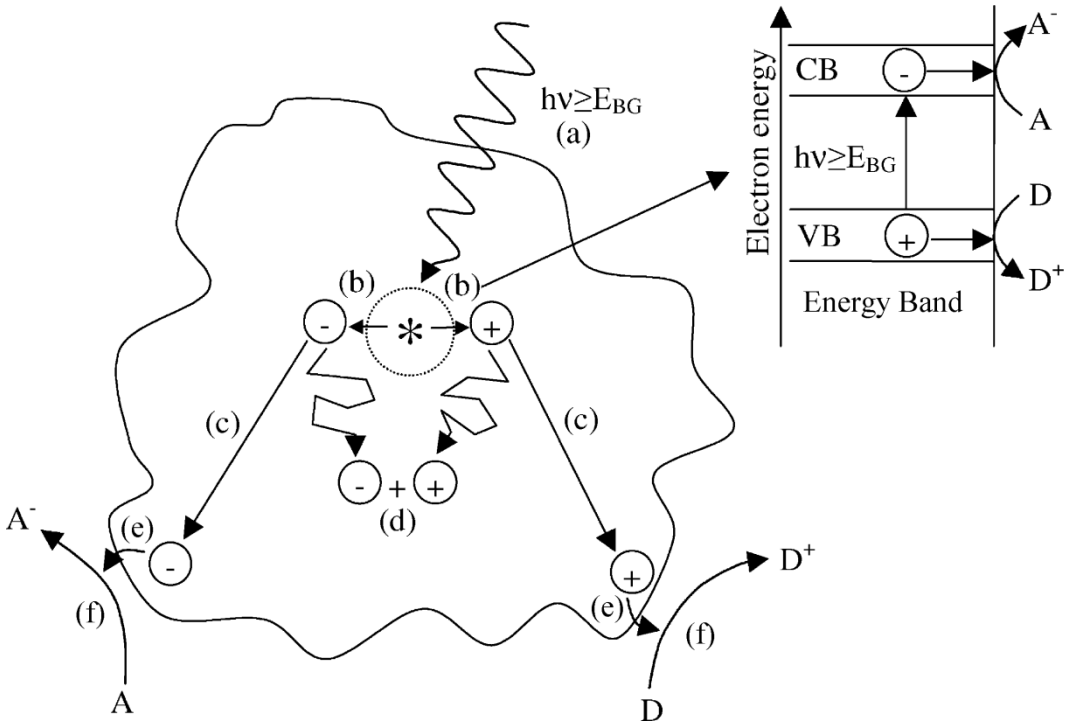

Figure 2.2 Schematic illustration of the major processes that occur on a semiconductor particle upon absorption of a photon of ultra-band gap light [Mills and Lee, 2002]

2.1.3 Titanium dioxide (TiO_2)

In the field of semiconductor photochemistry, TiO_2 is the most widely used photocatalyst. Although there are many semiconducting materials on the earth, only a few are very effective as semiconductor photocatalysts. In order to photo-reduce a chemical species, the conductance band of the semiconductor must be more negative than the reduction potential of the chemical species; to photo-oxidize a chemical species, the potential of the valence band of the semiconductor must be more positive than the oxidation potential of the chemical species. Fig. 2.3 shows an energy level diagram indicating the energy positions of the conduction and valence bands for various semiconductors in aqueous media. It can be seen that the oxidation and

reduction power of TiO_2 is strong enough to produce OH· and HO_2· radicals which are very strong oxidants as well.

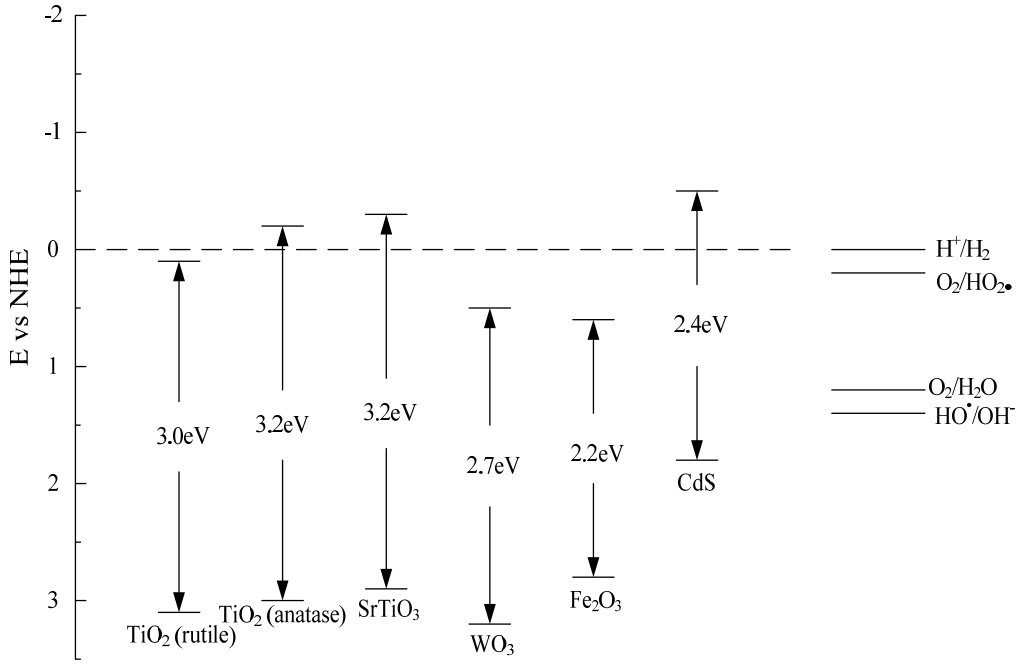

Figure 2.3 Valence and conductive band positions for various semiconductors at pH 0, E (Electric potential) vs NHE (Normal Hydrogen Electrode potential) [Mills and Hunte, 1997]

TiO_2 is a common semiconductor material which has been used as a white pigment in paints, cosmetics and foodstuff since ancient times [Fujishima et al., 1999]. It has three crystal structures: anatase, rutile and brookite. The anatase type is more widely used because it has a higher photoactivity than the other two types of TiO_2. The extensive use of TiO_2 in photocatalytic building materials is attributed to the following characteristics [Agrios and Pichat, 2005]:

(a) Cheap, safe, water insoluble, chemically inert and biologically safe;

(b) High photocatalytic activity compared with other semiconductor

photocatalysts;

(c) Effective under weak solar irradiation in ambient atmospheric environment.

TiO_2 displays all the desired features of an ideal semiconductor photocatalyst, with the exception that it does not absorb visible light. The band gap of TiO_2 varies from 3.0 to 3.2 eV, corresponding to light with wavelength less than 390 nm. Therefore, it is a UV light absorber and can only absorb a small fraction (5%) of the solar spectrum. Despite this limitation, its positive features far outweigh this negative one. Its dominant position extends not only to basic research but, more importantly with respect to commercial applications.

2.2 Photocatalytic Decomposition of Air Pollutants

2.2.1 Reaction mechanisms

It has been demonstrated that both organic pollutants and common oxides such as NO, NO_2 and SO_2 at low concentration levels can be converted by TiO_2 photocatalysis under UV irradiation. The mechanism of pollution decomposition is illustrated by Fig. 2.4. The reaction begins with the irradiation of light over TiO_2. When TiO_2 absorbs a photon containing the energy equal to or larger than the band gap, an electron will be promoted from the valence band to the conduction band. The activation of the electrons results in the generation of “holes” (electron vacancy) in the valence band. In this reaction, h^+ and e^- are powerful oxidizing and reducing agents respectively. The electron-hole pairs may recombine in a short time or take part in chemical reactions depending on reaction conditions and molecular structures of the semiconductors. The strong oxidation power of h^+ enables it to react with

water molecule to generate the highly active hydroxyl radical (·OH) which is also a powerful oxidant. In addition, the reducing power of the electrons can induce the reduction of molecular oxygen (O_2) to superoxide ($\cdot O_2^-$). It has been confirmed that the superoxide is almost as effective as the holes and hydroxyl radicals in the chain reactions for the breaking down of organic compounds. Most organic air pollutants can be degraded completely by either the hydroxyl radicals or the holes themselves to innocuous final products (e.g. CO_2 and H_2O) [Fujishima et al., 1999; Agrios and Pichat, 2005].

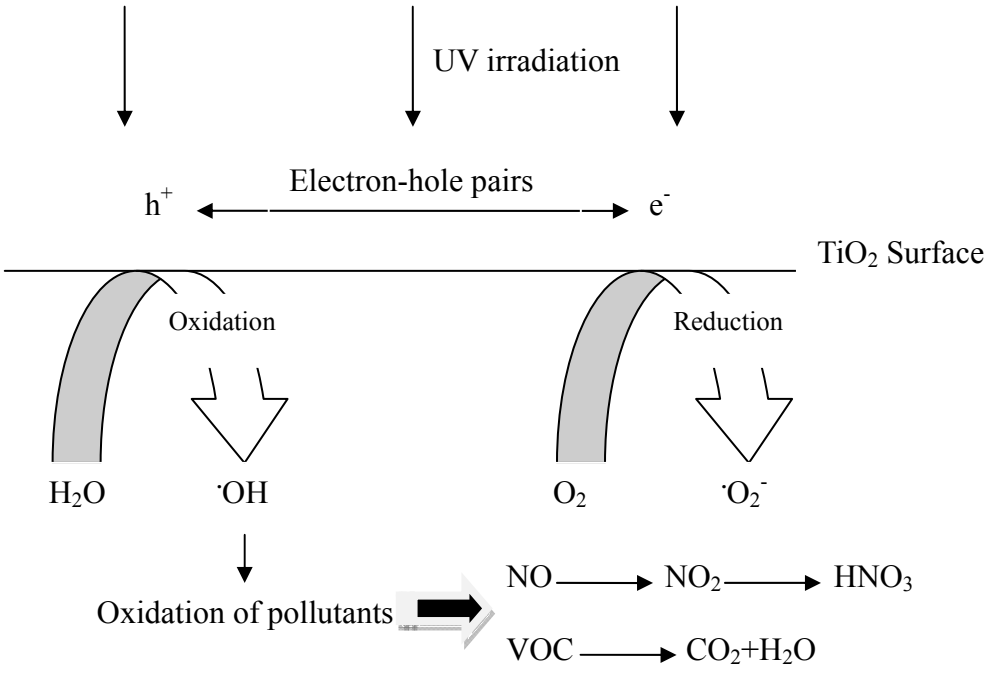

Figure 2.4 Gaseous Pollutants removal mechanism of TiO_2 photocatalysis

An example of photocatalytic conversion of nitric oxide to nitric acid is illustrated as follows [Lim et al., 2000; Dalton et al., 2002]:

(a) After irradiation of UV light ranging from 300 to 400 nm, the photocatalytic reaction begins with the generation of electron-hole pairs;

$$TiO_2 \xrightarrow{h\nu} h^+ + e^-$$

(b) The h^+ reacts with OH^- dissociated from water to form the hydroxyl radical;

$$h^+ + OH^- \rightarrow OH^\bullet$$

(c) The e^- reacts with molecular oxygen to form the superoxide anion;

$$e^- + O_2 \rightarrow O_2^-$$

(d) The superoxide anion further reacts with H^+ dissociated from water to produce $HO_2^\bullet$ radicals;

$$H^+ + O_2^- \rightarrow HO_2^\bullet$$

(e) NO diffuses to the surface of TiO_2 and is oxidized to NO_2 by $HO_2^\bullet$ radicals;

$$NO + HO_2^\bullet \rightarrow NO_2 + OH^\bullet$$

(f) Finally NO_2 reacts with hydroxyl radicals to form nitric acid.

$$NO_2 + OH^\bullet \rightarrow HNO_3$$

The great redox power of the UV induced electron-hole pair of photocatalysts can also decompose the organic pollutants. An example of degradation of palmitic acid is shown below [Peruchon et al., 2008]:

$$TiO_2 \xrightarrow{h\nu} h^+ + e^-$$

$$n-C_{15}H_{31}-COO^-H^+ + h^+ \rightarrow n-C_{15}H_{31}-COO^\bullet + H^+ \rightarrow n-C_{15}H^\bullet_{31} + CO_2 + H^+$$

After the release of the first carbon atom, the $n-C_{15}H_{31}^\bullet$ radicals are oxidized by $OH^\bullet$ radicals to an alcohol:

$$n-C_{15}H_{31}^\bullet + OH^\bullet \rightarrow n-C_{15}H_{31}OH$$

The produced $n-C_{15}H_{31}OH$ undergoes oxidation into aldehyde, and then further to acid $n-C_{14}H_{29}-COOH$. Subsequently, a second photo-Kolbe reaction takes place to release the second CO_2. The chain reactions continue until the palmitic acid is completely mineralized to CO_2 and H_2O. Some side reactions may also be induced to generate volatile compounds, accelerating the oxidation process.

2.2.2 Reaction kinetics

Reaction kinetics gives information about the reaction rate and the mechanisms by which the reactants are converted to the products. A common way to express the reaction rate is to use the power law:

$$-\frac{\mathrm{d}C}{\mathrm{d}t} = kC^{\mathrm{n}}$$

Where *k* is the rate constant, *C* is the concentration of the reactant, and n is the order of the reaction. In general, first-order and second-order models are more common.

A heterogeneous catalytic reaction consists of the following processes [Yamazaki et al., 1999]:

(a) mass transfer of reactants (contaminants) to the catalyst surface;

(b) Adsorption of reactants on the catalyst surface;

(c) Photochemical reaction on the surface;

(d) Desorption of products from the surface;

(e) Mass transfer of products from the surface into the bulk of the fluid (air).

The kinetic models were developed to express one or several of these processes mathematically. The Langmuir-Hinshelwood (L-H) model is the most widely used model to describe the kinetics of gas-solid phase reaction in heterogeneous photocatalysis. The model assumes that [Fox and Dulay, 1993]:

(a) At equilibrium the number of surface adsorption sites is fixed;

(b) Only one substrate may bind at each surface site;

(c) The heat of adsorption by the substrate is identical for each site and is independent of surface coverage;

(d) There is no interaction between adjacent adsorbed molecules;

(e) The rate of surface adsorption of the substrate is greater than the rate of any subsequent chemical reactions;

(f) No irreversible blocking of active sites by binding to product occurs.

The surface coverage (θ) is related to the apparent adsorption equilibrium constant (K) by the following equation:

$$\theta = \frac{KC_o}{1 + KC_o} \quad (2.1)$$

The rate of product formation can be expressed as L-H kinetic rate expression, in which the reaction rate (r) varies proportionally with the surface coverage:

$$r = k\theta = \frac{kKC_o}{1 + KC_o} \quad (2.2)$$

Where k is the apparent reaction rate constant occurring at the active site of the photocatalyst surface and C_o is the initial concentration of the pollutant. By rearranging equation 2.2, a linear form of the L-H model can be obtained:

$$r = \frac{kKC_o}{1 + KC_o} \rightarrow \frac{1}{r} = \frac{1 + KC_o}{kKC_o} \rightarrow \frac{1}{r} = \frac{1}{kKC_o} + \frac{KC_o}{kKC_o}$$

$$\rightarrow \frac{1}{r} = \frac{1}{kKC_o} + \frac{1}{k} \quad (2.3)$$

The linearity of the data by plotting the reciprocal of the reaction rate versus the reciprocal of the initial concentration is a standard method to test whether the kinetics can be expressed by the L-H model. In addition, the values of the rate constant (k) and the equilibrium constant (K) can be obtained by the intercept and the slope of the graph, respectively.

Several researchers [Zhang et al., 1994; Cho et al., 2004] have also used the residence time of the pollutants in reactors to study the heterogeneous photocatalytic

reaction kinetics. Integrating equation 2.2,

$$r = -\frac{dC}{dt} = \frac{kKC}{1 + KC}$$

$$-\int_0^t dt = \int_{C_o}^{C} (\frac{1}{kKC} + \frac{1}{k}) dC$$

$$\ln\frac{C_o}{C} + K(C_o - C) = kKt \quad (2.4)$$

Substitute $t = V/Q$ into equation 2.4, where V is the volume the reactor and Q is the flowrate of the reactant.

$$\ln\frac{C_o}{C} + K(C_o - C) = kK\frac{V}{Q} \quad (2.5)$$

$$\frac{V}{Q} = \frac{1}{kK}\ln\frac{C_o}{C} + \frac{1}{k}(C_o - C) \quad (2.6)$$

$$\frac{V/Q}{C_o - C} = \frac{1}{k} + \frac{1}{kK}\frac{\ln(C_o/C)}{(C_o - C)} \quad (2.7)$$

By rearranging equation 2.6, a linear plot of $\frac{V/Q}{C_o - C}$ versus $\frac{\ln(C_o/C)}{(C_o - C)}$ can be obtained to ventilate the L-H model, as shown by equation 2.7.

2.2.3 Effects of environmental factors on photocatalytic pollution degradation

Based on kinetic models and experiments, the dependence of photocatalytic reaction rate on some influencing factors, such as temperature, humidity, light intensity, pollutant concentration and residence time, have been extensively studied as follows.

2.2.3.1 Effects of temperature

Temperature not only affects the kinetic reaction but also the adsorption of the gas phase compounds on the photocatalyst. The reaction rate constant (k) followed an Arrhenius temperature dependence formula [Obee and Hay, 1997]:

$$k \propto f\left(\exp\left(\frac{-E}{RT}\right)\right)$$

Where E is an apparent activation energy; T is the temperature; and R is the gas constant (1.99×10^{-3} kcal $(\text{mol K})^{-1}$). Therefore, it is obvious that temperature enhancement can positively affects the kinetic reaction.

During an adsorption process, the coverage of photocatalyst surfaces by the pollutants decreases progressively with increasing temperature. The adsorption equilibrium coefficient (K) also followed a temperature dependent equation, similar to the Arrhenius one [Pichat and Herrmann, 1989]:

$$K \propto f\left(\exp\left(\frac{-H}{RT}\right)/\sqrt{\mathrm{T}}\right)$$

Where H is the change of enthalpy in the adsorption of the adsorbed reactant.

The total photocatalytic degradation rate is the combined process of kinetic reaction and adsorption. Under the reaction kinetic limit process, increasing temperature will enhance the reaction rate and the negative effect on adsorption becomes negligible. On the contrary, under the mass transfer limit process, the increase of temperature decreases the amount of adsorbed pollutants on the reaction surface so that it will lower the reaction rate. Therefore, a maximal reaction rate should appear at an optimal temperature [Pichat and Herrmann, 1989]. The optimal temperature seems to be in a narrow range. It was found that increasing the reaction temperature from 30 to 77 °C increased the reaction rate constant of vapor acetone at a 95% confidence level; however, increasing the temperature from 77 to 113 °C did not have a significant effect [Zorn et al., 1999].

Different VOC compounds under various temperature conditions were investigated to identify the effect of temperature. Toluene [Obee and Brown, 1995], trichloroethylene (TCE) [Sanchez et al., 1999], perchloroethylene (PCE) [Hager and Bauer, 1999] and acetaldehyde [Sano et al., 2004] were found to have decreasing reaction rates with increasing temperatures. However, for the compounds of formaldehyde [Obee and Brown, 1995] and ethylene [Obee and Hay, 1997], the reaction rates increased with increasing temperatures.

2.2.3.2 Effects of relative humidity

Humidity represents one of the most important parameters for photocatalysis applications in the gaseous pollutant mitigation. Many studies have confirmed a significant impact of humidity on the degradation efficiency of air contaminants. Logically, the presence of OH· (and therefore precursor water molecules) should

significantly promote photocatalytic reactions. It has been reported that under UV illumination, the number of hydroxyl radicals formed is directly proportional to the adsorbed water molecules [Boonstra and Mutsares, 1975]. However, the effects of humidity levels on photodegradation rate are quite controversial.

Amama et al. (2004) reported that degradation of TCE to CO_2 in gas phase during heterogeneous photocatalytic degradation reaction increased from 52% at 0% RH to 71% at 100% RH. Wu et al. (2005) also observed that the removal ratio of benzene increased with humidity in the range of 15000-28000 ppmv of water. Conversely, it has been demonstrated that humidity inhibits the photocatalytic decomposition reactions in many cases. For example, Oua and Lo (2007) pointed out that the water molecules deliver inhibitory effect on the TCE degradation, reporting that the value of the rate constant of TCE degradation at 10% RH is larger than that at 55% RH by a factor of 2.5. Sleiman et al. (2008) found that the mineralization of pesticide dichlorvos in gas phase dropped drastically with the increase of RH and reached a plateau at a RH value of 50%. In addition, there are other studies finding that the photocatalytic oxidation rate increased to an optimum level with increasing RH and then decreased or reached a steady state [Obee and Brown, 1995; Demeestere et al., 2005].

The discrepancy between the reported phenomena cannot be explained simply by the change of hydroxyl radical population levels. In the case of inhibition effect, the general acceptable explanation is that diffusion driven adsorption competition occurs on the active sites of TiO_2 surface between the target contaminants and water vapors can result in the decrease in conversion rate [Obee and Brown, 1995; Kim and Hong,

2002]. It was also proposed that the hydrophilic or hydrophobic property of gaseous reactants which dominates the mass transport mechanisms account for the detrimental effect of water vapors. The surface of the TiO_2 is strongly hydrophilic and preferential adsorption of water. Multiple layers of water molecules can be formed at the TiO_2 interface with air, even at low relative humidity [Cao et al., 2000]. Therefore, the hydrophilic/hydrophobic nature of a given chemical could promote or retard it to reach the reactive TiO_2 surface through multiple-layered water film, determining it reaction rate with radical species in boundary layers [Zhang et al., 2007]. Regarding to the observed enhancement of the decomposition of a target contaminant with increasing humidity, it is believed that water molecules are needed to generate sufficient hydroxyl radical for photodegradation. Thus, an increase of conversion rate is observed with increasing water vapor concentration to a certain level [Peral and Ollis, 1992]. However, when excess water vapor is provided, the competition effect between pollutant and water vapor become dominant and could decrease the conversion rate.

Moreover, RH was found to significantly affect the mineralization extent and the formation of reaction intermediates. Ameen and Raupp (1999) showed that the deactivation caused by o-Xylene decreased with increasing water vapor concentrations. High water vapor concentrations favor the generation of reactive hydroxyl radicals, which serve to attack adsorbed reactant molecules and partial oxidation intermediates, thereby decreasing the surface coverage by these compounds. Kim and Hong (2002) also showed a similar result in toluene photodegradation. They reported that at low humidity level, the color of the photocatalyst changed to brown. With increasing water vapor concentrations, the

intermediates which accumulated on the catalyst surface were desorbed or degraded.

2.2.3.3 Effects of UV-light intensity

The UV-light irradiation has the dramatic effect (as the energy provider) on the photocatalytic degradation of the reactants. The reaction rate increases with increasing light intensity or the photon flux on the surface of the catalyst, as the heterogeneous photocatalytic reaction depends on the irradiation of TiO_2 surface by UV light to produce electron/hole pairs even though part of them may recombine. Generally, UV light with the wave length of near 300-370 nm is used to provide energy to the photocatalytic degradation process. The types of light sources used in the research include Xe arc lamp, Hg-arc lamp, Hg-Xe lamp and Black-light lamp [Zhao and Yang, 2003].

The dependence of the oxidation rate on UV intensity is well established [Ollis et al., 1991; Peral and Ollis, 1992]. The functional dependence of the PCO (photocatalytic oxidation) reaction rate (r) on UV light intensity is:

$$r = KI^n \ (\mathrm{n} = 0.5, \mathrm{when:\ I} > \mathrm{S}_\lambda;\ \mathrm{n} = 1, \mathrm{when\ I} < \mathrm{S}_\lambda)$$

where K is a constant; I is the UV intensity; S_λ is the one sun equivalent under the λ wavelength. For illumination levels appreciably above one sun equivalent (1-2 mW cm^{-2} with wavelengths below 350 and 400 nm respectively), the oxidation rate increases with the square root of the intensity. For UV intensities below that level, the oxidation rate increases with the intensity linearly. Obee and Brown (1995) applied formaldehyde, toluene and 1, 3-butadiene as the target pollutants to study the effect of light source on photocatalytic oxidation and confirmed above conclusions.

They showed that the oxidation rate dependence of toluene on UV light intensity followed a power law with an exponent of 0.55 ± 0.03, and the same exponent was found for formaldehyde and 1, 3-butadiene in the UV intensity range of 10-40 mW cm^{-2}. Obee (1996) also indicated that the internal shading in the porous structure (e.g., titania-coated alumina struts) affected the adsorption rate of the photons so as to influence the conversion rate.

The impact of UV-light intensity on the degradation rate was also confirmed by using different air pollutants. Yamazaki et al. (1999) showed that the reaction rate of photo assisted degradation of ethylene over TiO_2 catalysts was first-order with light intensity, which indicates that the higher intensities can produce the higher rates without losing efficiency if constant quantum yield can be maintained. Wang et al. (1998a) observed that the reaction rate of TCE was enhanced from 0.08×10^{-6} to 0.25×10^{-6} mol s^{-1} g^{-1} as the light intensity increased from 0.08 mW cm^{-2} to 0.45 mW cm^{-2} under humidity of 3800 ppmv, but the quantum yield decreased as the UV light intensity increased. The first order dependence of the TCE oxidation rate on the intensity of the incident radiation was also confirmed in the range of 5.2-20.8 W m^{-2} [Puddu et al., 2009]. Benoit-Marquie et al. (2000) found that an Xe-excimer lamp with a higher incident emission than a medium pressure Hg-arc light increased the conversion rate of 1-butanol from 50% to 85% and the conversion rate of 1-butylamine from 30% to 60%.

2.2.3.4 Effects of initial pollutant concentration

It can be seen from equation 2.5 that different inlet pollutant concentrations and retention time lead to different reaction rates. Obee and Hay (1997) found that the

reaction rate of ethylene was enhanced with the increase of inlet concentration from 10 to 260 ppmv. Kim and Hong (2002) showed that the photocatalytic degradation rate of volatile organic compounds (VOCs) including gaseous TCE, acetone and methanol gradually increased in the concentration range of 0.005 to 0.020 mol m^{-3}. They also pointed out that a good fitting of the L-H model to the experimental data, proving the L-H nature of the photocatalytic degradation reaction mechanism. However, there are also several studies reporting the decrease in reaction rate with increasing pollutant concentration due to the blockage of active sites by the intermediates (Li et al., 1998; Duan et al., 2002; Demeestere et al., 2005).

Mohseni and David (2003) suggested that the removal rate of gas phase vinyl chloride (VC) followed pseudo-first order reaction rate kinetics at low pollutant concentration levels where the oxidizing species (i.e. OH radicals and/or UV photons) were in excess. The reaction kinetics then approached to zero order at higher VC concentrations and the rate was less dependent on concentration. Under such conditions, the concentrations of OH radicals and/or UV photons as oxidizing species were likely the limiting factors. A similar finding was shown by Noguchi et al. (1998), the increasing rate of the reaction rate slowed down when the inlet concentration of formaldehyde was higher than 600 ppmv. This indicated that the reaction kinetics was mass-transfer limited in low concentration region, so they concluded the reaction rate was determined by the adsorption of contaminants on the catalyst surface.

In summary, when the initial pollutant concentration is lower than a certain level, the reaction rate increases with increasing initial concentration and can be described by

the L-H model. When the initial pollutant concentration is relatively high, an opposite trend is observed due to the deactivation of photocatalysts.

2.2.3.5 Effects of retention time

The effect of residence time is widely studied together with the initial pollutant concentration. Similar to the effects of initial pollutant concentration, two opposite effects are observed. The influence of mass transfer played a significant role in the effect of residence time. When the reaction is mass transfer controlled, the degradation rate of reactants increased with decreasing residence time [Alberici and Jardim, 1997]. With the contact time further decreasing, the photodegradation rate changes from mass transfer control to reaction kinetic control and can be described by the L-H model. In this case, the degradation rate increases with the increase of residence time [Mohseni and David, 2003; Stokke and Mazyck, 2008].

2.2.4 Standardization of photocatalytic air pollutants degradation test

The market for photocatalytic air purification has been growing very fast. It has been shown that the photocatalytic air pollutant degradation process is significantly influenced by the operating and environmental parameters. Thus, the performance of photocatalytic products cannot be reasonably compared without a standard evaluation method. In the academic field, it is also necessary to establish a set of reliable and rapid test methods to harmonize the results reported in a huge number of articles.

The standardization of photocatalytic air pollutants degradation test was first started in Japan in 2002 [Fujishima and Zhang, 2006]. In Europe, test standards for photocatalysis CEN/TC 386 are also under development. Up to now, Japanese Industrial Standard JIS R 1701 is consisted of the following 5 parts under the general title “Fine ceramics (advanced ceramics, advanced technical ceramics)—Test method for air purification performance of photocatalytic materials”: Part 1: Removal of nitric oxide; Part 2: Removal of acetaldehyde; Part 3: Removal of toluene; Part 4: Removal of formaldehyde; Part 5: Removal of methylmercaptan. The testing apparatus set-up, equipment requirements, general test conditions and procedures specified in these standards are summarized as follows.

The testing facilitates consist of a testing gas supply, a photo-reactor, a light source and pollutant concentration measurement equipments. A typical equipment set-up is shown in Fig. 2.5. The testing-gas supply prepares air polluted with the model contaminants at a predetermined concentration, temperature, and humidity, which are continuously supplied to the photo-reactor at a fixed flowrate. The photo-reactor holds a planar test piece above and in parallel to an optical window for photo irradiation. The test piece is separated from the window by a 5 mm thick air layer. The reactor is fabricated from materials that adsorb little testing gas and withstand irradiation of near-UV light. The testing gas passes only through the space between the test piece and the window. Quartz or borosilicate glass that absorbs little light at wavelengths longer than 300 nm shall be used for the window. The ultraviolet fluorescent lamp (wavelength range, 300 to 400 nm) is used as the light source to irradiate the test piece uniformly through the window. The distance between the light source and the reactor is adjusted so that the irradiance of UVA at the sample surface

is 10 W m^{-2}. The reactor is shielded from external light. Analyzers, such as chemiluminescent NO analyzer and gas chromatograph (GC) is used to record the pollutant concentration change during test.

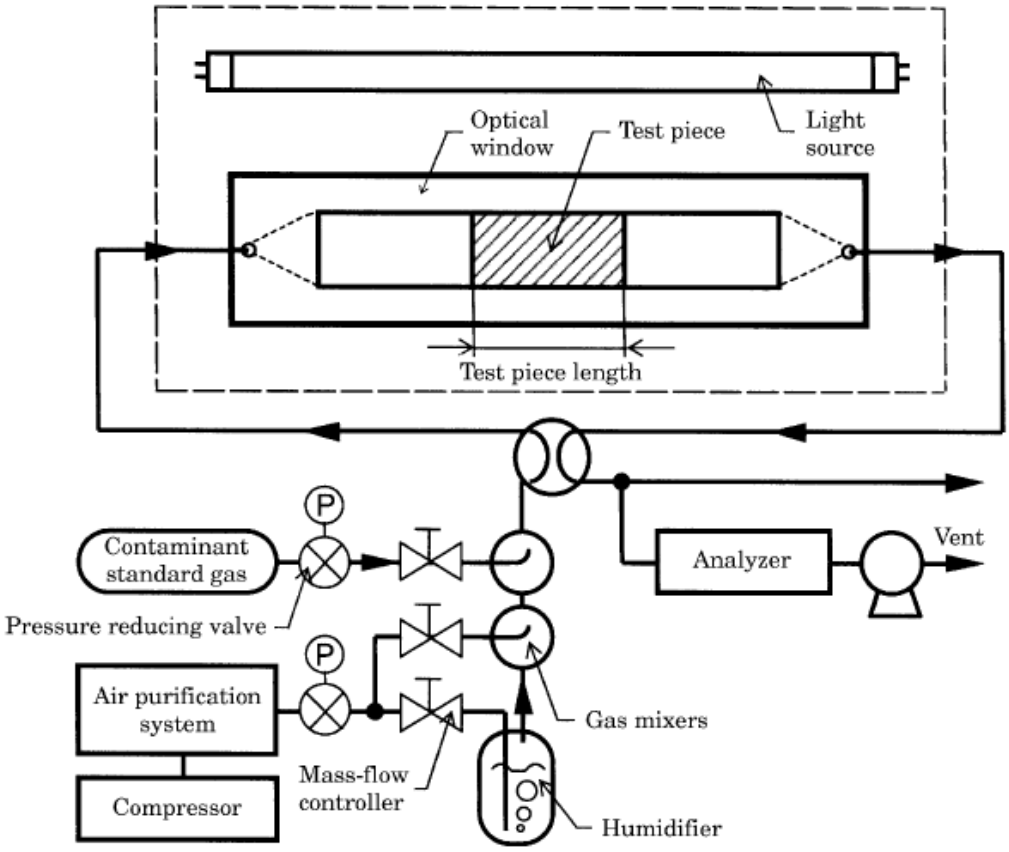

Figure 2.5 Schematic illustration of testing equipment [JIS R 1701-1]

The testing procedure is summarized here taking NO photocatalytic removal as an example [JIS R 1701-1]:

(a) Adjust the testing gas supply beforehand so that it can stably supply the testing gas containing 1.0 ppmv NO (25.0 ± 2.5 ^{o}C and 50% RH). Fix the flow rate at the inlet of the photo-reactor at 3.0 L min^{-1} (0 ^{o}C, 101.3 kPa, dry gas base). Measure and record the irradiance from the light source. NO

analyzer should be warmed up and calibrated before the measurement.

(b) Put a test piece in the middle of gas flow channel in the photo-reactor and adjust the space between the window plate and the test piece to be 5 mm. Then attach the glass window and check that the reactor is completely sealed.

(c) Introduce the testing gas into the photo-reactor. Continue the adsorption process for 30 min and record the change in the concentrations of NO and NO_2 under dark conditions. If the concentration of NO at the outlet is confirmed to be identical with the supplied testing gas concentration, irradiation may start at that point.

(d) Turn the light source on and record the NO and NO_2 concentrations at the reactor outlet under irradiation for 5 h. Stop irradiation, switch to the zero-calibration gas under the same temperature, humidity and flow conditions and record the NO_x concentration at the reactor outlet for 30 min. The recording may be finished before that, if the NO_x concentration is confirmed zero.

(e) Stop air supply to the reactor and take out the test piece of the reactor.

2.3 Cement-based Materials

2.3.1 Cements

2.3.1.1 Introduction

There is a wide variety of cements that are used in the construction and building industries, but by far the greatest amount of concrete used today is made with Portland cements. The name “Portland” was used as a trade name and thus gives no indication of composition or properties. The name now applies to a family of closely related cements that have an overall similarity of properties. Portland cement is essentially a calcium silicate cement, which is produced by firing an intimate mixture, usually of limestone and clay, in a kiln at a temperature of approximately 1500 ^{o}C. At this temperature, the two materials interact chemically to form the calcium silicates [Mindess et al., 2003].

The first calcium silicate cements were produced by the Greeks and Romans, who discovered that volcanic ash, if finely ground and mixed with lime and water, produced a hardened mortar, which was resistant to weathering. The reaction is known as the pozzolanic reaction and it is the basis of the contribution made to strength and concrete performance by materials such as fly ash, microsilica and metakaolin in modern concrete [Newman and Choo, 2003]. A typical chemical composition of an ordinary Portland cement is given in Table 2.1. It should be noted that the quantities do not add up to 100%, the missing percentages being account for by impurities [Mindess et al., 2003].

Table 2.1 Typical composition of ordinary Portland cement [Mindess et al., 2003]

Chemical name	Chemical formula	Shorthand notation	Weight percent
Tricalcium silicate	$3CaO \cdot SiO_2$	C_3S	55
Dicalcium silicate	$2CaO \cdot SiO_2$	C_2S	18
Tricalcium aluminate	$3CaO \cdot Al_2O_3$	C_3A	10
Tetracalcium aluminoferrite	$4CaO \cdot Al_2O_3 \cdot Fe_2O_3$	C_4AF	8
Calcium sulfate dihydrate	$CaSO_4 \cdot 2H_2O$	$C\bar{S}H_2$	6

Cement-based materials are referred as composites with cements as binder, including concrete (containing coarse and fine aggregates), mortar (only containing fine aggregate) and cement paste (containing no aggregate). The coarse aggregate is typically stones such as gravel. The fine aggregate is typically sand. These aggregate are chosen because their low cost and wide availability. Aggregates serve as fillers, while cement serves as binders. Mixing these materials together forms cement-matrix composites. Concrete is the form that is mostly commonly used in structures. Mortar is used in masonry, coating and some forms of repair. Cement paste itself is not used in structural applications, but it is a basic component of concrete and mortar [Chung, 2003].

2.3.1.2 Hydration of cement

When cement is mixed with water, its constituent compounds undergo series of chemical reactions that lead to subsequently setting and hardening, thereby allowing cement to be used conveniently as the matrix in concrete structures essentially any

shape. Reactions with water are designated hydration, and the new solids formed during hydration are collectively referred to as hydration products. The hydration reactions proceed until either a lack of reactants or a lack of space to deposit the hydration products. All hydration reactions can be described by reaction stoichiometries, rates of reaction, and heats of reactions. An example of the hydration of C_3S under ambient conditions is described by reaction (2.8) [Gartner et al., 2002].

$$C_3S + (3 - x + n)H \rightarrow C_xSH_n + (3 - x)CH \ [\Delta H = -121 \text{ kJ mol}^{-1}] \quad (2.8)$$

In major applications (concrete or mortars, etc.), the setting process is the consequence of a change from a concentrated suspension of flocculated particles to a visco-elastic skeletal solid capable of supporting an applied stress. The continued development of the solid skeleton is called hardening — a physic-chemical process leading to the development of ultimate mechanical properties. In addition, all the hydration reactions of cement are exothermic. Thus, during the hardening process, the concrete is being continually warmed by the internal heat generated. The extent of temperature rise depends on how quick the heat is liberated and how quickly it is lost from the concrete to the surroundings. Therefore, the rate of heat evolution is an important quantity. The hydration characteristics of the cement compounds and their contribution to the strength of the hydrated cement are summarized in Table 2.2.

Table 2.2 Characteristics of hydration of the cement compounds [Mindess et al., 2003]

Compounds	Reaction rate	Amount of heat liberated	Contribution to cement	
			Strength	Heat liberation
C_3S	Moderate	Moderate	High	High
C_2S	Slow	Low	Low initially, high later	Low
$C_3A+ C\bar{S}H_2$	Fast	Very high	Low	Very high
$C_4AF+ C\bar{S}H_2$	Moderate	Moderate	Low	Moderate

The hydration of a Portland cement is much more complicated than the hydration of individual components, because it is a sequence of overlapping chemical reactions. The reactions of the different components proceed simultaneously at different rates and can influence each other in complex ways. The principal stages of hydration of Portland cements in concrete are summarized as follows and corresponding rate of heat evolution is illustrated in Fig. 2.6 [Mindess et al., 2003]

Stage I (First minutes: wetting and mixing):

(a) Chemical processes: Rapid dissolution of free lime, sulphates and aluminate phases; immediate formation of ion substituted ettringite (AFt); superficial hydration of C_3S. Hemihydrates dissolve but gypsum or syngenite can form.

(b) Physical processes: Large initial burst of heat, mainly from dissolution of aluminate phases, plus some from alit and CaO.

(c) Relevance to physical properties of concrete: Rapid formation of aluminate hydrates, gypsum and syngenite influences rheology and may also affect the subsequent microstructure.

Stage II (Induction period: agitation, transport, placing and finishing)

(a) Chemical processes: Nucleation of "CSH(m)"; Rapid decrease in [SiO_2] and [Al_2O_3] to very low level; CH becomes supersaturated and portlandite nucleates; [R^+] (alkali metal ions), [SO_4^{2-}] stay fairly stable.

(b) Physical processes: Low heat evolution rate; slow formation of early CSH and more AFt leads to continuous increase of viscosity.

(c) Relevance to physical properties of concrete: Continued formation of AFt and iron substituted monosulfate (AFm) phases can influence workability, but the formation of CSH usually leads to the onset of normal set.

Stage III (Acceleration period: setting and early hardening)

(a) Chemical processes: Hydration of C_3S accelerates and reaches maximum; CH supersaturation decreases; [R^+], [SO_4^{2-}] stay fairly stable.

(b) Physical processes: Rapid formation of hydrates leads to solidification and decrease in porosity; high rate of heat evolution.

(c) Relevance to physical properties of concrete: Change from plastic to rigid consistency (initial and final set); early strength development.

Stage IV (Post acceleration period: demoulding; continued hardening)

(a) Chemical processes: Decelerating rate of formation of CSH and portlandite from both C_3S and C_2S; $[R^+]$ and $[OH^-]$ increase but $[SO_4^{2-}]$ falls to very low levels; renewed hydration of aluminates forms AFm phases. AFt may redissovle or recrystallize.

(b) Physical processes: Decrease in rate of heat evolution; continuous decreasing in porosity; particle to particle and paste to aggregate bond formation.

(c) Relevance to physical properties of concrete: Continuous strength increase due to decreasing porosity, but at an ever-diminishing rate; decrease in creep capacity; hydration continues for years if water is available; paste will shrink due to drying.

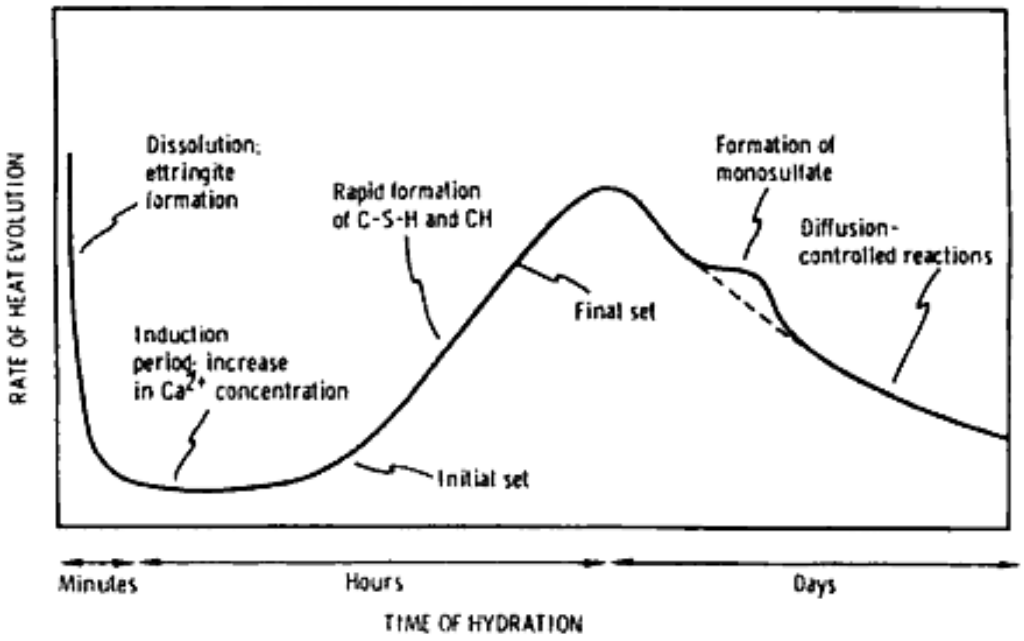

Figure 2.6 Schematic representation of heat evolution during hydration of a Portland cement [Gartner et al., 2002]

2.3.1.3 Hydration and properties of cement with nano-particle admixtures

One of the definitions of an admixture given by ASTM C 125-07 is “a material other than water, aggregates, hydraulic cement and fiber reinforcement that is used as an ingredient of concrete or mortar and is added to the batch immediately before or during its mixing”. Admixtures are added at less than 5% of the cement weight in the mix but the majority of admixtures are used at less than 2% and the typical range is 0.3-1.5% [Newman and Choo, 2003]. They can modify concrete properties either in the wet state immediately after mixing or after the mix has hardened. Admixtures can be single chemical or a blend of several chemicals in the form of powders or aqueous solutions. A wide range of materials are used as admixtures in modern concrete technology and can be divided into two categories: one is finely divided solids (mineral admixtures) and another one is water-soluble compounds (chemical admixtures). These substances are blended with Portland cement to improve workability and water retention [Mindess et al., 2003]. Considering the nature of materials used in this research, this section will confine the review to mineral admixtures with nano-particle size.

Nano-SiO_2 is the most widely used nano-particle admixture in cement-based building materials. The microstructure of nano-SiO_2 blended cement-based materials has been investigated by several studies. Tao (2005) studied the water permeability resistant behavior and microstructure of concrete with nano-SiO_2. The water permeability test showed that for concretes of similar 28-day strength incorporation of nano-SiO_2 can improve the resistance of water penetration of concrete. SEM observation revealed that the microstructure of concrete with nano-SiO_2 is more uniform and compact than that of normal concrete. The nano-SiO_2 particles can fill the voids of the CSH gel

structure and act as nucleus to tightly bond with CSH gel particles, making binding paste matrix denser. Li et al. (2004) also found that nano-Fe_2O_3 and nano-SiO_2 could fill up the pores of cement mortar and reduced CH compound among the hydrates. They concluded that nano-particles are valuable for reinforcing cement mortar based on the experimental results that the compressive and flexural strengths of cement mortar with nano-SiO_2 or nano-Fe_2O_3 were both higher than that of plain cement mortar with the same w/b.

The influence of adding nano-SiO_2 on the hydration and properties of cement are also extensively studied. Lin et al. (2008a) found that adding nano-SiO_2 into sludge/fly ash mortar promoted the crystal growth and aluminate dissolution in CSH gel through the nucleation of hydrates. It could accelerate the hydration reaction and improve the properties of the specimens. The compressive strength of mortar samples was increased and the negative effects caused by sludge/fly ash on the early strength of mortar were overcome. They demonstrated that the amount of water needed at standard consistency increased as more nano-SiO_2 was added. Their research results also confirmed the improvement of compressive strength due to the addition of nano-SiO_2. Senff et al. (2009) showed that spread diameter, setting time and the time to reach maximum temperature of nano-SiO_2 containing cement decreased 33%, 60% and 51.3%, respectively, when compared with samples without nano-SiO_2.

There are other researches trying to compare the influence of nano-SiO_2 addition with silica fume or fly ash addition. Ye et al. (2007) compared the difference through the measurement of compressive and bond strengths of hardened cement paste, and by XRD and SEM analysis. Their results indicated that nano-SiO_2 made cement

paste thicker and accelerated the cement setting process as compared with silica fume. Compressive strengths and bond strengths of paste-aggregate interface incorporating nano-SiO_2 were obviously higher than those incorporating silica fume, especially at early ages. With 3% nano-SiO_2 added, the orientation of CH crystals was decreased, reducing the crystal size of CH gathered at the interface and improving the interface more effectively than silica fume. Jo et al. (2007) showed that the compressive strengths of mortars with nano-SiO_2 particles were all higher than those of mortars containing silica fume at 7 and 28 days. It is demonstrated that the nano-particles are more valuable in enhancing strength than silica fume. The results indicate that nano-SiO_2 behaves not only as a filler to improve microstructure, but also as an activator to promote pozzolanic reaction. Li (2004) found that the addition of fly ash leaded to higher porosity at short curing time, while nano-SiO_2, acting as an accelerating additive, leaded to more compact structures, even at shorter curing times. They also demonstrated that fly ash had low initial activity, but the pozzolanic activity could be significantly increased after incorporating a little nano-SiO_2. Both short-term strength and long-term strength were increased due to the addition of nano-SiO_2 into high-volume high-strength concrete.

2.3.2 Aggregates

2.3.2.1 Introduction

Aggregates are granular materials, derived the most part from natural rock and sands, although recycled crushed concrete and synthetic materials such as slag and expanded clay are used to some extent. Sources of aggregates fall into the broad categories of sands, gravels and crushed rock. Sand and gravels are the products of

erosion of pre-existing rocks and are usually transported by water. They are typically deposited as relatively thin layers at the foot of mountains, in river valleys or along shorelines. By contrast, crushed rock is obtained from rock quarries by drilling and blasting the quarry face with explosives to maximize the fragmentation. The blasted fragments are then crushed and passed through a series of vibrating screens to produce the particles size fractions required [Newman and Choo, 2003].

Aggregate particles generally occupy 70 to 80% of the volume of a normal concrete and therefore have an important influence on its properties. The important properties of aggregates to proportion suitable concrete mixes include shape and texture, size gradation, moisture content, specific gravity and bulk unit weight. Aggregates should be hard and strong, free of undesirable impurities, and chemically stable. Soft, porous rock can limit strength and wear resistance. It may also break down during mixing and adversely affect workability. Rocks that tend to fracture easily along specific planes can also limit strength and wear resistance. Therefore, it is best to avoid aggregates that contain a significant proportion of weak or friable materials. Aggregates should also be free of impurities such as silt, clay, dirt or organic matter. If these materials coat the surfaces of the aggregate, they will isolate the aggregate particles from surrounding concrete, causing a reduction in strength. Although aggregate strength can play an important role in high-strength concretes, for most applications the strength of concrete and mix design are essentially independent of the composition of aggregates. However, durability may be affected [Mindess et al., 2003].

2.3.2.2 Recycling of waste glass as aggregates in concrete

Based on the chemical composition, glasses can be classified into the three major groups: soda-lime glass, lead glass and borosilicate glass. Glasses in these categories account for at least 95% of all glass types. With very few exceptions, most glasses are silicate based glasses, the major component of which is SiO_2. Small amounts of additives are often added during the production of glasses to give glasses different colors or to improve specific properties. Soda-lime glass is most widely used to manufacture containers, float and sheets. It consists of approximately 71-75% SiO_2, 12–16% Na_2O and 10-15% CaO [Pfaender, 1996]. In waste glasses, soda-lime glass is over 80% by weight. On a color basis, 63% are clear, 25% are amber, 10% are green and 2% are blue or other colors [Shi and Zheng, 2007].

Quantities of waste glasses have been on the rise in recent years due to the rapid improvement in the standard of living. Unfortunately, container glass is the only type of glass that can be recycled in large quantities for making new glass. But due to various reasons, in Hong Kong, the supply of waste glass containers far exceeds the recycling capacity. Also, in a traditional recycling process, some of the collected glass becomes broken, color-mixed, or otherwise contaminated, and cannot be used in container manufacturing. Recyclers are beginning to develop alternative markets for such glass. The use of recycled glass in construction is among the most attractive options because of the large quantity and low quality requirements. The main applications include aggregate replacement in concrete, fine aggregate in unbond base course, pipe bedding, landfill gas venting systems and gravel backfill for drains.

In recent years, the use of glass as a partial replacement of aggregates has become a hot research topic due to high disposal costs for waste glasses and environmental regulations. Chen et al. (2006) studied the properties of concretes containing various waste E-glass particle contents. They found that compressive strength and resistance of sulfate attack and chloride ion penetration were significantly improved by utilizing proper amount of waste E-glass in concrete. The workability decreased as the glass content increased due to reduction of fineness modulus, and the addition of high-range water reducers was needed to obtain a uniform mix. Little difference was observed in alkali-silica reaction (ASR) testing results between control and E-glass specimens. Based on the properties of hardened concrete, optimum E-glass content was found to be 40-50% by mass. Kou and Poon (2009) found that although the compressive strength, tensile splitting strength and static modulus of elasticity of the self-compacting concrete containing recycled glass were decreased with an increase recycled glass aggregate content, the resistance to chloride ion penetration increased and the drying shrinkage decreased. The results showed that it is feasible to produce self-compacting concrete with recycled glass cullet. Ismail and AL-Hashmia (2009) showed that the flexural strength and compressive strength of concrete with a replacement of 20% aggregates by waste glass were higher than those of control specimens at 28 days. The mortar bar tests demonstrated that the finely crushed waste glass helped reduce expansion by 66% as compared with the control mix. They concluded that there is a promising potential for the use of waste glass in concrete.

The expansion and cracking of concrete containing glass aggregates due to alkali-silica reaction is one of the biggest obstacles in real application [Shi et al., 2005; Lam et al., 2007]. Two main theories have been proposed to explain the

mechanism of expansion caused by ASR [Hobbs, 1988]. One attributes the induced stresses within the concrete to the growth of the gel caused by absorption of pore fluid. Another one, known as the osmotic cell pressure theory, proposes the hydraulic pressure developed across an impermeable membrane is the cause of the expansion. Different attempts have been made to solve this concern. Supplementary cementitious materials such as ground blast furnace slag, fly ash, silica fume and metakaolin are often used to reduce the alkali-silicate reactions. Several studies have indicated that the use of these materials can effectively reduce the expansion of concrete containing glass aggregates [Hobbs, 1988; Zhu and Byars, 2004; Lam et al., 2007]. Another method is using porous lightweight aggregate or introducing air entrainment because the expansive reaction products can permeate into porous structure and then relieve the expansive pressure [Ducman et al., 2002].

2.4 Photocatalytic Construction and Building Materials

Since 1970s, the fundamentals and applications of photocatalytic oxidation (PCO) reaction have received significant attention. In the past decade, many research studies were devoted to explore the function of photocatalysts including photocatalytic water and air purification, self-cleaning and photocatalytic anti-bacterial effect. All these functions can be attributed to two fundamental photochemical phenomena that occur on the surface of photocatalysts under UV irradiation. One is the photo-induced redox reaction of adsorbed substances, and the other is the photo-induced superhydrophilicity. The synergy of these two properties is also the foundation of its application in building and construction materials.

2.4.1 Air depollution building materials

2.4.1.1 Outdoor air

In big cities with dense population the pollutant concentration at street level is quite high because the dispersion of the exhaust generated by a large number of vehicles is hindered by surrounding tall buildings. For these cities applying TiO_2 modified cementitious materials onto the external covering of buildings or roads may be a good supplement to conventional technologies such as catalytic converters fitted on the vehicles for reducing gaseous exhaust emission. Concrete pavement surfaces and external building surfaces are optimal media for applying the photocatalytic materials because the relatively flat configuration of the building materials can facilitate the exposure of the photocatalyst to sun-light. In addition, the nature of cement matrix is particularly suitable for incorporating TiO_2 particles and other

photo-oxidation products. Under irradiation of solar light, gaseous pollutants can be degraded on the surface of construction materials which can be eventually washed away by rain (Fig.2.7). The whole removal process of pollutants is driven by natural energy alone.

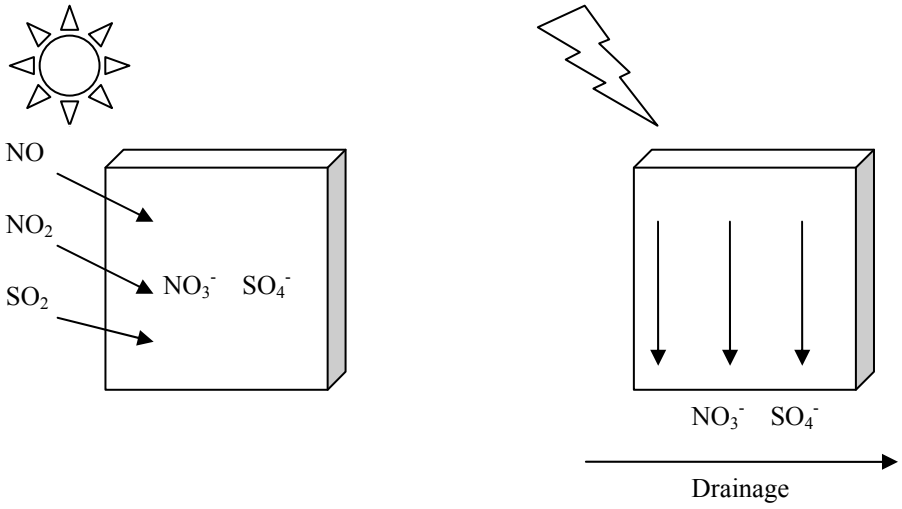

Figure 2.7 Illustration of pollutant removal by photocatalytic building materials in ambient environment

The depollution effect of photocatalytic cementitious materials has been demonstrated by many laboratory studies [Poon and Cheung, 2006; Beeldens, 2007; Strini et al., 2005; Hüsken et al., 2007; Demeestere et al., 2008]. NO_x and VOCs have been chosen by most studies as representative airborne pollutants due to their potential health risks and ability to generate photochemical smog. The NO removal efficiency of paving blocks made by waste materials and TiO_2 was evaluated by Poon and Cheung (2006). They found that an optimum mix design which incorporated recycled glass, sand, cement and 10% TiO_2 achieved 4.01 mg h^{-1} m^{-2} NO removal under a test condition of 1000 ppb initial NO concentration, a flowrate

of 6 L min^{-1} and a 10% RH. A typical performance of NO removal by the photocatalytic paving blocks obtained in the laboratory is shown in Fig. 2.8. Beeldens (2007) also investigated the feasibility of using TiO_2 on the surface of pavement blocks. It was reported that the air cleaning capacity can be enhanced by increasing the surface area, reducing the air flowrate and increasing the turbulence of the pollutant in the test chamber. Hüsken et al. (2007) carried out a comparative analysis of different photocatalytic cementitious products in an optimum laboratory conditions. They pointed out that the efficiency with respective to NO_x degradation varied significantly, with some products achieving 40% degradation whereas others showing almost no effect.

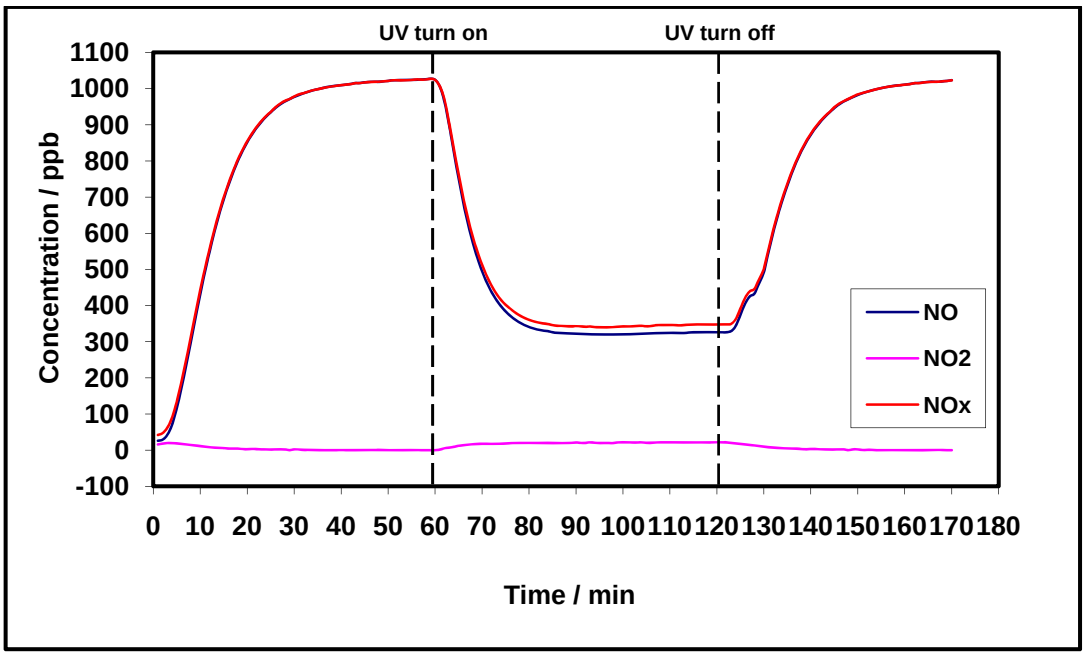

Figure 2.8 Photocatalytic NO_x removal results of photocatalytic paving block obtained in laboratory

Regarding the degradation of VOCs, Strini et al. (2005) measured the photodegradation of organic compounds (at ppb level) at the surface of photocatalytic materials using a stirred flow reactor with 50% RH and a 100 ml min^{-1} flow. They observed that the photocatalytic activity of pure TiO_2 sample was three to ten times greater than the cementitious sample that was prepared with the incorporation of 3% catalyst. The decomposition rate of BTEX was linearly dependent on the concentration of the reactant and the intensity of the irradiation. However, the catalytic activity was not linearly dependent on the TiO_2 content in the samples probably because the formation of catalyst clusters in the cementitious paste was influenced by the different viscosity of the paste. Demeestere et al. (2008) studied the potential of using TiO_2 as a photocatalyst in building materials, i.e. roofing tiles and corrugated sheets, for the removal of toluene from air at ambient conditions (T=25.0 °C; relative humidity RH=47%; toluene inlet concentration $[TOL]_{in}$=17–35 ppbv). It was reported that a toluene removal efficiency of 78 ± 2% and an elimination rate of higher than 100 mg h^{-1} m^{-2} were obtained under an optimal condition. Their results showed that low toluene removal performance occurred at high relative humidity and high inlet concentration, whereas better performance was observed with increased residence time. They also found that a decrease of photocatalytic activity by a factor of 2 when the photocatalytic building materials were operated at high pollutant concentration levels ($[TOL]_{in}$ > 76 ppmv). Also, washing the building materials with deionized water could partially regenerate the catalyst's activity.

Motivated by the promising results of the laboratory scale investigation, several pilot projects have been carried out to verify the effectiveness of the photocatalytic

cementitious materials in ambient environment. In Bergamo (Italy), a street in the city centre was re-paved by the photocatalytic concrete paving blocks (total area of about 12000 m^2). Environmental monitoring was conducted on two locations: one was at the area where photocatalytic blocks were laid, and the other was at the extension of the road paved by normal bituminous concrete which was used as a reference. NO_x concentration was measured by chemiluminescence analyzers simultaneously on the two sites. A successive air monitoring campaign, lasting two weeks, showed an average NO_x abatement of 45% in daytime (from 9 am to 5 pm) [Guerrini and Peccati, 2007a]. A similar project was carried out in Antwerp (Belgium), where 10000 m^2 photocatalytic pavement blocks was laid on a parking lane. Measurements on the site indicated an evident decrease of the NO_x peak concentration due to the presence of the photocatalytic materials. The photocatalytic activity of these blocks was retested in laboratory after they were in service for 2 years. The results showed that there was no reduction in NO_x removal efficiency after washing the paving blocks with distilled water [Beeldens, 2007]. In Guerville (France), three artificial street canyons were built to evaluate the depollution performance of walls covered with a photocatalytic mortar. Continuous NO_x and meteorological measurement were taken. NO_x concentration recorded in the TiO_2 treated canyon were 36.7% to 82.0% lower than the ones observed in the reference canyons [Maggos et al., 2008].

2.4.1.2 Indoor air

Indoor air pollutants mainly include NO_x, VOCs and particulates. These pollutants are emitted from different sources such as combustion, construction materials and consumer products. Many VOCs are known to be toxic and carcinogenic. PCO is one

of the most feasible options to improve indoor air quality because of two reasons [Wang et al., 2007]:

(a) PCO can mineralize many organic pollutants to harmless substrates, such as CO_2 and H_2O;

(b) The concentration level of pollutants in indoor environment is usually quite low (at ppb level), so the depollution function of the photocatalyst can be maintained for a long time.

The most frequently used building material aimed at removing indoor airborne impurities are photocatalytic paints incorporated in different binders, such as lime, polyorganic siloxane, silica sol-gel and organic binders. Maggos et al. (2007) tested the depollution efficiency of a TiO_2-containing paint in an indoor car park under real scale configuration. The ceiling of the car park was painted with a white acrylic TiO_2-containing paint. The artificially closed area of the car park was polluted by car exhaust during the testing period. As soon as the system reached a steady state, the UV lamps were turned on for 5 h. Results showed that photocatalytic oxidation of NO_x gases was significant. The photocatalytic removal of NO and NO_2 was 19% and 20%, respectively. Guarino et al. (2008) chose two identical mechanical ventilated farrowing rooms in a swine farm, where NH_3 was the main pollutant, to study the pollution removal performance of a TiO_2 catalytic paint. Environmental parameters, ventilation rate and gas concentrations were continuously monitored in the catalytic painted room and a reference room. NH_3 average concentration of 5.41 mg m^{-3} (in the reference room without treatment) and 3.76 mg m^{-3} (in the experimental room) have been reported during a full farrowing cycle.

Other building materials including composite sheets and wall papers are also modified with photocatalysts to reduce indoor pollutants. Ichiura et al. (2003) fabricated a composite TiO_2-zeolite sheet using a papermaking technique. The pollutant removal efficiency was tested using toluene and formaldehyde as target indoor pollutants under UV irradiation. The composite sheet with a Ti/zeolite ratio of 1:4 seemed to be the most effective for the removal of toluene, while no optimum composition was found for formaldehyde due to the high formaldehyde adsorptivity of Y type zeolite. The study showed this kind of sheets had potential to be placed on walls and ceilings for the removal of various indoor pollutants. Taoda et al. (2006) developed a photocatalytic wall paper by coating a visible light type photocatalyst on a wall paper. Their experimental results indicated that toluene and acetaldehyde could be decomposed efficiently even under irradiation of a fluorescent lamp, although using UV irradiation had better performance.

Regarding indoor environment where additional UV source is not applicable, TiO_2 containing building materials can also remove odors. This is because the odour which is sensitive to human noses is caused by chemical substances in the order of 10 parts per million by volume. Weak UV intensity of 1 $\mu W\ cm^{-2}$ was found to be sufficient to decompose these substances in the presence of photocatalysts [Ohko et al., 1997].

2.4.1.3 Problems and limitations

Although the depollution effect of photocatalytic building and construction materials is evident, it is noticed that there are still unresolved problems when these materials are used in real-life applications. Immobilization of TiO_2 by the construction

materials can lead to significant loss of the photocatalytic activity. Rachel et al. (2002) pointed out that TiO_2-cement mixtures and red bricks containing TiO_2 were significantly less efficient than TiO_2 slurries in decomposing 3-nitrobenzenesulfonic. It is thought that the reduction of active surface and the presence of ionic species, which contributed to the charge recombination, are the reasons for the catalytic activity loss. Lackhoff et al. (2003) stated that the carbonation of the TiO_2 modified cements led to a noticeable loss in catalytic efficiency over several months because of the changes in cement surface structure. The report published by the Hong Kong Environmental Protection Department claimed that the photocatalytic activity of TiO_2 coated paving blocks decreased significantly after 4 months exposure in a downtown area due to the accumulation of contaminants on the block surface [Yu, 2003]. This means periodic servicing (washing or replacement) of the TiO_2 materials may be necessary to maintain the pollution reduction effect. It also should be noticed that the photocatalytic air purification function is usually restricted to pollutants which are adsorbed on the surface of the construction materials. In widely open spaces, the pollutant removal efficiency may be low as only a small fraction of the pollutants can be trapped. It is believed that the pollution elimination effect is more easily quantified using continuous monitoring data for confined spaces such as canyon streets where dispersion and ventilation is poor [Bygott et al., 2007].

Immobilization of TiO_2 compatible with organic substrates also triggers some challenges: (1) the limited thermal tolerance of organic surfaces precludes the sintering temperatures used on glass or metals to better anchor the TiO_2 layer; (2) the substrates themselves are prone to photocatalytic degradation [Agrios and Pichat, 2005]. As far as indoor application is concerned, controversy surrounds the question

of whether it is safe to apply the photocatalytic materials, especially on the possible health effects of byproducts formed in incomplete photo-oxidation [Auvinen and Wirtanen, 2008]. In addition, the potential impacts of nano-materials on human health should also be assessed. The particle size of nanoscopic photocatalysts is so small that it is possible it could enter into the human body triggering adverse health effects during the production, transportation, storage, and use [Wang et al., 2008].

2.4.2 Self-cleaning building materials

2.4.2.1 Principle

Super-hydrophilicity is a phenomenon that occurs when a TiO_2 film is subject to UV irradiation a very small water contact angle appears. On this surface, water tends to spread out flat instead of beading up. It has been shown that the reciprocal of the contact angle corresponds to the density of the surface hydroxyl groups reconstructed by UV irradiation [Sakai et al., 2003]. The binding energy between Ti atom and the lattice oxygen atom is weakened by the hole generated after UV irradiation. Therefore, the adsorbed water molecules can break a Ti-O-Ti band to form two new Ti-OH bands resulting in super-hydrophilicity (Fig. 2.9). In fact, TiO_2 film is not only hydrophilic but also amphiphilic after UV irradiation. The surface may adsorb both polar and nonpolar liquids. When water is rinsed over the surface, contaminations like oil can be washed away [Wang et al., 1997].

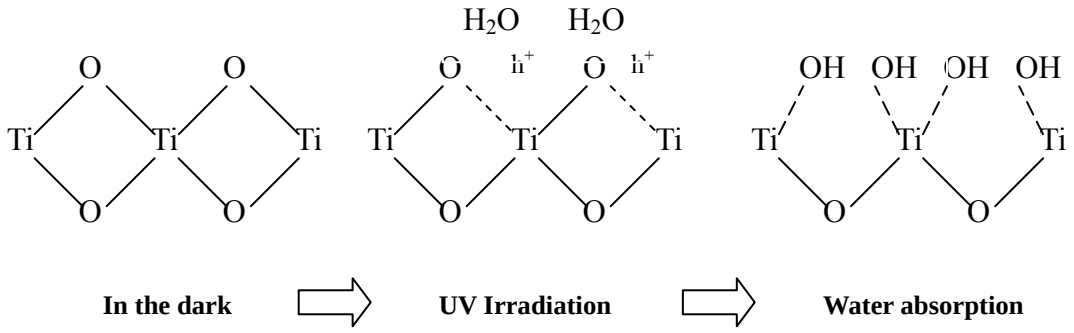

Figure 2.9 Photo-induced hydrophilic TiO_2 surface

The macro effect of self-cleaning is, in fact, a combined effect of super-hydrophilicity and degradation of organic deposits. Although the photo-induced super-hydrophilicity and degradation of organic contaminants are different processes, they may take effect simultaneously. It is difficult to distinguish which mechanism is more important for self-cleaning. Also worth noting is the interesting fact that, to some extent, there might be synergetic effect of photocatalysis and super-hydrophilicity promoting self-cleaning. Hydroxyl radicals play an important role in the decomposition of organic compounds. If more hydroxyl groups can occur on the surface of TiO_2 due to super-hydrophilicity, the efficiency of degradation of organics may also be improved [Schwarz et al., 1997]. On the other hand, the adsorption of organic compounds on the film surface may lead to a conversion of hydrophilic surface to hydrophobic surface. The photocatalytic decomposition of these organic contaminants can restore the super-hydrophilic property [Guan, 2005]. Thus the synergetic effect of photocatalysis and super-hydrophilicity ensure the self-cleaning character of TiO_2 film can be maintained continuously.

2.4.2.2 Research development and practical applications

It is a common phenomenon that the aesthetic and luster of the surface of ordinary buildings are gradually lost with time. Visible stains on building surface are constituted by composite materials mainly originated from the atmospheric aerosol pollutants. Small particles and greasy deposits are adhered to building surface by organic binders such as hydrocarbons and fatty acids [Peruchon et al., 2008]. Taking fatty acid molecules for example, their carboxylic groups (-COOH) enable them to stick on building surface via chemical binding with calcium ions present in concrete; on the other hand, their long chains link with other hydrophobic molecules perpendicularly to the surface, resulting in fatty stains which trap many atmospheric particles and dusts. As a result, dirt built up on the surface reduces the visual appearance. Without constant and proper maintenance, it is difficult to restore the buildings' aesthetic properties. The applications of self-cleaning building materials provide an excellent solution to this problem. The adsorbed organic soilage can be decomposed to water and CO_2, while other residues and dust can be washed away by rainwater. This application can save much time and money spent on cleaning maintenance, particularly for tall buildings where such maintenance may be very difficult and costly.

Several research studies have confirmed the effectiveness of this method. Cassar (2004) mixed a suitable amount of TiO_2 into white cement pastes to endow the structure with photocatalytic function. In order to verify the self-cleaning property, white cement disks were impregnated with a phenanthroquinone solution (0.1 mg cm^{-3}) showing homogeneous yellow surfaces. After UV irradiation, a rapid restoration of the clean surface was possible for the treated specimens. Similar

experiments were carried out under the framework of a European Project PICADA. Two cementitious products, a 10 mm thick rendering (mixture of cement, lime and sand) and a 1 mm thick mineral paint (mixture of cement and fillers), both containing nano-sized TiO_2, were developed. The self-cleaning effect of these samples was determined by monitoring the rate of photocatalytic decomposition of an organic dye rhodamine B by colorimetric measurements. The experimental results showed that the samples recovered about 65% of their initial coloration in less than a day of exposure to artificial sunlight [Vallee et al., 2004]. In addition, the validity of self-cleaning cementitious products was demonstrated by colorimetric monitoring of buildings constructed using this kind of materials. A church "Dives in Misericordia" in Rome and a music and art city hall in Chambery (France) were both built with photocatalytic concrete and had been monitored since the beginning of their service life. For the church in Rome, after 6 years monitoring, only a slight different between the external and internal values of the lightness was observed. It was also found that the color variations of the panels caused by inorganic substance could be completely eliminated by washing with water. Regarding the city hall in Chambery, the primary color almost remained constant for approximately 5 years in different positions of the facade (West/North/East/South) [Guerrini et al., 2007b].

Besides self-cleaning cementitious materials, TiO_2-based self-cleaning exterior building products including tiles and glass have been widely commercialized and applied. About 270 patents have been registered in the photocatalytic technology domain by TOTO Ltd. Their representative products are white ceramic tiles for exterior walls and home environments. They are fabricated by spraying a liquid suspension containing TiO_2 powder or gel on the surface and then heated to 600-800℃.

Through the heat treatment, the TiO_2 is sintered and strongly attached to the tile surface forming a micrometer thick layer [Shimohigoshi and Saeki, 2007]. The self-cleaning and stain free performance is confirmed by hung up samples outdoor for six months [Wang et al., 1998b]. For interior tiles used in washrooms or bathrooms, soilage and dirt are always a problem. The fatty acids from soap can form chemical bonds with calcium and magnesium in hard water and adhere to the tile surface, which are difficult to clean after the accumulation of dirt. The tiles with TiO_2 film surface can break the binding between the organic compounds and the ceramic tiles, which make the washing process easier.

Another important commercial product among the photocatalytic building materials is TiO_2 based self-cleaning glass. Its successful application is not only due to the self-cleaning function but also strengthened by the light-induced anti-fogging property. Fogging of the surfaces of mirrors or glass happens when steam is cooled down on the surface to form fine water droplets. As droplets fall or form on a hydrophilic surface, they rapidly coalesce to form a water sheet. The visible view behind the glass can still be observed without blockage or distortion. Moreover, the super-hydrophilic layer makes the glass dry without leaving the traditional droplet marks [Sanderson et al., 2001]. The challenge faced, when coating TiO_2 thin film on glass, is that the film should be highly active and stable, while at the same time the optical clarity and appearance cannot be deteriorated [Wang et al., 1998b]. The physical properties and photocatalytic activity of the TiO_2 film significantly depend on factors such as calcination temperature, flowrate of the carrier gas and partial pressure of starting materials during the fabrication process [Kaneko and Okura, 2002].

2.4.2.3 Problems and limitations

Durability of the performance is one of the most important factors for photocatalytic self-cleaning building materials. For tiles and glass, because of the high temperature treatment, the photocatalyst layer is usually stable and permanent. However, organic building materials, such as PVC (polyvinylchloride), can not tolerate the high sintering temperature to anchor the photocatalyst layer. Another problem is that organic building materials themselves tend be decomposed by photocatalytic reactions, resulting in not only reduced photocatalytic activity but also structure and strength destruction. Therefore, an intermediate layer must be placed between organic materials and photocatalysts. This dramatically increases the difficulty and manufacturing cost. In current market, it is claimed that various commercial TiO_2 containing paints can be coated on the building surface directly to impart self-cleaning capability. These products may demonstrate the self-cleaning effects in a short period of time, but the durability is quite poor. A 5.5 years outdoor exposure test of photocatalytic coating materials showed that most paints made of organics lost photocatalytic capability. Significant degree of chalking has been observed probably due to the decomposition of organic binders [Motohashi and Inukai, 2007]. In the case of concrete surfaces, the use of organic admixture for concrete and other cementitious materials must be minimized to avoid possible reduction of the photocatalytic activity. The self-cleaning effect may also be limited due to the physical anchoring of the dirt in large pores of concrete.

2.4.3 Self-disinfecting building materials

2.4.3.1 Principle

A number of researches have shown that typical bacteria such as *Escherichia coli* can be effectively killed by TiO_2 under UV irradiation [Bekbolet, 1997; Dadjour et al., 2005]. However, the biological inactivation mechanism of illuminated TiO_2 is still a debatable subject. Two major explanations have been proposed so far. One explanation attributes the death of microorganism to the attack of chemical species. Hydroxyl radical is assumed to be the lethal chemical species because it is a key factor in the decomposition of pollutants. In the early studies, the decrease of intracellular coenzyme A (CoA) in TiO_2-treated cells was detected for various microorganisms. The direct oxidation of CoA that inhibited cell respiration and subsequently caused cell death was proposed as the killing mechanisms [Matsunaga et al., 1985]. A ^{14}C radioisotope labeling experiment has demonstrated that the carbon content of *E. coli* could be oxidized to form CO_2 with substantial closure of the mass balance, which proved that the organic matter in the whole cells can be completely oxidized [Jacoby et al., 1998]. In support of this explanation, it has been reported that the reaction of Fe^{2+} with H_2O_2 photo-generated by the TiO_2/UV system constituted a supplementary source of hydroxyl radicals resulting in the increase of bacterial inactivation rate [Rincon and Pulgarin, 2007]. However investigations conducted by other researchers concluded that biological structure destruction account for the inactivation of microorganisms. Saito et al. (1992) found that TiO_2 photocatalytic reaction could cause a significant disorder in cell permeability inducing a fast leakage of potassium ions and a slow leakage of RNA and proteins. Sunada et al. (2003) investigated the bactericidal activity of copper-deposited TiO_2

thin film under very weak ultraviolet light illumination. The effective bactericidal activity was explained by a two-step process. The first step is the partial decomposition of the outer membrane in the cell envelope by a photocatalytic reaction, followed by the permeation of copper ions into the cytoplasmic membrane. The second step is a disorder of the cytoplasmic membrane caused by the copper ions, which results in a loss of the cell's integrity. A second killing mode was therefore proposed by Huang et al. (2000) who suggested that when microorganisms undergo TiO_2 photocatalysis, the cell wall will be damaged followed by cytoplasmic membrane damage, leading to a direct intracellular attack. Subsequently, essential functions that rely on intact cell membrane architecture, such as respiratory activity, are lost, and cell death is inevitable.

2.4.3.2 Research development and practical applications

With the increasing concern for human health and quality of life, the use of TiO_2 for disinfection becomes more and more important. In the ceramic and building industry, there is a special interest for the photo-induced bactericidal effect of TiO_2. This is particularly true when the ceramic is going to be placed in microbiologically sensitive environments, such as medical facilities and food industries where biological contamination must be prevented [Amézaga-Marid et al., 2002]. Applying self-disinfecting TiO_2 building materials to indoor furnishing have been proved to be an effective way to decrease bacteria counts to negligible levels. It was reported that in an operating room in a hospital the number of bacteria on the wall surface was reduced to zero and the bacteria in the air was also decreased significantly after installing photocatalytic tiles. The longer term effect was much better than the spraying of disinfectants [Fujishima et al., 1999]. Several companies, such as TOTO,

Karpery and Biocera, have commercialized the concept of a deposited thin film semiconductor photocatalyst on ceramics as an antimicrobial agent. Their semiconductor photocatalyst thin film ceramic products exhibit both UV light induced antimicrobial agent and deodorizing properties [Mills and Lee, 2002].

The light-induced bactericidal activity of TiO_2 can also be used to control the biological growth on concrete surfaces. Unsightly stains due to the growth of biofilm may cause the loss of aesthetic beauty particularly at places where design features or maintenance faults result in frequent wetting of the building surface [Dubosc et al., 2001]. This also could trigger chemical changes of concrete surfaces and decrease the durability [Kurth et al., 2007]. The photosynthetic algae can only grow where sunlight is available, so that photocatalytic technology is an ideal control method. Linkous et al. (2000) employed TiO_2 and WO_3 as surfacing agents to inhibit the attachment and growth of Oedogonium, a filamentous algae. It was demonstrated that coating cement substrates with a dispersion of 10% TiO_2 powder could achieve a 66% reduction in the growth of algae in comparison to the unprotected cement surface. Adding a 1.0% loading of a noble metal such as Pt or Ir to the photocatalyst enabled an 87% reduction.

2.4.3.3 Problems and limitations

Compared with the other two major applications, less research work has been conducted in the self-disinfecting building material area. So far, standardized protocols for evaluating the light-induced anti-bacterial activity have not been established. The stated efficiency of different self-disinfecting products cannot be verified and compared. Moreover, effective and reliable coating techniques are

needed to anchor the nano-photocatalysts to interior building surface in the event that the dispersion of fallen nano-particles could cause potential health threats. A cost benefits analysis is also needed to further evaluate the applicability of self-disinfecting building materials.

Chapter 3 Methodology

3.1 Introduction

In this chapter, the materials used in this research, preparation methods for photocatalytic cement-based materials, experimental set-up and testing protocols of photocatalytic NO_x degradation tests are presented. Experimental details for the determination of properties of photocatalytic cement-based materials are also described. The final part of this chapter explains two monitoring methods adopted for the evaluation of NO_x removal efficiency by photocatalytic paving blocks in field trials.

3.2 Materials

3.2.1 Photocatalysts

Three kinds of TiO_2 sourced from different suppliers were used in this research. The TiO_2 (98.5% anatase) used in surface layer fabrication was purchased from Ke Xiang Chemical Co., Ltd. (China). The TiO_2 used in paste and mortar fabrication were P25 (75% anatase & 25% rutile, Degussa, Germany) and Anatase (99% anatase, Sigma-Aldrich, USA). The primary particle size of P25 and Anatase were 21 nm and 350 nm respectively. The N_2-BET surface areas of Anatase (China), Anatase (USA) and P25 were 8.8 $m^2 g^{-1}$, 7.5 $m^2 g^{-1}$ and 58.8 $m^2 g^{-1}$ respectively, measured using a Micrometritics ASAP2010 system.

3.2.2 Cement-based materials

3.2.2.1 Cement

ASTM Type I Ordinary Portland cement (OPC, Green Island Cement Limited, Hong Kong) and white cement (WC, TAIHEIYO Cement Corp., Japan) were used in this study. The physical properties and chemical compositions of the cement are presented in Table 3.1 and Table 3.2.

Table 3.1 Physical properties of cement according to manufacturers' specifications

Properties	Ordinary Portland Cement	White Cement
specific surface / $cm^2\ g^{-1}$	3520	3660
Density / $kg\ m^{-3}$	3160	3088

Table 3.2 Chemical properties of cement determined by X-ray fluorescence analysis

Components	Ordinary Portland Cement (Mass %)	White Cement (Mass %)
SiO_2	22.18	21.36
Al_2O_3	5.95	5.27
Fe_2O_3	3.37	0.2
CaO	62.46	67.49
MgO	1.56	1.14
K_2O	0.48	0.077
Na_2O	0.24	0.048
TiO_2	0.37	0.14

SO_3	2.25	2.6
P_2O_5	0.1	0.03
Loss on ignition	0.64	1.58

3.2.2.2 Fine aggregate

Fine natural river sand (mainly quartz sand) sourced from the Pearl River was used in the reference samples. The saturated surface dry density of the sand was 2650 $kg\,m^{-3}$. The waste beverage glass bottles were provided by a local eco-construction material company (Laputa Co., Ltd.). All the bottles were made of soda-lime glass which consists of approximately 71-75% SiO_2, 12-16% Na_2O and 10-15% CaO. These bottles were washed, sorted by type and color and then crushed by a mechanical crusher in the laboratory. The crushed glass cullets were further sieved to different particle sizes. The characteristics of the five types of recycled glass cullets used in the experiment are shown in Table 3.3.

Table 3.3 Characteristics of recycled glass cullets

Properties	Milk bottle I (MI)	Milk bottle II (MII)	Soft drink bottle (SD)	Wine bottle (W)	Beer bottle (B)
Color	Clear	Clear	Light green	Dark green	Brown
Particle size / mm	d<1.16 1.16<d<2.36	d<1.16 1.16<d<2.36	d<1.16 1.16<d<2.36	d<2.36	d<2.36

3.3 Sample Preparation

3.3.1 Fabrication of surface layers

Concrete surface layers with different mixing design were made in the laboratory. The mixing proportions are shown in Table 3.4. Five types of recycled glass cullets with different particle sizes were used in the experiment. The details are provided in Table 3.5. The surface layers were fabricated in steel moulds with an internal dimension of 200 × 100 × 5 mm (Fig. 3.1). For each concrete surface layer, 250 g well mixed materials (cement, sand, glass, TiO_2 powder and water) were weighted. The steel moulds were over filled with the mixed materials and hand compacted, and further compressed twice using a compression machine at a rate of 500 kN min^{-1}, firstly to 500 kN and secondly to 600 kN. For every type of the surface layer, four identical samples were made for subsequent tests. After one day, the surface layers were removed from their moulds and were cured in a chamber with controlled humidity of 95% and temperature of 25 °C until testing.

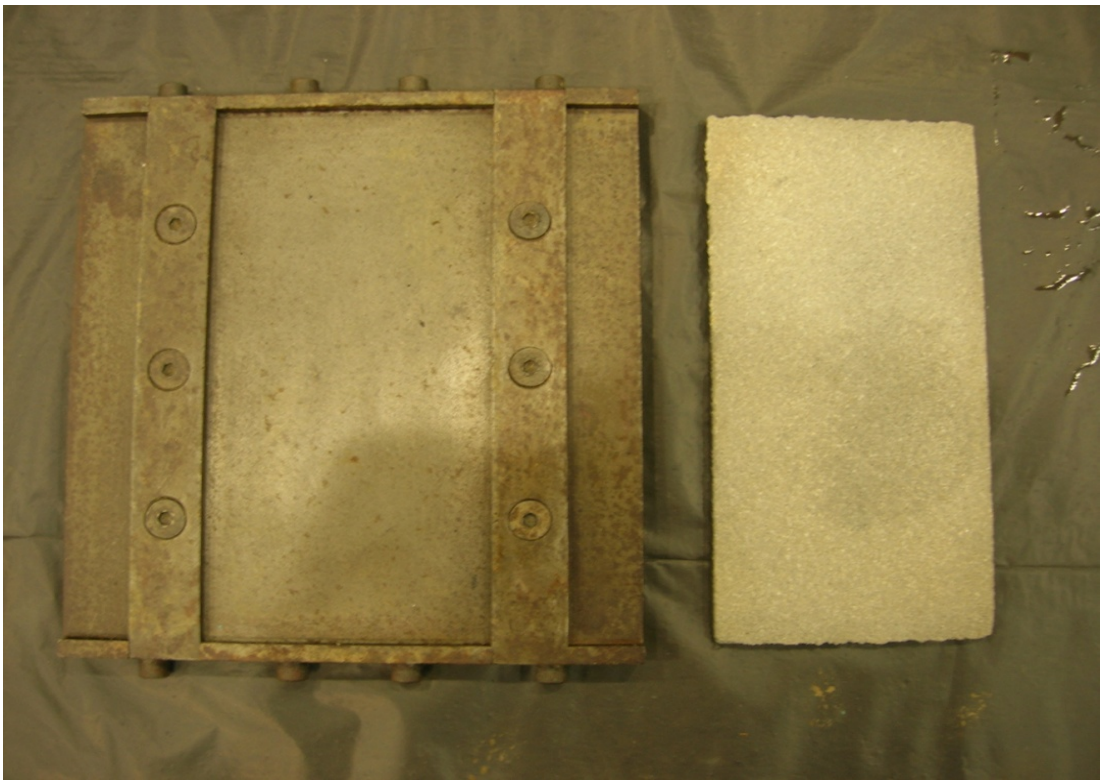

Figure 3.1 Steel mould and surface layer sample

Table 3.4 Mixing proportions of concrete surface layers

Mix proportion	Sand / kg	Glass / kg	OPC / kg	TiO_2 / kg	Water / kg
Pure sand	1.5	N/A	0.5	0.04	0.14
50% glass	0.75	0.75	0.5	0.04	0.14
100% glass	N/A	1.5	0.5	0.04	0.14

Table 3.5 Classification of concrete surface layers by mix proportion, glass color and particle size

Types of glass	MI	MII	SD	W	B
Color / Particle size	Clear	Clear	Light green	Dark green	Brown
d<1.16	50% glass, 50% sand	50% glass, 50% sand	50% glass, 50% sand	N/A	N/A
d<1.16	100% glass	100% glass	100% glass	N/A	N/A
1.16<d<2.36	50% glass, 50% sand	50% glass, 50% sand	50% glass, 50% sand	N/A	N/A
1.16<d<2.36	100% glass	100% glass	100% glass	N/A	N/A
d<2.36	N/A	N/A	N/A	100% glass	100% glass

3.3.2 Fabrication of cement paste cubes

Cubic cement paste samples were made in the laboratory using the two types of cement (OPC and WC) blended with P25 and Anatase respectively. Reference samples without TiO_2 addition were also made for comparison. The water to cement ratio was 0.35 and the amount of additional mixing of nano-TiO_2 was 5% and 10% of the total weight of cement. A smooth and well blended paste was produced using a mechanical mixer, and then was cast into laboratory made moulds (dimensions 40 x 40 x 40 mm). The moulds were vibrated by a vibrating table to ensure thorough compaction. After that, the paste samples were cured in an environmental chamber at 25 ºC and 95% RH for 24 h. After one day, the hardened pastes were removed from

their moulds and placed back into the same chamber at the same conditions until the time of testing. The paste samples were prepared for the photocatalytic NO_x conversion, porosity, XRD, TG, SEM-EDX tests. Details of those tests were given in Section 3.4 and Section 3.5.2.

3.3.3 Fabrication of cement mortar cubes

For the study of compressive strength, mortar cubes (dimensions 50 x 50 x 50 mm) were prepared in accordance with ASTM C109. The cement to sand ratio was 1: 2.75, and water to cement ratio was 0.485. Water content for samples containing TiO_2 was adjusted to obtain a flow of 110 ± 5 in 25 drops of the flow table. Detailed mixing proportions are shown in Table 3.6. All test samples were kept in the molds on the base plates in the moist room (at a temperature of 23.0 ± 2.0 °C and a relative humidity of not less than 95%) immediately after molding until they are 24 h old. Then the samples were immersed in saturated lime water in storage tanks (at a temperature of 23 ± 2 °C) until time of testing.

Table 3.6 Mixing proportions

	OPC / g	Sand / g	Water / mL	TiO_2 / g
Control	1000	2750	485	0
5% P25	1000	2750	527	50
10% P25	1000	2750	560	100
5% Anatase	1000	2750	489	50
10% Anatase	1000	2750	493	100

3.4 Photocatalytic Conversion of NO_x

3.4.1 Experimental set-up

The instruments were configured according to the specifications of JIS R 1701-1 with slight modifications. Fig. 3.2 shows a schematic diagram of the equipment configuration. A zero air generator (Thermo Environmental Inc. Model 111, Fig. 3.3) was used to supply the calibration gas. The testing gas was a mixture of zero air and standard NO (Arkonic Gases, Hong Kong). The humidity in the reactor was controlled by passing the zero air stream through a humidification chamber. A thermometer, a humidity sensor and an adjustable rack supporting specimens were placed inside the reactor. The UV lamps were positioned outside the reactor and the distance between the lamps and the reactor could be adjusted to achieve a required intensity. The UV intensity was measured by a digital radiometer equipped with a DIX-365A UV-A sensor (Spectroline DRC-100X, spectronics corporation, USA). The NO_x concentration was continuously measured using a chemiluminescence NO_x analyzer (Thermo Environmental Instruments Inc. Model 42c, USA, Fig. 3.4). The reactor was completely sealed with no detectable leakage.

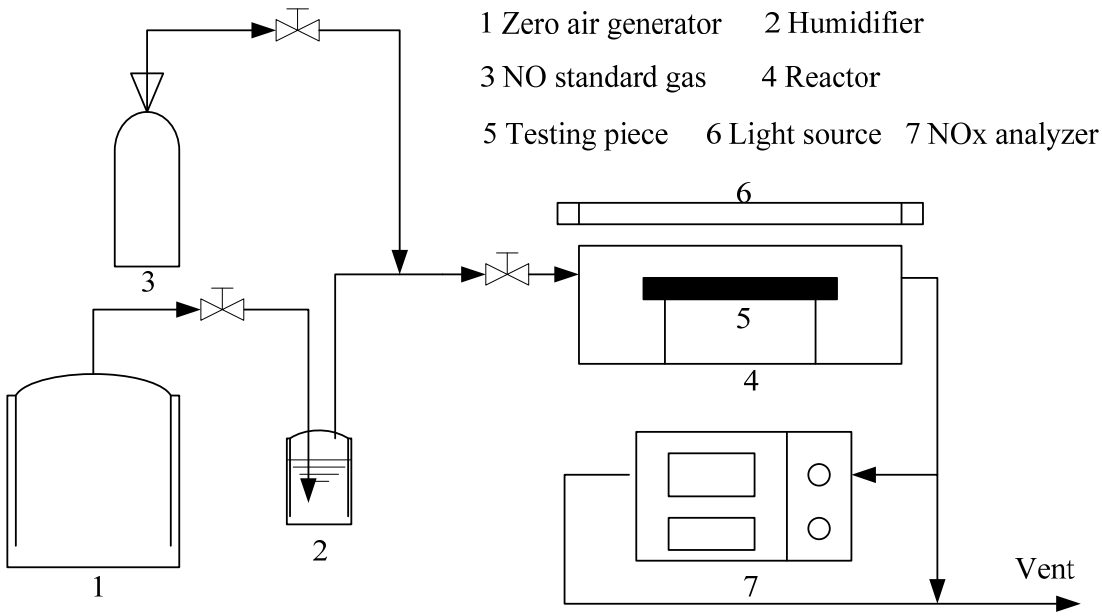

Figure 3.2 Schematic diagram of the experimental set-up

Figure 3.3 Zero air generator

Figure 3.4 Chemiluminescence NO_x analyzer

3.4.1.1 Original reactor design

The dimension of the origin reactor made with stainless steel was 700 mm in length, 400 mm in width and 130 mm in height (Fig. 3.5). Three 8W UV-A fluorescent lamps (TL 8W/08 BLB, Philips, Holland) were used to provide UV radiation. The wavelength of the lamps ranged from 300 to 400 nm with a maximum intensity at 365 nm. The UV intensity was maintained at 10 W m^{-2} at the center of the reactor. No air leakage and nitric oxide photolysis were found during several blank tests. This reactor was used in the test of photocatalytic conversion of NO_x by the concrete surface layer.

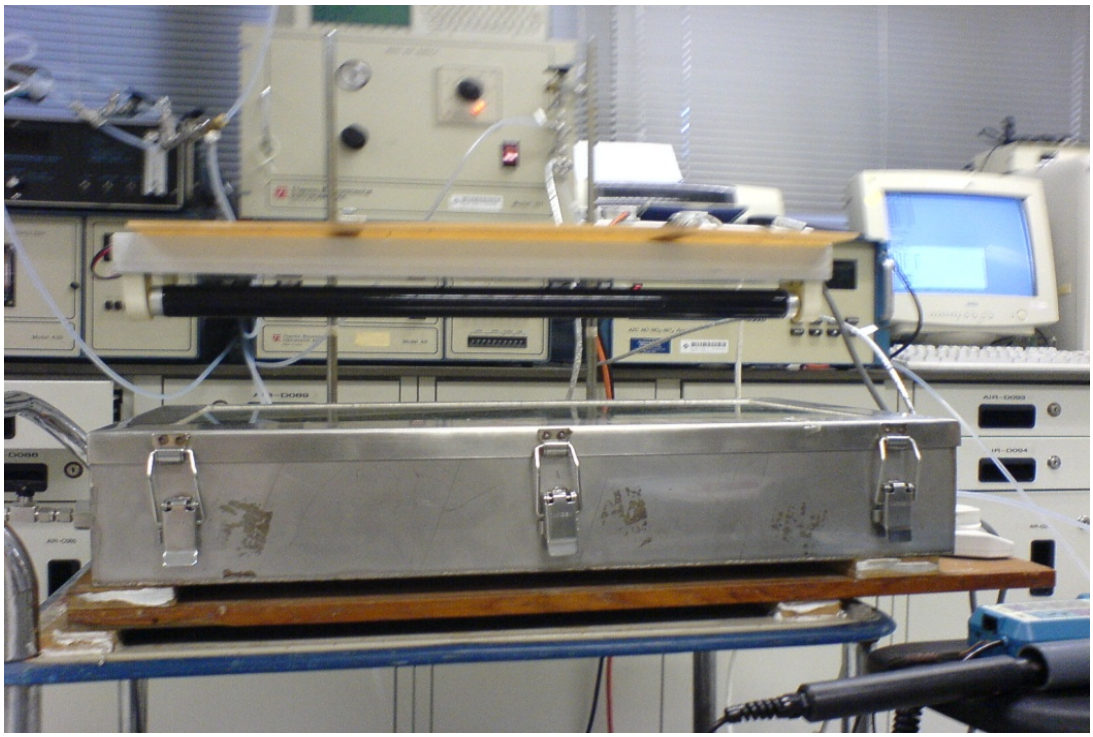

Figure 3.5 Original reactor

3.4.1.2 Revised reactor design

The main reason for the revised design of reactor was the equilibrium time of NO_x in the original reactor is too long (about one hour). Therefore, a new reactor with revised dimensions (300 mm long, 150 mm wide and 100 mm high) was fabricated (Fig. 3.6). The irradiation system was also updated. A halogen photo optic lamp (QUADX 3000, BOEWNS, UK), which has a similar spectrum to sunlight, was used as a sunlight simulator to provide irradiation. The calibrated relative irradiance spectrum of the lamp measured by a wideband Spectroradiometer (ILT900-R International light technologies, USA) is shown in Fig. 3.7. The UV intensity in the center of the reactor was 0.6 ± 0.1 W m^{-2}. The intensity of the entire spectrum illuminance was 40000 ± 1000 Lux measured by a heavy duty light meter (407026, Extech Instruments, USA). Air leakage and nitric oxide photolysis were also not

observed in several blank tests. This reactor was used in the test of photocatalytic conversion of NO_x by the cement paste cubes.

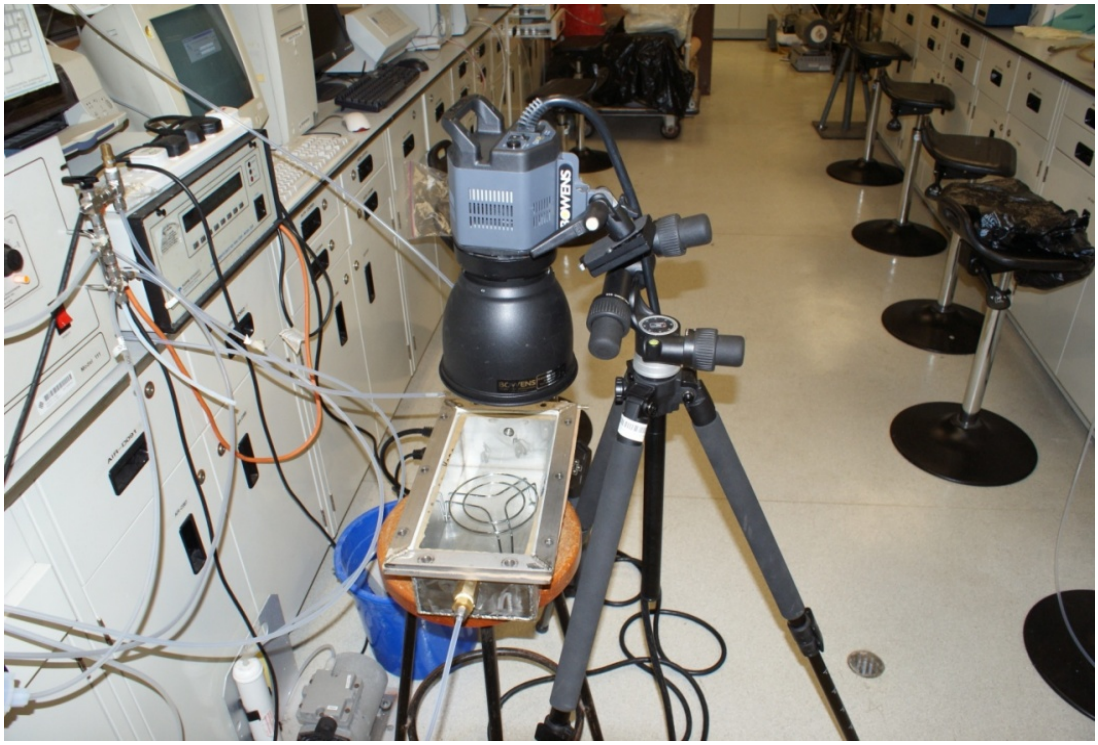

Figure 3.6 Revised reactor

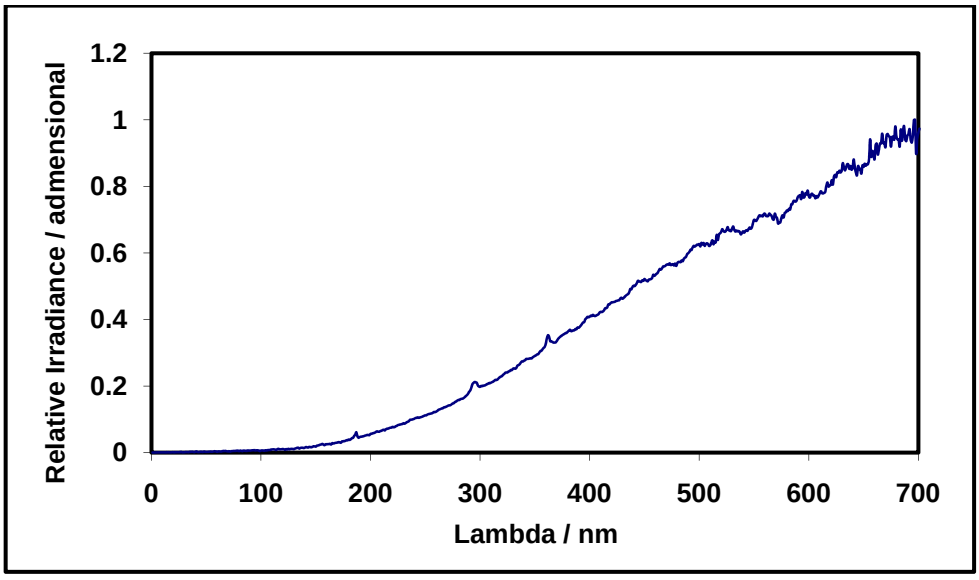

Figure 3.7 Calibrated relative irradiance spectrum of the lamp

3.4.2 Testing protocol

For every test, the concrete surface layers or the cement paste cubes (four side faces were covered with aluminum foil so that only the top surface was exposed to the external irradiation) were put at the centre of the reactor. 1000 ppb NO gas was allowed to continuously flow through the reactor at a flowrate of 3 L min^{-1} in a laminar plug flow pattern. When the NO concentration in the reactor reached equilibrium, the lamp was turned on and the photocatalytic NO conversion process began. The experiment was carried out at room temperature (25 ± 2 ^{o}C) and the relative humidity was controlled at 50 ± 5%. Each test lasted for 1 h and the changes of NO and NO_2 concentrations at the outlet were continuously measured. The calculation of the amount of NO_x removal is shown below:

$$Q_{NOx} = \frac{\left(\frac{f}{22.4}\right)\{\int([NO]_0 - [NO])dt - \int([NO_2] - [NO_2]_0)dt\}}{A \times T}$$

Where, Q_{NOx} : the amount of nitrc oxides removed by the test sample, μmol m^{-2} h^{-1};

$[NO]_0$: inlet concentration of nitrogen monoxide, ppm;

$[NO]$: outlet concentration of nitrogen monoxide, ppm;

$[NO_2]_0$: inlet concentration of nitrogen dioxide, ppm;

$[NO_2]$: outlet concentration of nitrogen dioxide, ppm;

t : time of removal operation, min;

f : flow rate converted into that at the standard state (0 ^{o}C, 1.013 kPa), L min^{-1};

A: surface area of cement paste samples, m^2;

T: duration of the photocatalytic process, 1 h for all experiments;

22.4: the volume of 1 mole ideal gas at the standard state is 22.4 L (ideal gas law).

3.5 Determination of Properties of Photocatalytic Cement-based Materials

3.5.1 Surface layers

3.5.1.1 Porosity test

The porosity of the concrete surface layer was determined using the Vacuum Saturation Apparatus developed by Cabrera and Lynsdale (1988). The samples were dried at 100 ± 5 °C until constant weight had been achieved and were then placed in a desiccator under vacuum for 4 h. After that the desiccator was filled with distilled water. The porosity was calculated using the following formula:

$$P = \frac{W_{\text{sat}} - W_{\text{dry}}}{W_{\text{sat}} - W_{\text{wet}}}$$

where, P :vacuum saturation porosity, %;

W_{sat} : weight in air of saturated sample;

W_{wet} : weight in water of saturated sample;

W_{dry} : weight of oven-dried sample.

3.5.1.2 Simulation of UV absorption by glass cullets

To clarify how much UV radiation would be absorbed by glass cullets, a simulation study was carried out using original glass cullets, TiO_2 coated glass cullets and sand. Both the influence of glass color and aggregate particle size were investigated. In the experiment, different glass cullets and sand were first washed by hydrochloric acid (1 mol L^{-1}). Then the acid residue was rinsed out by distilled water. Subsequently ethanol (10%) was passed through the cullets to remove organic contaminates. Finally the glass cullets were dried at 60 ^{o}C in an oven for 24 h.

The TiO_2 coating materials were prepared using the method reported by Stathatos et al. (1997). Triton X-100 (Sigma-Aldrich) and distilled water were added to cyclohexane (99.9%, TEDIA) to prepare a solution with Triton X-100 concentration of 0.2 M and the molar ratio of water to the Triton X-100 was 1.5. After stirring for 2 h, the solution was mixed with titanium isopropoxide (97%, Sigma-Aldrich). The alkoxide solution was being continuously stirred at room temperature for hydrolysis and condensation of the titanium alkoxide for 1 h. 50 ml prepared titanium alkoxide solution was added to the samples of weighed glass cullet (10 g) in separate beakers. The mixture of TiO_2 gel and glass cullets were calcined at a heating rate of 3 $^oC\ min^{-1}$ up to 500 ^oC in a normal atmospheric environment and were kept at 500 ^oC for about 1 h. After calcination, the coated glass was washed by distilled water to remove the excess TiO_2 powder residues.

For the UV absorption experiment, 5 g TiO_2 coated glass cullets and sand were placed evenly in 10 mm thick glass vessels separately. To allow a better comparison, a granulated sugar solution (80% wt/vol, refraction index 1.49) which had almost the same refraction index as soda-lime glass (refraction index 1.52) was injected into the vessel to reduce the reflection caused by air. The UV adsorption of the sugar solution was measured separately as a reference. The UV absorption characteristics of different glass cullets were determined by scanning the filled vessels using a VIS-UV spectrophotometer (Spectronic Genesys2, USA) within the UV-A range (320 to 400 nm). The schematic diagram of the simulation study is shown in Fig. 3.8.

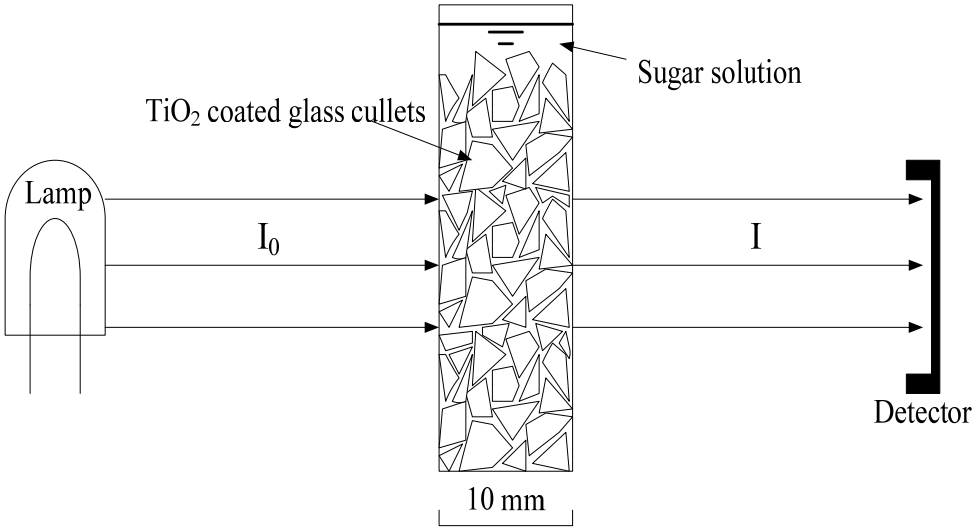

Figure 3.8 Schematic illustration of the simulation study

The absorbance, A, was calculated using following formula.

$$A = -\log_{10}(I/I_0)$$

Where A is the measured absorbance, I_0 is the intensity of the incident light at a given wavelength, I is the transmitted intensity.

3.5.2 Pastes and mortars

3.5.2.1 Chemical composition analysis

X-Ray diffraction (XRD) and thermal gravimetric (TG) techniques were used to evaluate the chemical stability of TiO_2 and the degree of hydration in the hardened cement pastes. Samples for these analyses were obtained by crushing the hydrated cement pastes using a compression machine on the 3rd, 7th and 28th day of curing. In order to eliminate any further hydration the crushed pieces were soaked in acetone

for a minimum of 7 days. The specimens were oven dried at a temperature of 60 ºC for 24 h before analysis.

The components of the photocatalytic cement pastes and their amount at different curing age were determined by an internal standard method of XRD measurement. A piece of crushed sample was ground by a rotating ball mill for 20 min. 1.000 g weighted ground powder was mixed with 0.111 g of ZnO (AR grade) and then the mixture was passed through a 125 μm sieve three times to ensure the two materials were thoroughly mixed. The X-ray diffraction data was collected by an X-ray diffractometer (Bruker D8 Discover, Philip, Holland) under ambient conditions. The samples were X-rayed from 5 to 65 degrees two-theta using monochromatic Cu K–alpha radiation, with a step size of 0.02 degrees two theta, and a count time of 2 seconds per step. The semi-quantitative X-ray diffraction analysis was conducted using the equation proposed by Copeland and Bragg (1958). The ratio of the integrated intensities (I_0 and I_1) of the X-ray diffraction lines of two components in a mixture is proportional to the ratio of the weight fractions (w_0 and w_1) of those components,

$$\frac{I_1}{I_0} = k\frac{w_1}{w_0}$$

where k is a proportionality constant.

The non-evaporable water, defined as the mass loss due to decomposition between the boiling temperature and 900 °C, can be used as a relative measurement of the degree of hydration of the Portland cement [Escalante-Garcia, 2003]. The content of

the chemically bound water and portlandite (CH) in the hardened cement pastes was evaluated by TG analysis. 10 mg samples were heated at a rate of 10 °C min^{-1} up to 1000 °C under an Argon atmosphere using a TG/DSC analyzer (STA 449C Jupiter, NETZSCH, Germany). The content of non-evaporable water was calculated from the ignited weight loss between 120 ^{o}C and 900 ^{o}C. A correction was made by subtracting the mass loss due to decarbonation within a temperature range of 575-650 °C from the value of the non-evaporable water. The amount of CH content was estimated from the weight loss between 350 ^{o}C and 500 ^{o}C due to the dehydration of portlandite (Betioli et al., 2009). The CH content was determined using the following equation:

$$CH(\%) = \Delta_{CH}(\%) \times M_{CH} / M_{h}$$

where CH(%) is the content of portlandite, $\Delta_{CH}(\%)$ is the weight loss during the dehydration of CH, M_{CH} is the molar weight of CH and M_{h} is the molar weight of water.

3.5.2.2 Microstructure analysis

Mercury intrusion porosimetric (MIP) measurements were conducted to study the change of the microstructure of the hydrated cement pastes at the specified curing ages. The pore size distribution and total volume of porosity of the samples at different curing ages were determined by MIP analysis. The MIP measurements were taken by a mercury intrusion porosimeter (Poresizer 9320, micromeritics, USA, Fig. 3.10) with a maximum intrusion pressure of 210 MPa. A contact angle θ of 140º and a cylindrical pore geometry were assumed. The mercury intruded pore diameter d_p at an intrusion pressure of P_{In} was calculated using following equation:

$$d_p = -4\gamma\cos\theta / P_{In}$$

where $\gamma = 0.483$ N m^{-1}, is the surface tension of mercury.

Figure 3.9 Poresizer 9320 mercury intrusion prosimeter

Energy Dispersive X-ray (EDX) element mapping analysis was conducted to get a profile of TiO_2 distribution in the cement paste. A thin slice of cement paste sample polished with fine (600/1200 grade) SiC paper was examined by an energy dispersive X-ray (EDX) spectrometer connected to a SEM (JSM-6335F, JEOL, Japan). The analytical time was 10 min for EDX scan.

3.5.2.3 Hydration heat test

The heat of hydration and its releasing rate were measured using a JAF isothermal conduction calorimeter. The calorimeter has a heat sink maintained at constant temperature and the heat generated by the chemical reaction from the cement hydration flows through a known thermal path. There is an interface module which allows the heat evolution to be recorded in the form of a calibration curve. The samples were prepared by mixing cement and TiO_2 in a polythene bag. Mix proportions for this study are given in Table 3.7. The measurement of the hydration heat was conducted over a 72 h period.

Table 3.7 Mix proportions for hydration heat experiment (P25 and Anatase were added separately)

Material	0% TiO_2 (Ref)	5% TiO_2	10% TiO_2
Cement / g	30	30	30
Water / mL	10.5	10.5	10.5
P25 / g	N /A	1.5	3.0
Anatase / g	N /A	1.5	3.0

3.5.2.4 Standard consistence and setting time test

The standard consistence and setting time of the cement pastes were determined using a Vicat apparatus (Fig. 3.10) according to the specification of BS EN 196-3. 500 g of cement, 25 g or 50 g TiO_2, and a quantity of water was mixed using a mechanical mixer. The time to the nearest minute of the start of the mixing was recorded as “zero time”. The total mixer running time was 3 min. The paste was

transferred immediately to the lightly oiled mould which was filled to excess without undue compaction or vibration. The excess was removed by a gentle sawing motion with a straight-edged implement in such a way as to leave the paste filling the mould and having a smooth upper surface. Immediately after leveling the paste, the mould and base-plate were transferred to the Vicat apparatus and were positioned centrally under the plunger. The plunger was lowered gently until it was in contact with the paste. Then the moving part was released quickly and the plunger penetrated vertically into the centre of the paste. The scale reading was recorded, which indicates the distance between the bottom face of the plunger and the base-plate. The test was reported with pastes containing different water contents until one was found to produce a distance between plunger and base-plate of 6 ± 2 mm. The water content of the paste was expressed as a percentage by mass of the cement, and was recorded to the nearest 0.5% as the water for standard consistence.

Figure 3.10 Vicat apparatus

The initial and final setting time was determined as follows:

A Vicat mould was filled with paste of standard consistence. The filled mould and base-plate were placed in the container. Water was added and the surface of the paste was submerged to a depth of at least 5 mm. The container was stored in a temperature controlled enclosure at 20.0 ± 1.0 °C. After a suitable time, the mould, base plate and container was positioned under the needle of the Vicat apparatus. The needle was lowered gently until it was in contact with the paste. The moving part was released quickly and the needle penetrated vertically into the paste. The scale readings together with the time from zero were recorded. The elapsed time, measured

from zero to the time at which the distance between the needle and the base-plate was 6 ± 3 mm, was reported as the initial setting time of the cement, to the nearest 5 min.

The filled mould used in initial setting time determination was inverted on its base-plate so that the tests for final set were made on the face of the specimen originally in contact with the base-plate. The mould and base-plate were immersed in the container and stored in the temperature controlled enclosure at 20.0 ± 1.0 °C. After a suitable time, the mould, base-plate and container were positioned under the needle of the Vicat apparatus. The needle was lowered gently until it was in contact with the paste. Then the moving part was released quickly and the needle penetrated vertically into the paste. The time at which the needle first penetrated only 0.5 mm into the specimen, together with the time from zero was recorded as final setting time.

3.5.2.5 Determination of Compressive strength

The compressive strength measurements of the cement mortars were conducted after 3, 7 and 28 days of curing in accordance with ASTM C109. Each specimen was wiped to a surface-dry condition, and removes any loose sand grains or incrustations were removed from the faces. The faces were checked by applying a straightedge. If there was appreciable curvature, the specimen was discarded. If the cross-sectional area of a specimen varied more than 1.5 % from the nominal, the actual area was used for the calculation of the compressive strength. A loading on the specimen with 1000 N s^{-1} was applied using a Denison compression machine (Fig. 3.11). The compressive strength was calculated using following equation:

$$f_m = P/A$$

Where, f_m = compressive strength, MPa;

P = total maximum load, N;

A = area of loaded surface, mm^2.

Figure 3.11 Denison compression machine

The compressive strength of all acceptable test specimens made from the same sample and tested at the same period was averaged and reported to the nearest 0.1 MPa. The maximum permissible range between specimens from the same mortar batch, at the same test age is 8.7% of the average when three cubes represent a test age.

3.6 Evaluation of NO_x Removal Efficiency by Site Monitoring

3.6.1 Original monitoring method

To investigate the NO_x removal performance of photocatalytic paving blocks in real environment, a large number of photocatalytic blocks manufactured by a local factory were paved on a road at the campus of The Hong Kong Polytechnic University. The road is located next to the Hong Kong Cross Harbor tunnel, where the level of air pollution is relatively high due to vehicle exhaust emissions (Fig. 3.12). 500 m^2 photocatalytic blocks and 500 m^2 normal blocks were paved on that road and the NO_x concentration was monitored (Fig. 3.13). The air quality monitoring was carried out by collecting air bag samples from designated sampling points from March 2007 to March 2008. For both the photocatalytic block zone and the normal block zone three fixed sampling points were chosen. At each sampling point, two air samples were collected monthly, one from the ground level (Fig. 3.14) and another from the breathing zone (about 1.5 m high from the ground, Fig. 3.15). At the same time, environmental parameters such as temperature, relative humidity and UV intensity were also measured. After sample collection, the air bags were taken back to the air laboratory where the concentration of NO_x was analyzed. The average concentration of NO_x of the three different sampling points was used for statistic analysis to eliminate the influence of sampling locations.

Figure 3.12 Location of the road

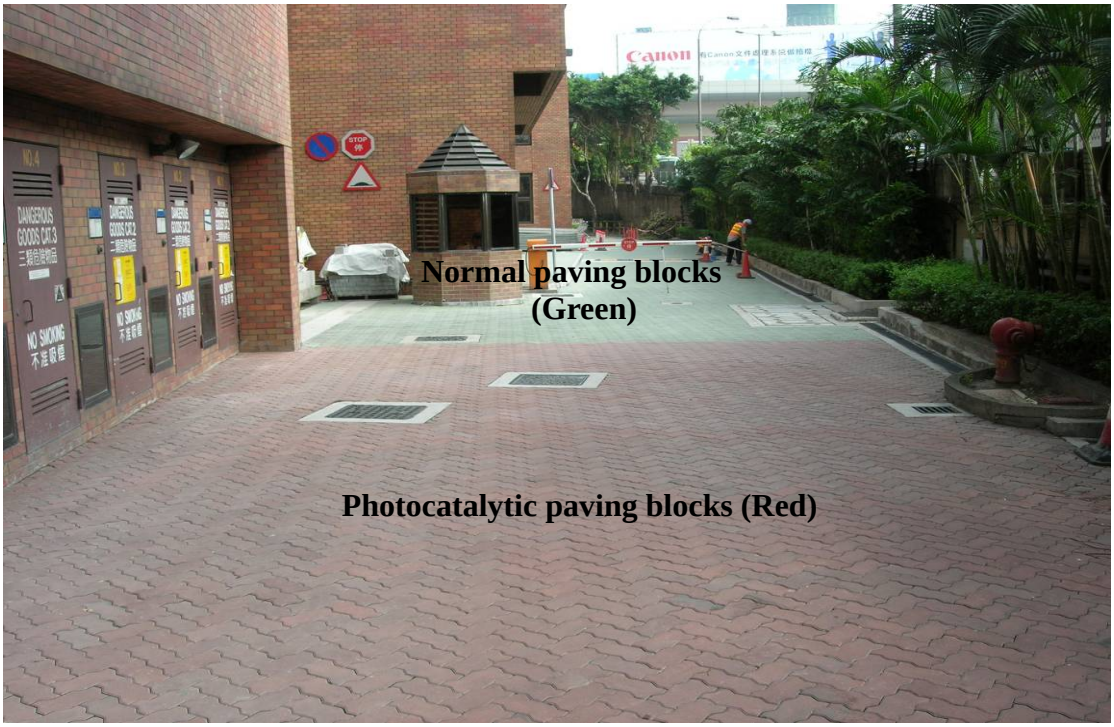

Figure 3.13 View of the paved road

Figure 3.14 Air sampling at ground level

Figure 3.15 Air sampling at breathing zone

3.6.2 Revised monitoring method

During the monitoring project mentioned in Section 3.6.1, it was found that the fluctuation of meteorological factors (e.g. wind direction) may influence the accuracy of NO_x sampling. Therefore, a new sampling plan was developed to monitor the NO_x removal performance of photocatalytic paving blocks from February 2009 to April 2009. As the NO_x removed from ambient air by the blocks should be oxidized to nitrite (NO_2^-) and nitrate (NO_3^-), and these ions eventually deposit in the matrix of the block surface. The amount of NO_2^- and NO_3^- deposited in a certain period of time can reflect the photocatalytic NO_x removal efficiency of the blocks. The details of this method are provided below.

As shown in Fig. 3.16, a plastic box covered by a transparent glass plate was used as the sampling box. A rectangular hole was cut on each face of the box to allow air flow through it. The glass cover is not only transparent to sun-light, but also can prevent the soluble ions to be washed out by rain. This field trial was conducted at three primary schools in different districts with different air pollution levels (Mong Kok, Kowloon City and Tseung Kwan O, Fig. 3.17). Sampling boxes each contained three paving blocks were put at each monitoring site. Two of the boxes contained photocatalytic paving blocks and the other one contained normal paving blocks. The photocatalytic blocks in one of the boxes were tested every month together with the normal blocks; the photocatalytic blocks in the other one were tested every three months. Passive air samplers (Ogawa Co. Inc., USA, Fig. 3.18) were placed near the sampling sites to record the background NO_x concentration, which was used to quantify the effect of the local air quality on photocatalytic pollutant removal.

Figure 3.16 Sampling box

Figure 3.17 Locations of sampling boxes: (a) Mong Kok; (b) Kowloon City; (c) Tseung Kwan O

Figure 3.18 Passive air quality sampler

Elution tests were conducted after the blocks were taken back to the laboratory. The surfaces of the paving blocks were immersed in 100 mL deionized water in a container for 1 h. Then the test piece was taken out and the volume of the water remained in the container was recorded (Washing 1). The washing process was repeated again using fresh deionized water, and hereafter was referenced as Washing 2. The concentrations of nitrate and nitrite ions in the elution were measured by ion chromatography (IC). The equipment and procedures of the IC test are described in Appendix A. The amount of nitrogen eluted is calculated by the following formula:

$$n = n_{w1} + n_{w2} = V_{w1}\left(\frac{\rho_{NO_3^-,w1}}{62} + \frac{\rho_{NO_2^-,w1}}{46}\right) + V_{w2}\left(\frac{\rho_{NO_3^-,w2}}{62} + \frac{\rho_{NO_2^-,w2}}{46}\right)$$

Where, n is the amount of nitrogen eluted from the test piece, μmol;

V is the volume of collected washings, mL;

$\rho_{NO_3^-}$ is the nitrate ion concentration in the eluent from the test piece, mg L^{-1};

$\rho_{NO_2^-}$ is the nitrite ion concentration in the eluent from the test piece, mg L^{-1};

$w1$, $w2$ (subscripts) are the 1st and 2nd elutions, respectively.

Chapter 4 Influence of Utilizing Recycled Glass Cullets as Aggregates on Photocatalytic Pollution Degradation

4.1 Introduction

This chapter presents the results on assessing the effect of using recycled glass cullets as a replacement of fine aggregate in concrete surface layers on the photocatalytic NO_x removal. The experimental results were verified and explained by a separate simulation study. The mechanism of the photocatalytic activity improvement by incorporating glass cullets in concrete surface layers was proposed based on the results of experimental and simulation studies. The influence of glass color, aggregate size and curing age on photocatalytic NO_x removal was also reported.

4.2 Effect of Utilization of Glass Cullets as Aggregates on NO_x Photodegradation

Fig. 4.1 compares the NO_x removal ability of the samples with different mix proportions. It is clear that the photocatalytic activity of the concrete surface adopting recycled glass cullets as fine aggregates improved significantly compared with the reference (100% sand) sample. The amount of NO_x removed by the 100% MI (milk bottle I) glass sample was three times of that removed by the reference

sample. For every sample prepared with different types of glass (soft drink bottle, milk bottle I and milk bottle II), when a higher percentage of glass cullets was incorporated, an increase of NO_x removal was observed. It is likely that the light-transmitting characteristic of the recycled glass cullets had a positive influence on the photocatalytic activity of the surface layers.

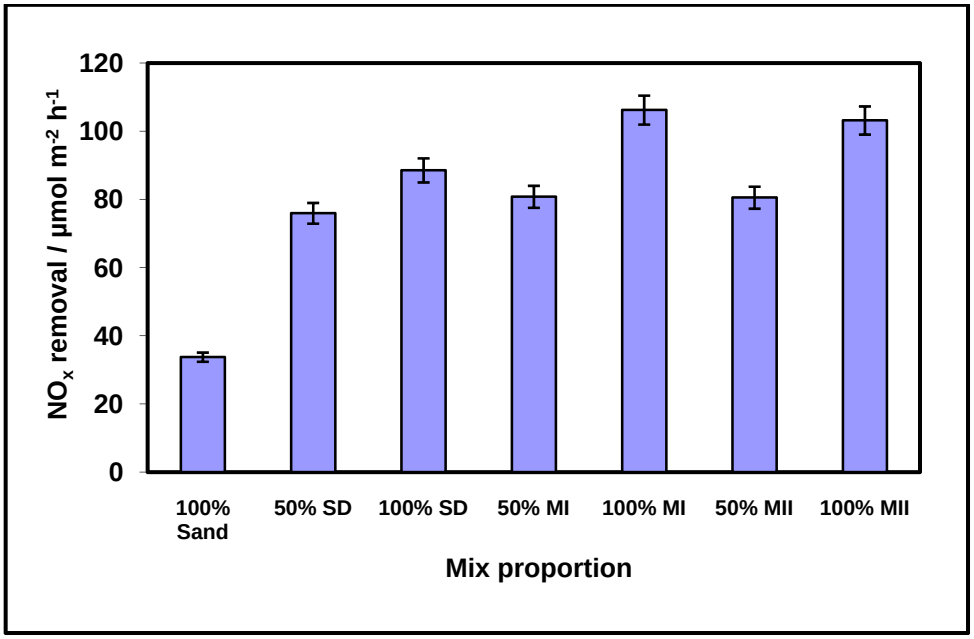

Figure 4.1 Comparison of NO_x removal by samples of different mix proportions based on 7-day curing age testing (d<1.16 mm)

The above results can be explained with reference to the results of the simulation study. The UV-A absorbance of the 80% wt/vol sugar solution is very low, as shown in Fig. 4.2. It can be seen from Fig. 4.3 that the absorption of UV (wavelength less than 370 nm) by the TiO_2 coating on the glass is clear. Similarly, the UV-A absorbance of the TiO_2 coated glass specimens are presented in Fig. 4.4, which shows that there were significant differences in the absorption of UV by sand and

different types of glass. The UV radiation was completely blocked (absorbed) by sand. While for the glass cullets, although some light was absorbed by TiO_2 or glass itself during the transmission process, a small fraction of light was still able to penetrate the 10 mm thick vessel.

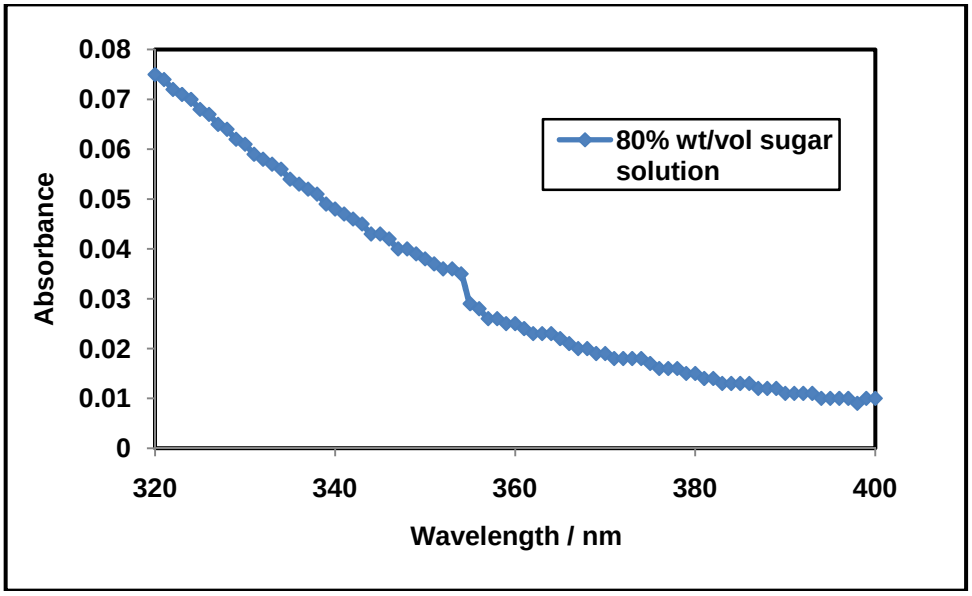

Figure 4.2 UV-A absorbance of 80% wt/vol sugar solution

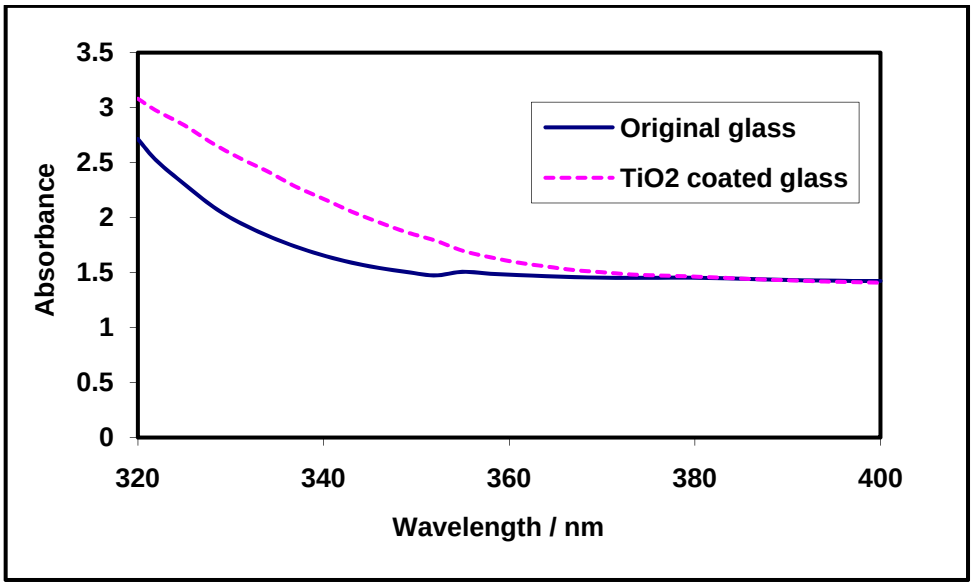

Figure 4.3 Absorbance difference between original glass and TiO_2 coated glass

(Clear glass, 1.16 mm<d<2.36 mm)

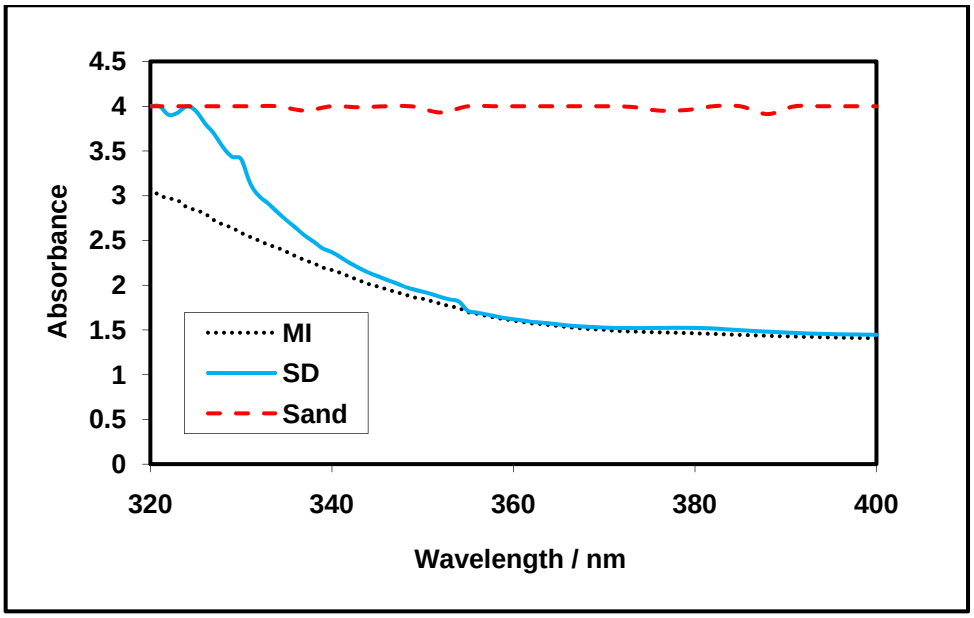

Figure 4.4 Comparison of UV-A absorption among Sand (without coating), milk bottle glass (MI, TiO_2 coated, 1.16 mm<d<2.36 mm) and soft drink bottle glass (SD, TiO_2 coated, 1.16 mm<d<2.36 mm)

In the concrete surface layers made with glass, it seems possible that light could be carried to a greater depth activating the TiO_2 within the inner part of the surface layer as well as those TiO_2 on the top of the surface. The proposed mechanism of the photocatalytic activity improvement by incorporating glass cullets in concrete surface layers is illustrated by Fig. 4.5.

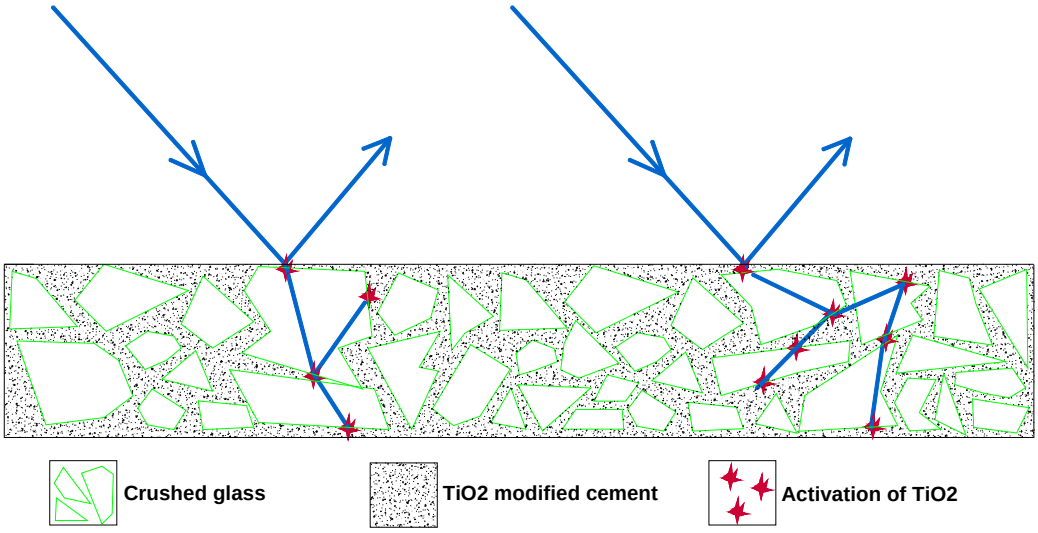

Figure 4.5 Pathways of light and activation of TiO_2 in concrete surface layer using glass as aggregates

4.3 Influence of Glass Color on NO_x Photodegradation

Fig. 4.6 shows there was a clear trend of increasing NO_x removal as the glass color became lighter. It is indeed interesting to note that the sample incorporating brown glass cullets showed the worst NO_x removal performance.

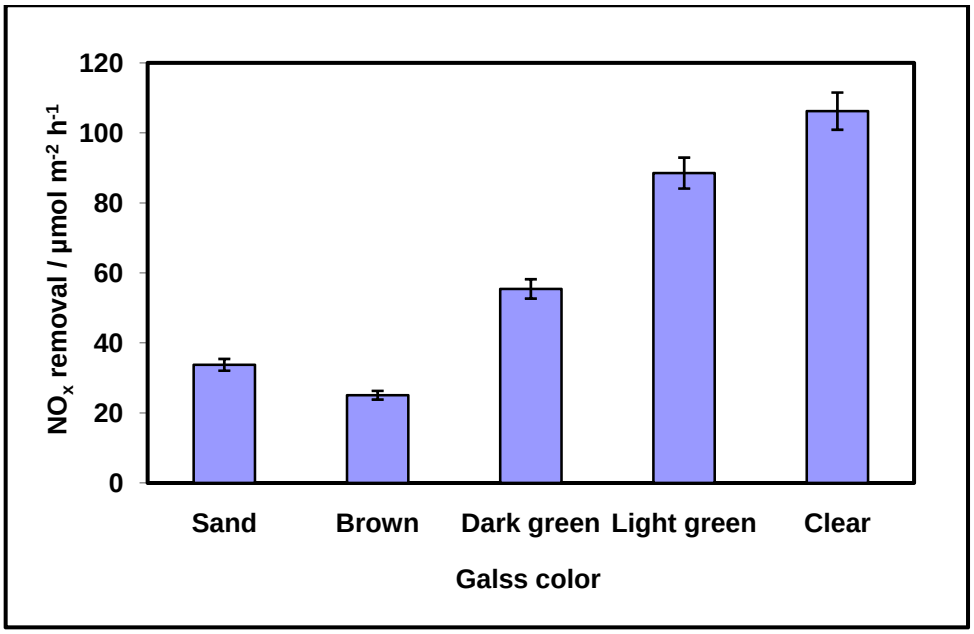

Figure 4.6 Comparison of NO_x removal by samples of different glass color based on 7-day curing age testing

The above results corresponded well with the UV absorption tests. The absorption spectrums of different colored glass are presented in Fig. 4.7. The brown glass had the highest UV absorbance, followed by the dark green, the light green and the clear glass sample. These results are consistent with the finding of Pfaender (1996) which stated that green glass would transmit ultraviolet light while brown one absorbed almost all. Green glass is produced by adding chromium oxide to the glass melts. For brown glass the coloring agent is either iron sulfide or Na_2SO_4 and carbon [Shelby, 1997]. The difference of activation energy for the transition metals (coloring agents) leads to the different UV absorption spectrum of colored glass. The strong correlation between the UV absorption of different colored glass and the photocatalytic activity further proves that the light transmitting property of glass aggregate is a key factor in influencing the photocatalytic NO_x removal performance of concrete surface layers.

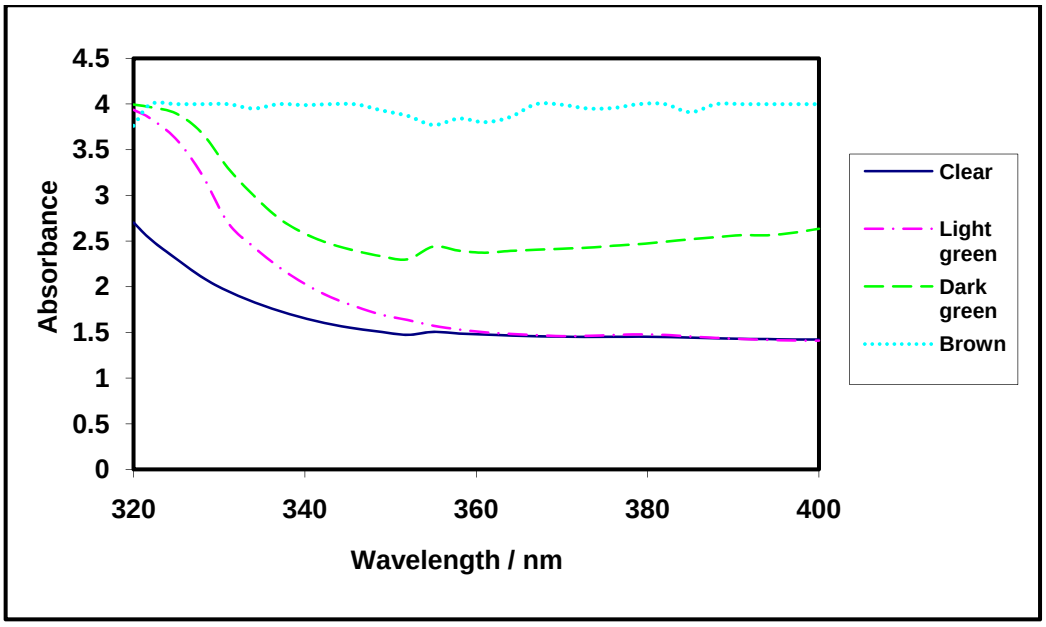

Figure 4.7 Comparison of UV-A absorption by glass cullets of different color (Uncoated glass, 1.16 mm<d<2.36 mm)

4.4 Effect of Aggregate Size on NO_x Photodegradation

It has been widely accepted that photocatalytic air purification is restricted to the pollutants which are in close contact with (or adsorbed by) photocatalysts. In general, porous structures which have large surface area are beneficial for the adsorption process. Therefore, the concrete surface layers fabricated with different sized aggregates, were assumed to have different pollutant degradation ability as changing the particle size distribution of aggregates could alter the porosity of concrete.

To investigate the influence of the aggregate size on NO_x removal, the porosity of samples prepared with two aggregate sizes (d<1.16 mm and 1.16 mm<d<2.36 mm) and their NO_x removal performance were examined. The results of the surface layer porosity analysis are summarized in Table 4.1. Unexpectedly, the surface layer

prepared with smaller glass cullets was found to have a slightly higher porosity than the sample made with larger glass cullets. The reason might be attributed to the fact that the shape and size of the aggregates were changed by the high compaction pressure during the fabrication process. It is possible that large glass cullet were crushed to smaller pieces, which changed the aggregate size distribution and the internal porous structure. Fig. 4.8 shows a comparison of the NO_x removal by the concrete surface layers made with two glass cullet sizes for all aggregate types. No significant difference was observed for the samples prepared with different aggregate sizes. However, the simulation study (Fig. 4.9) proved that the UV-A absorbance depended on the size of cullets, with large sized cullets showing lower absorption. Therefore, large sized aggregates which may induce higher porosity in concrete than small ones are still believed to facilitate pollutant reduction.

Table 4.1 Porosity of concrete surface layers

Aggregate type	d<1.16 mm	1.16 mm<d<2.36mm
100% Sand	22.1%	17.8%
100% Glass	20.9%	18.5%

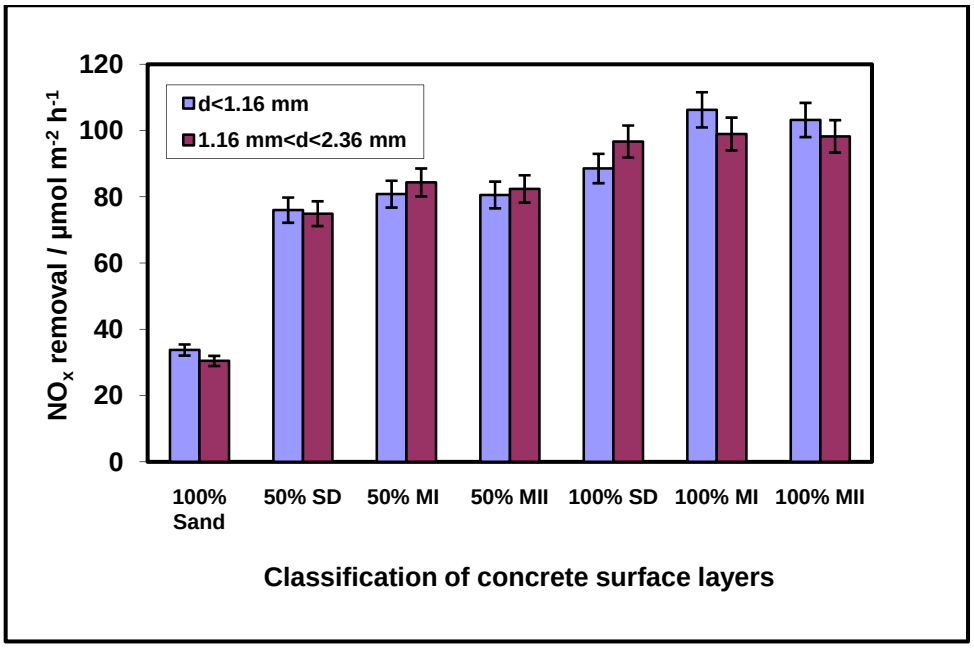

Figure 4.8 NO_x removal of the concrete surface layers with different aggregate sizes based on 7-day curing age testing

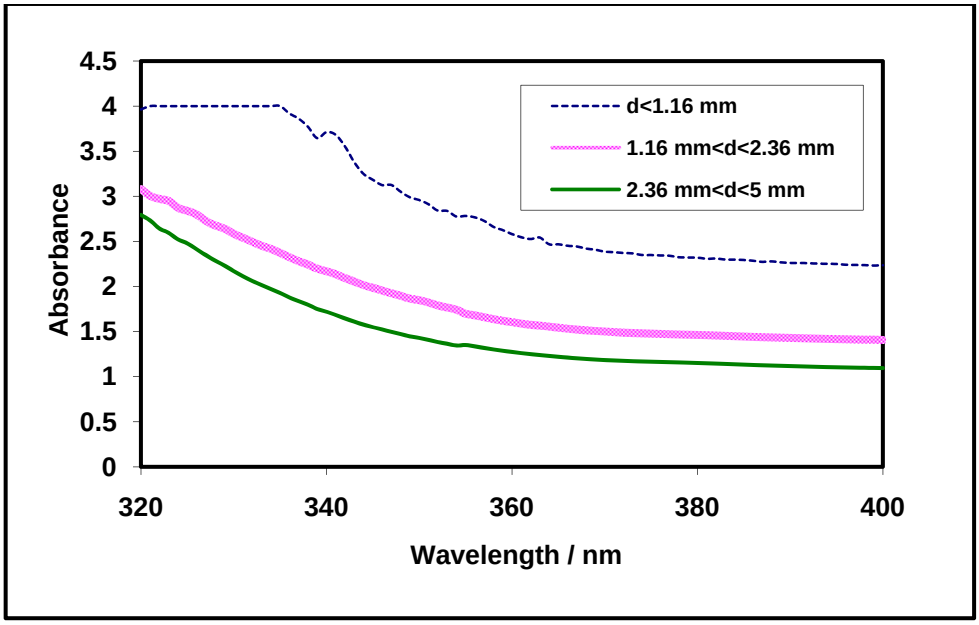

Figure 4.9 Comparison of UV-A absorption by glass cullets of different aggregate sizes (clear glass with TiO_2 coating)

4.5 Effect of Curing Age on NO_x Photodegradation

The photocatalytic activity of the surface layer samples at different curing ages was tested. Fig. 4.10 and Fig. 4.11 illustrate the influence of curing age on the photocatalytic activity of the concrete surface layers with different aggregate sizes. Compared with the NO_x removal after a curing age of 7 days, the average loss of the photocatalytic activity after 28 days and 56 days curing were 7.7% and 21.1% respectively. These findings are consistent with those of Lackhoff et al. (2003) who showed that photocatalytic activity of hardened cement pastes decreased with cement aging.

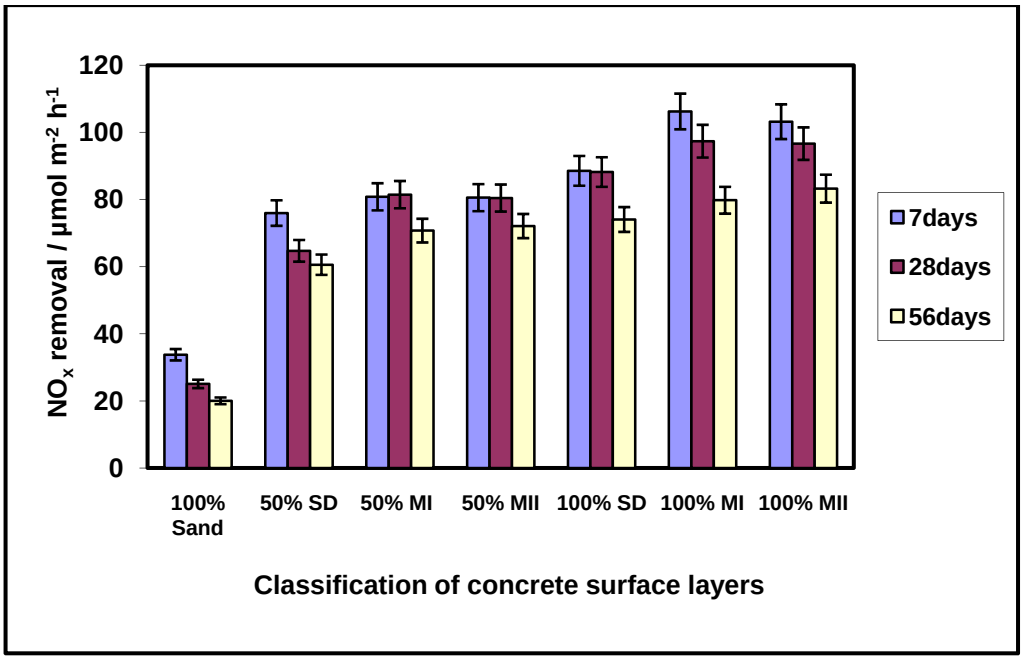

Figure 4.10 Comparison of NO_x removal by concrete surface layers after different curing ages (d<1.16 mm)

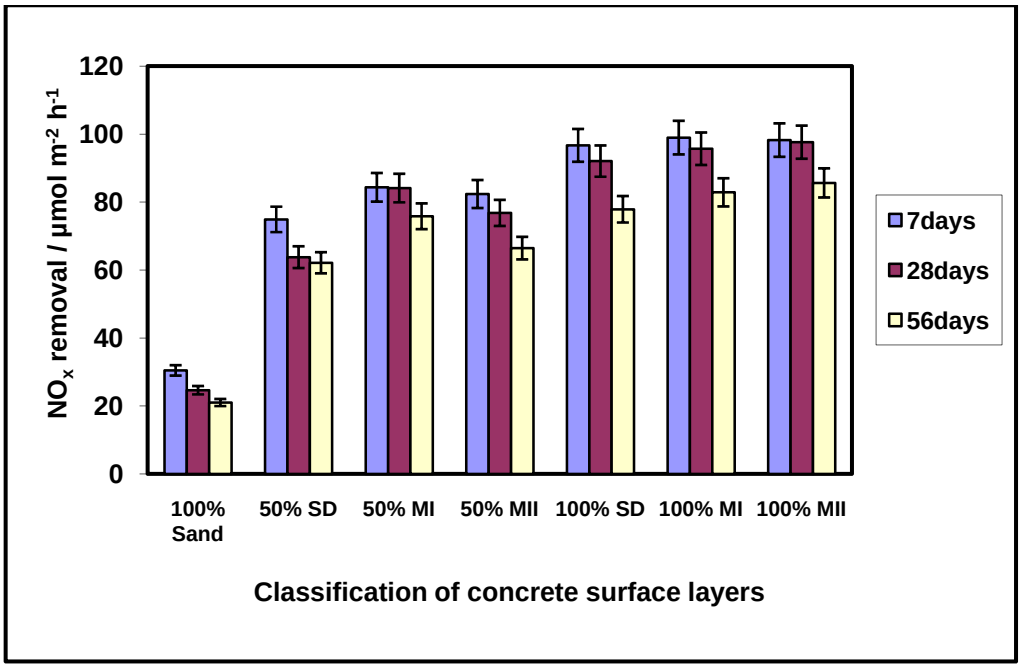

Figure 4.11 Comparison of NO_x removal by concrete surface layers after different curing ages (1.16 mm <d<2.36 mm)

One possible explanation for the loss of photocatalytic activity over time might be due to the change of the internal microstructure of concrete caused by cement hydration reaction. The adsorption and transportation of air pollutants in concrete may follow different mechanisms, depending on the pore structure of concrete, exposure conditions and the characteristics of the diffusing substance. Chen et al. (2001) have demonstrated that dynamic adsorption equilibrium, adsorption rate, internal mass transfer, and effective diffusivity have an effect on the rate of photocatalytic degradation. It also has been proved that there is a strong positive relationship between sorptivity coefficient and porosity [Gonen and Yazicioglu, 2006]. The hydration of cement has a strong influence on the change of the pore structure. Espinosa and Franke (2006) reported that both the amount of capillary pores and the total pore volume decreased with curing age. Therefore, the shrinkage

of pore structure during the cement hydration process may lead to a lower adsorption capacity for target pollutants.

4.6 Summary

In this study, recycled glass cullets derived from crushed waste beverage bottles, were used to replace sand in preparing the photocatalytic concrete surface layers. The photocatalytic activity of the samples was determined by photocatalytic NO_x removal test in the laboratory. Factors which may affect the pollutant removal performance of the concrete layers, such as glass color, aggregate size and curing age, were investigated. The results showed there was a significant enhancement of the photocatalytic activity due to the use of glass cullets as aggregates in the concrete layers. The samples fabricated with clear glass cullets exhibited three times of NO_x removal efficiency compared to the samples fabricated with river sand. The light transmittance property of glass was postulated to account for the efficiency improvement, which was confirmed by a separate simulation study. It was also found that the influence of the size of glass cullets was not evident because the shape and size of the aggregates may be changed by the high compaction pressure during the fabrication process. In addition, the photocatalytic activity of the concrete surface layers decreased with curing age, showing a loss of 20% NO_x removal after 56 days curing.

Chapter 5 Influence of the Microstructure of Cement Paste on Photocatalytic Pollution Degradation

5.1 Introduction

This chapter reports the results of the influence of the microstructure of cement-based composites on photocatalytic pollutant degradation. Nano-TiO_2 with two particle sizes was blended into cement pastes and mortars. Factors which may influence the depollution performance including TiO_2 type, cement type, chemical stability of TiO_2, microstructure of hardened cement paste and carbonation level are analysed and discussed based on experimental results.

5.2 Effect of Photocatalyst Types and Cement Types on NO_x Photodegradation

A typical photocatalytic NO_x removal performance of the cement paste samples obtained in the laboratory is shown in Fig. 5.1. An obvious decrease of NO together with a small increase of NO_2 was observed. The summary of the results of the photocatalytic NO_x removal by TiO_2 modified cement pastes are given in Fig. 5.2. The error bars represent the standard deviation of the removal rate based on data repeatability of three measurements. It is apparent that the photocatalytic activity of cement pastes containing P25 outperformed those containing Anatase. The difference in performance was likely due to the difference of catalysts' surface area [Stokke and Mazyck, 2008]. With higher surface area P25 could provide more active sites which

promoted the surface reactions. However, increasing the content of TiO_2 did not lead to a proportional increase of NO_x removal. The decrease of NO_x conversion for P25 blended cement pastes after a certain curing age was much higher than that of the Anatase blended cement pastes. Therefore, there must be other factors affecting the photocatalytic reactions in the cement matrix. For example, the kinetics of the reaction can also be limited by mass transfer of reactants or photons, which is discussed in the next section. One interesting finding was that the samples prepared with white cement showed higher photocatalytic activities than those prepared with OPC at all times. The reason for this result is not clear but it may be related to the light absorption characteristics of the different types of cement. The gray color of OPC is due to the presence of transition metals, such as manganese and iron, in its chemical composition. The amount of these elements in the white cement is much less (see Table 3.2). It is possible that the transition metal elements in OPC absorbed or blocked a portion of incident photons which otherwise could be utilized for the photocatalytic reaction. Another possible explanation is that the presence of the transition metal in the cement pastes contributed to the electron-hole recombination deactivating the photocatalysts. This assumption is supported by other research findings which attributed the reduction of the photocatalytic rate of surface modified TiO_2 to the transition metal species create acceptor and donor surface centers that behave as recombination sites for photogenerated electrons and holes [Rachel et al., 2002; Allen et al., 2008].

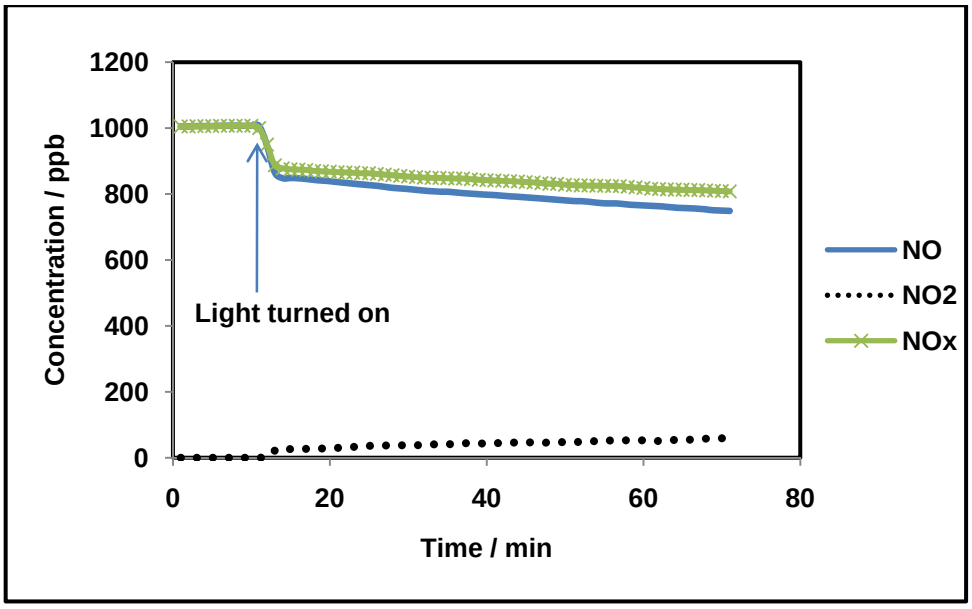

Figure 5.1 A typical photocatalytic NO_x removal profile (WC_5%P25, after 28 days of curing)

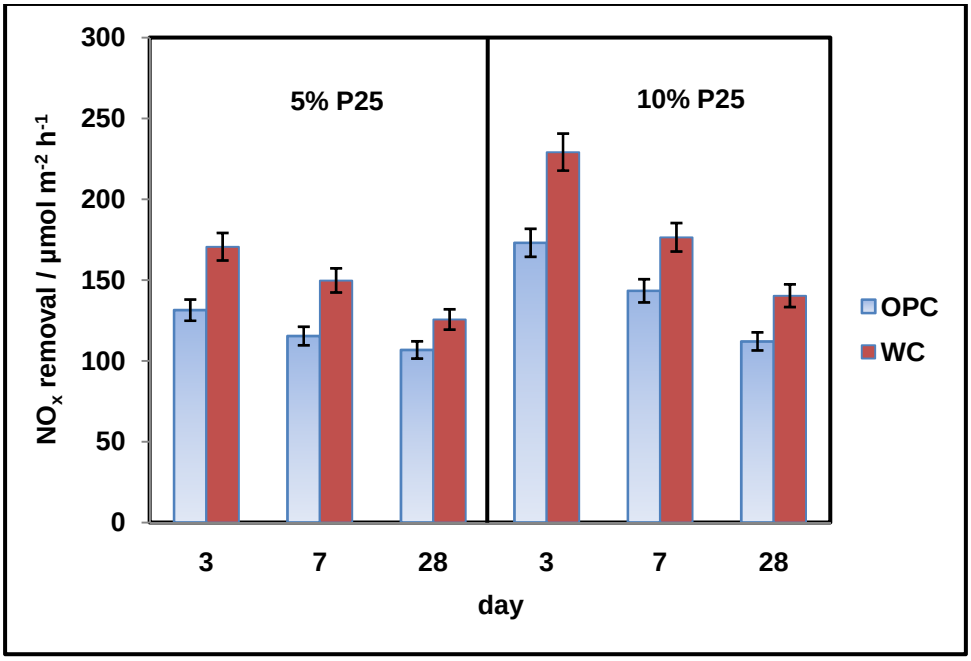

(a)

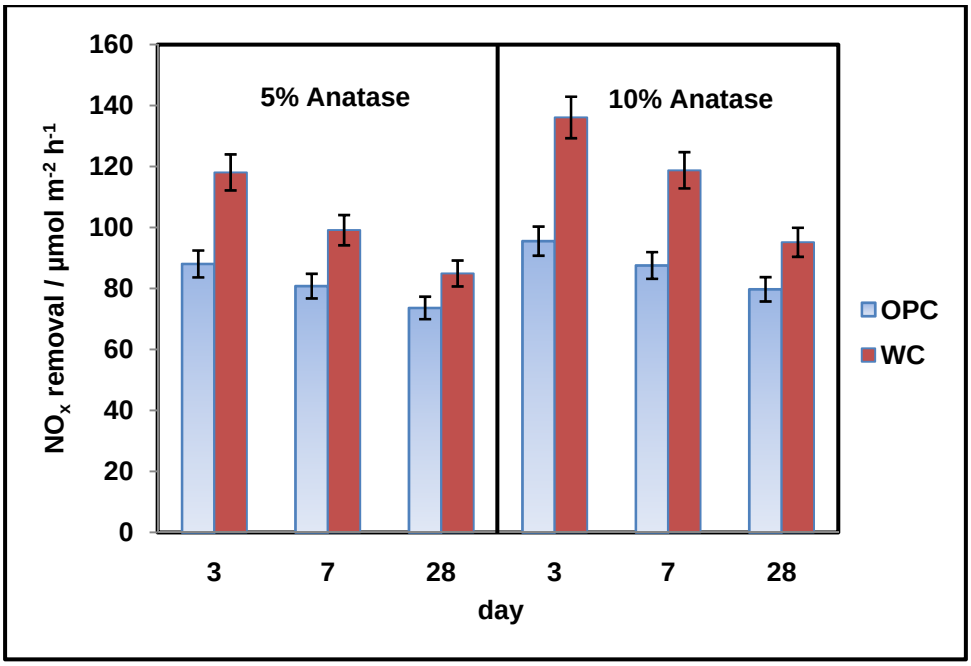

(b)

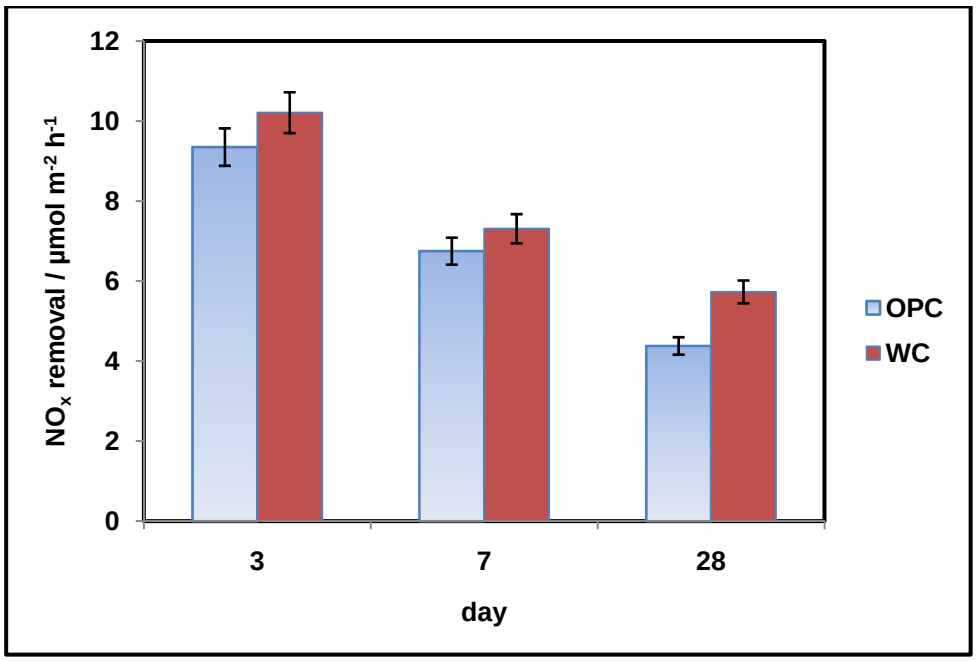

(c)

Figure 5.2 Photocatalytic NO_x removal performance of TiO_2 modified cement paste at different curing ages: (a) P25 mixture, (b) Anatase mixture, (c) Reference samples (without TiO_2 addition)

5.3 Effect of Curing Age on NO_x Photodegradation

The decreasing trend of NO_x removal ability with the increment of curing age observed in section 4.5 was confirmed again in this experiment. The loss of photocatalytic NO_x removal in curing progress ranged from 16.38% (OPC_5%Antase) to 38.77% (WC_10%P25) (Table 5.1). To investigate the reasons for the changes of photocatalytic activity in the cement hydration process, chemical composition and microstructure analysis were carried out. The XRD patterns of OPC_10%P25 and WC_10%P25 sample are shown in Appendix B. MDI Jade 5.0 was used for the identification of the chemical composition and the integration of their corresponding intensities. As shown in Table 5.2, no significant change of TiO_2 ratio was found, which indicates that TiO_2 was inert and chemically stable in the cement hydration reactions. This finding is contrary to those from a previous research [Lackhoff et al., 2003] which claimed that there were specific interactions between the cement matrix and the photocatalysts due to their pozzolanic activities (e.g. TiO_2 may react with $Ca(OH)_2$, such as SiO_2, to form a product similar to calcium silicate hydrates (CSH) gel). The above observations were further supported by the results of TG analysis (Table 5.3). The incorporation of TiO_2 into cement paste only reduced the amount of CH production slightly, ruling out the speculation for the pozzolanic activity of TiO_2. Therefore, it can be concluded that the reduction of photocatalytic activity in hydration is not caused by the reaction of TiO_2 with other chemicals.

Table 5.1 Reduction of NO_x removal ability during curing period (comparison between 3rd day's data and 28th day's data)

	5% P25	10 % P25	5% Anatase	10% Anatase
OPC	18.76%	35.26%	16.38%	16.54%
WC	26.37%	38.77%	28.06%	30.08%

Table 5.2 Weight ratios of the chemicals after 3, 7 and 28 days curing with respect to the 3 days' data

Sample	Chemical	3 days	7 days	28 days
OPC_10%P25 paste	TiO_2	1.00	1.02	0.97
	CH	1.00	1.15	1.31
WC_10%P25 paste	TiO_2	1.00	1.04	1.02
	CH	1.00	1.13	1.25

Table 5.3 The weight fraction of CH in the paste after 3, 7 and 28 days curing and their ratio with respect to the 3 days' data (Pure WC and WC_10%P25)

Sample		3 days	7 days	28 days
Pure WC	CH content / %	12.46	13.90	15.42
	Ratio	1	1.12	1.24
WC_10%P25	CH content / %	11.14	12.46	13.69
	Ratio	1	1.12	1.23

Table 5.4 shows the porosity decreased with cement aging for all the mixtures. A denser microstructure formed gradually with increasing curing age. The

neighbouring cement grains got in contact and a dense gel structure filled available voids during the progress of cement hydration [Brandt, 2009]. The pore size distributions of OPC_5%Anatase and WC_10%P25 samples after 3 days, 7 days and 28 days curing are compared in Fig. 5.3. It can be seen that the reduction of porosity mainly occurred within the capillary pore range (10 nm to 50 nm) [Aligizaki, 2006], which probably caused the continuous filling up of the pore space by hydration products. This may lead to a lower sorptivity of NO_x molecules. Fine TiO_2 particles might act as potential nucleation sites for the reaction products. CSH gel, a colloidal amorphous gel which is the main component of a cement paste, could form a dense coating on the TiO_2 surface. Similar to unreacted cement grains, the CSH surrounding TiO_2 particles were embedded in a porous groundmass constituted by undifferentiated materials containing CH and CSH gel [Gartner et al., 2002].

Table 5.4 Porosity of TiO_2 modified cement paste after different curing ages

	Porosity / %, v/v					
	OPC			WC		
	3days	7days	28days	3days	7days	28days
0% TiO_2	22.92	22.31	20.55	23.24	21.91	20.30
5% P25	21.56	19.76	18.15	23.04	19.61	19.23
10% P25	20.56	19.31	17.54	23.17	21.72	19.59
5% Anatase	21.63	19.47	16.16	22.01	19.08	16.81
10% Anatase	20.83	17.19	16.10	20.15	19.10	18.59

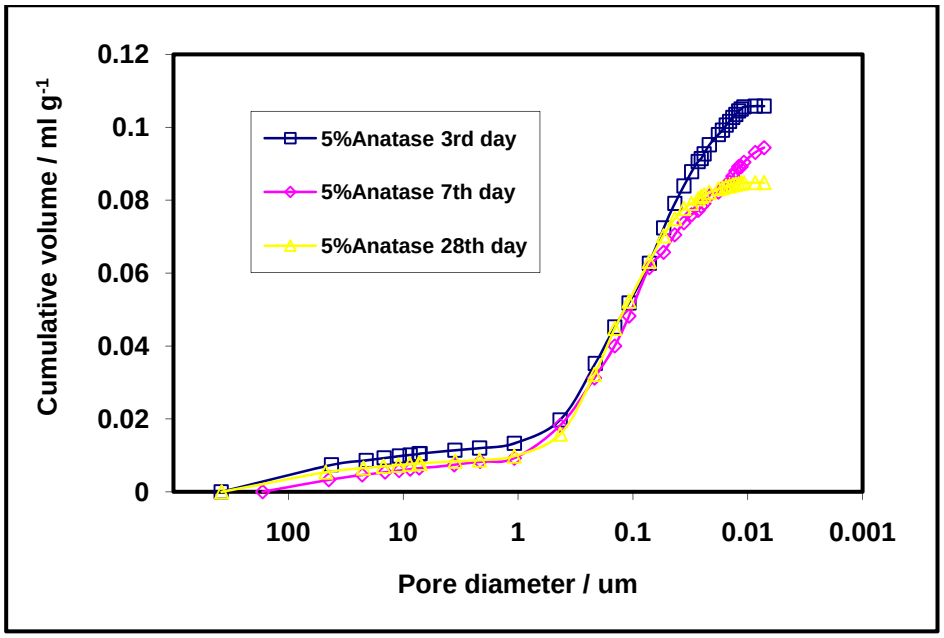

(a)

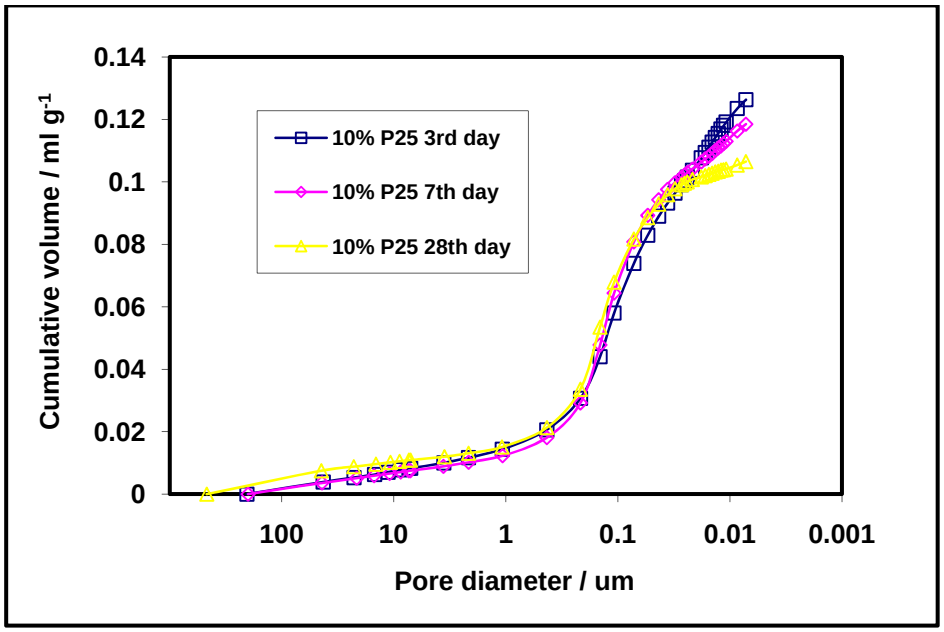

(b)

Figure 5.3 Pore size distribution of the photocatalysts blend cement paste at different curing ages: (a) OPC_5%Anatase sample, (b) WC_10%P25 sample

The photosensitivity of TiO_2 is considered to arise from localized sites on the crystal surface, and occupation of these sites by cement hydration products could inhibit its

photocatalytic activity. Compared with Anatase, it is obvious that P25 would lose much more reactive sites because of its large surface area. This can be used to explain the phenomena that the cement pastes containing P25 lost more photocatalytic activity than those containing Anatase as cement hydration progressed. The photocatalytic pollution degradation occurred in the cement matrix is a very complex interaction between photocatalysts, reagents and photons. The process may be controlled by the kinetics of the reaction, or by the transport of the reagents, or by the transport of the radiant energy or by a combination of these factors [Camera and Santarelli, 2007]. The variation of photocatalytic reaction rate with position in the catalyst layers is due to light intensity gradients caused by light absorption and concentration gradients caused by conversion or diffusion resistance [Herz, 2004]. Referring to the previous results, it is likely that the CSH coatings thickened with time and formed diffusion barriers to both reactants and photons resulting in the observed decrease of NO_x removal during the cement hydration period. In general, the continuous accumulation of cement hydration products which covers the active sites of TiO_2 blocking the adsorption of reactants and the transport of photons should be the major factor leading to the loss of photocatalytic activity in the cement hydration process.

5.4 Effect of Carbonation on NO_x Photodegradation

The equipment set-up and experimental details of this study are provided in Appendix C. The comparision of photocatalytic NO_x removal performance between samples in normal conditions and samples subjected to accelerated carbonation are shown in Fig. 5.4. The correlation of increased carbonation level (Table 5.5) and the loss of photocatalytic activity are well demonstrated. It also can be seen that the NO_x removal ability of normal samples was stable after the predominant period of cement hydration. The decrease of photocatalytic efficiency caused by carbonation may be attributed to the microstructure change occurred in the conversion of $Ca(OH)_2$ to $CaCO_3$. Around 11% solid volume increase in the conversion of $Ca(OH)_2$ to $CaCO_3$ was reported before [De Ceukelaire and Van Nieuwenburg, 1993]. The expansion of the solid volume in the paste results in a shift of pore size distribution towards smaller ones and a reduction of total porosity [Arandigoyen et al., 2006]. Therefore, the $CaCO_3$ deposition in pores could have a negative effect on the diffusivity of NO_x into the cement matrix reducing the photocatalytic reaction rate. This finding further proves that the accumulation of hydration products can influence the photocatalytic process, which also indicates that the photocatalytic pollution removal capability of the composite cementitious materials not only depends on the activity of TiO_2 but also the properties of the components of cement paste and their spatial relationship.

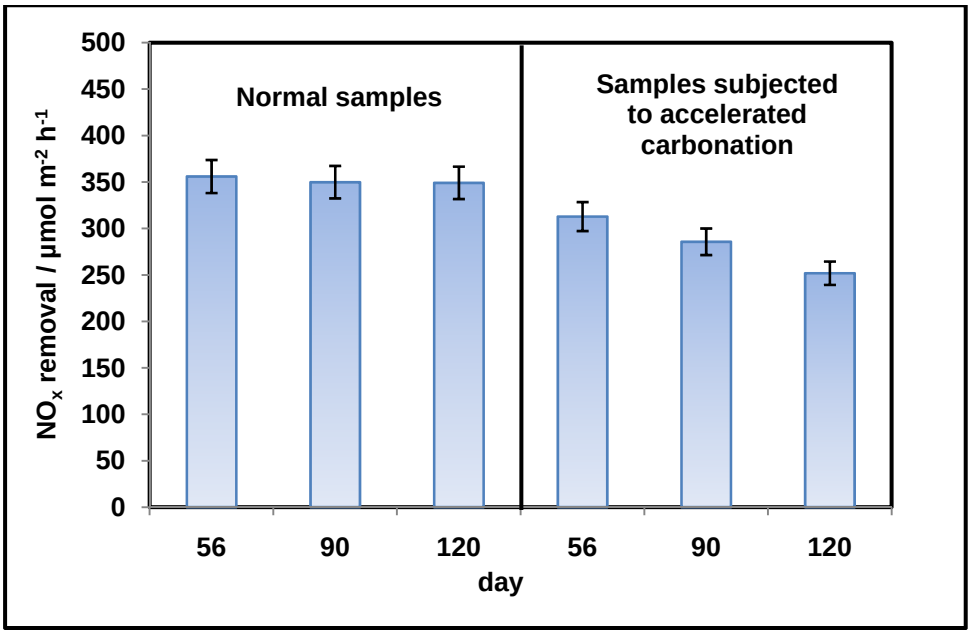

Figure 5.4 Comparison of Photocatalytic NO_x removal performance (OPC_10%P25) between samples in normal conditions and samples subjected to accelerated carbonation

Table 5.5 Carbonation depth of cement paste (accelerated carbonation)

	56 days	90 days	120 days
Carbonation depth (mm)	6.2	9.9	12.5

5.5 Summary

In this study, the photocatalytic NO_x conversion by TiO_2 modified cement pastes was used as a standard process to evaluate the internal factors which may influence the depollution performance. The chemical composition and microstructure of the TiO_2 modified cement pastes were characterized and analyzed. The active photocatalytic sites related to the surface area of TiO_2 are the key factor in determining the photocatalytic activity. Ordinary Portland cement pastes showed lower photocatalytic activity than white cement pastes probably due to the influence of minor metallic components. X-ray diffraction and TG analysis demonstrated that TiO_2 was chemically stable in hydrated cement matrix. The decreasing trend of NO_x removal ability with the increase of curing age was confirmed again. This could be attributed to the cement hydration products which filled up capillary pores forming diffusion barriers to both reactants and photons. It was also proved that surface carbonation could reduce the NO_x removal efficiency after the hydration of cement.

Chapter 6 Hydration and Properties of Nano-TiO_2 Blended Cements

6.1 Introduction

This chapter presents the results on investigating the hydration and properties of Nano-TiO_2 blended cements. Reference samples (pure cement) and cement/TiO_2 composite samples containing up to additional 10% TiO_2 by the weight of cement were prepared. The results of hydration heat measurements, TG analysis and MIP measurements are analyzed. The distribution of nano-TiO_2 in hardened cement paste is also presented. The secondary effects of nano-TiO_2 admixture on cement properties, such as standard consistence, setting time and compressive strength are discussed.

6.2 Hydration of nano-TiO_2 blended cements

6.2.1 Hydration heat measurements

The curves describing the rate of heat evolution for cement/TiO_2 mixtures with 0%, 5% and 10% addition of nano-TiO_2 are presented in Fig. 6.1 using mix proportions listed in Table 3.7. Because the mixtures were prepared outside the calorimeter, the first heat evolution peak resulted from the wetting of cement could not be recorded. As shown in the figures, the main peak occurred earlier for all the samples containing TiO_2 in comparison with the reference sample. The addition of fine TiO_2 powders

significantly increased the height of the heat peak and shortened its duration. The increase of TiO_2 dosage made this effect clearer, but did not trigger a proportional increase of heat release rate. Fig. 6.2 shows the curves of the total heat evolution during 72 h hydration. In correspondence with the trend of heat evolution rate, additional mixing of nano-TiO_2 powders resulted in a greater accumulative heat release, particularly in the first 30 h. The acceleration of hydration reactions by inert or active ultra fine fillers has been demonstrated by several studies [Gutteridge and Dalziel, 1990; Poppe and De Schutter, 2005; Kadri and Duval, 2009]. It was proposed that those filler particles could act as potential heterogeneous nucleation sites for hydration products [Gartner et al., 2002]. It is also noticed that the exothermic hydration process was accelerated more by P25 compared with Anatase, probably because the larger surface area of P25 could provide more sites for the hydrates to deposit.

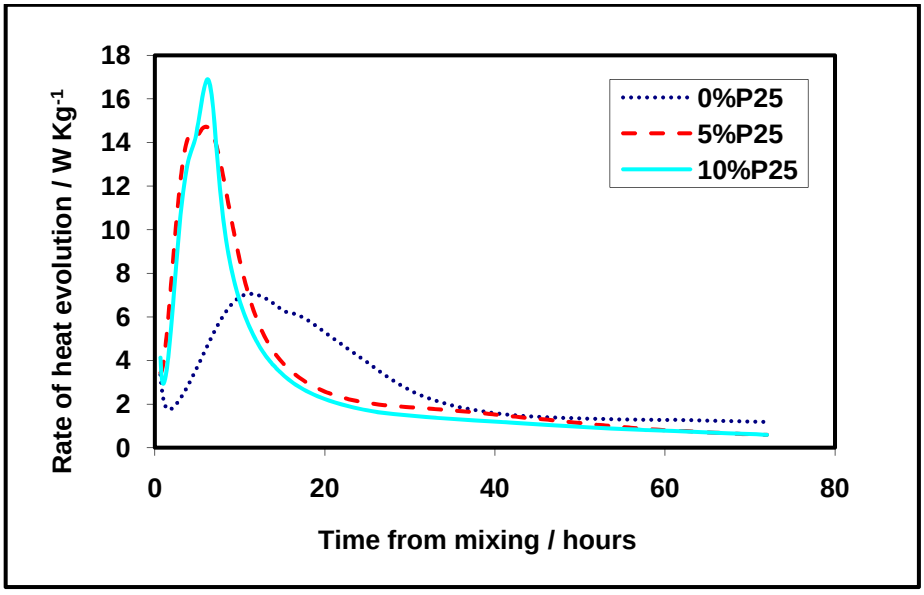

(a)

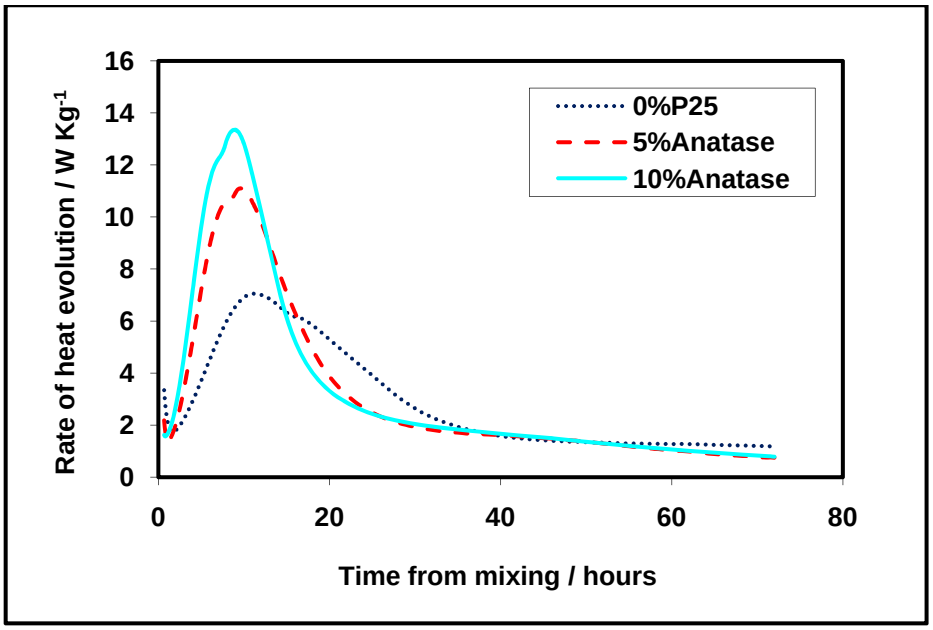

(b)

Figure 6.1 Rate of heat evolution for different TiO_2 content: (a) P25, (a) Anatase

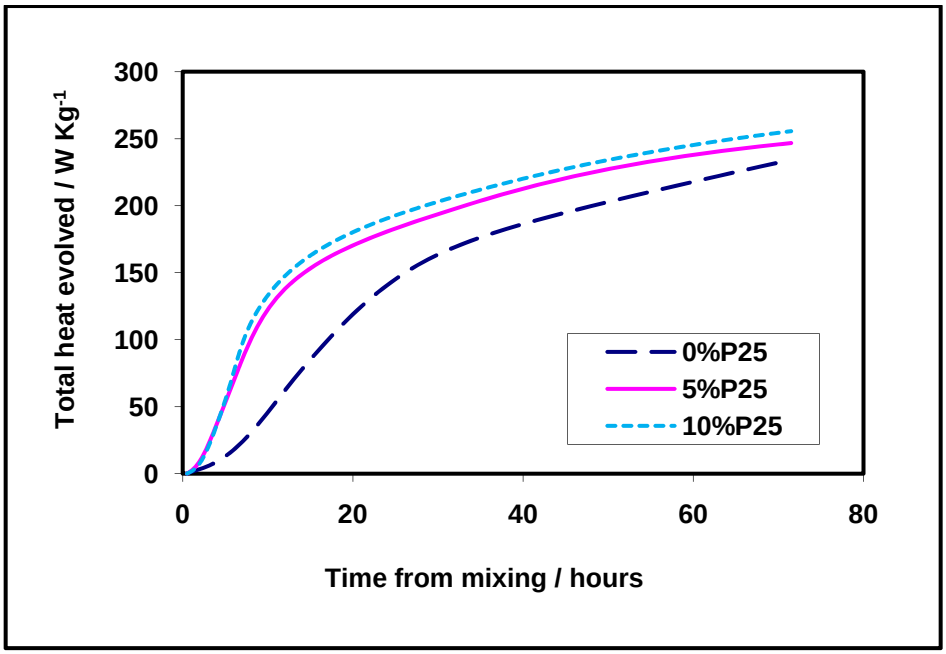

(a)

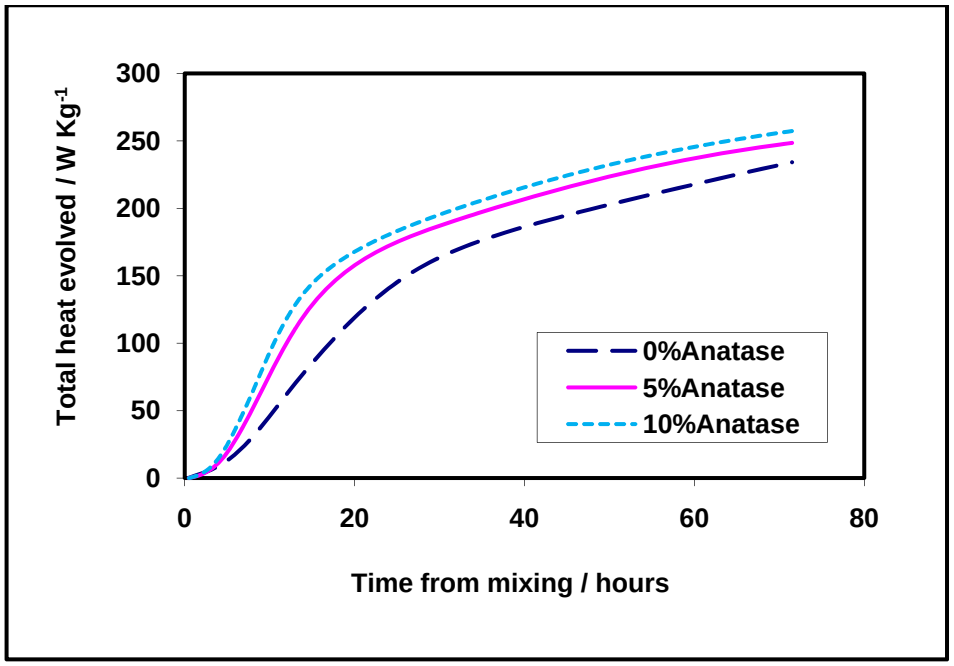

(b)

Figure 6.2 Total heat of hydration for different TiO_2 content: (a) P25, (b) Anatase.

6.2.2 TG analysis

Fig. 6.3 shows the TG curves of the pure cement sample and the 10% w/w P25 blended cement samples hydrated at 3, 7 and 28 days. The content of the non-evaporable water bound in cement pastes was determined as the weight loss between 120 ^{o}C and 900 ^{o}C on the TG curves. It was normalized with the mass fraction of cement in the composition, considering TiO_2 was a non-hydraulic additive. As shown in Fig. 6.4, the non-evaporable water content increased with hydration age. Dosing nano-TiO_2 powders into cements significantly increased the amount of chemically bound water, especially at the early curing ages, indicating that the hydration reactions were accelerated. Based on this result together with the isothermal calorimetric measurements, it is suggested that nano-TiO_2 particles could

accelerate the reaction rate during early hydration period and promote the formation and precipitation of hydration products.

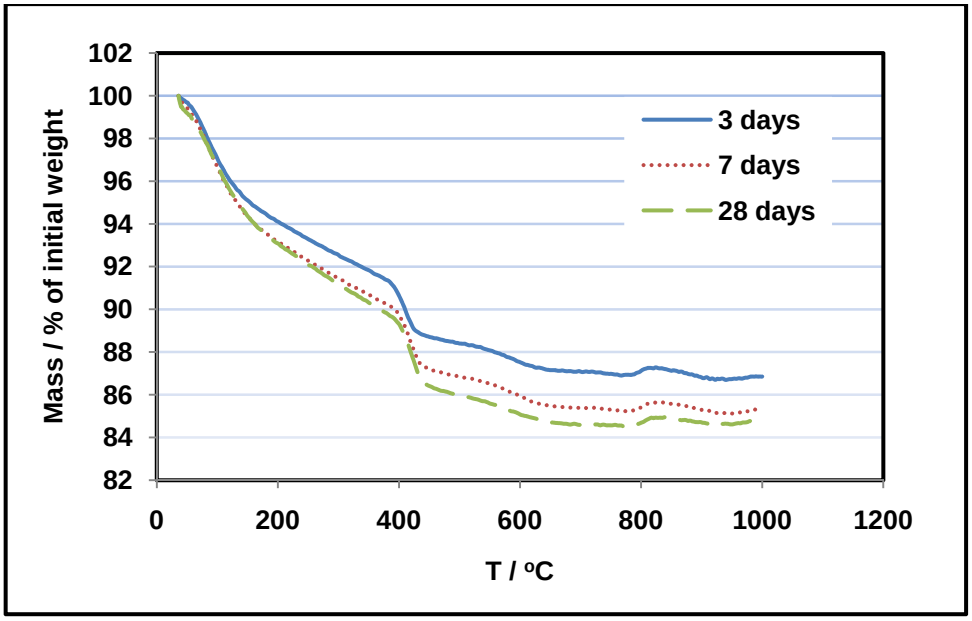

(a)

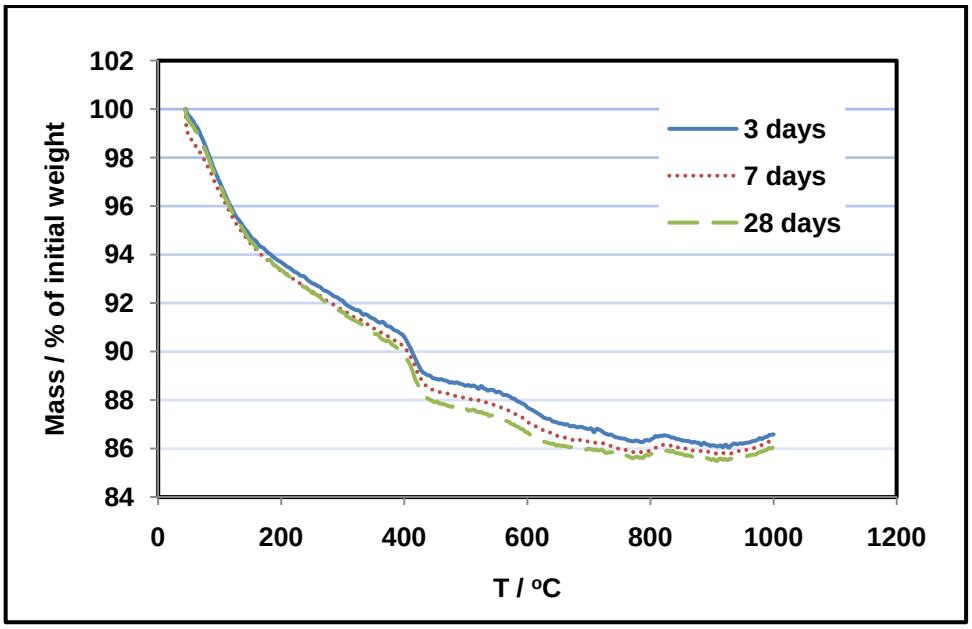

(b)

Figure 6.3 TG diagrams: (a) pure cement sample hydrated at 3, 7 and 28 days, (b) sample containing additional 10% w/w P25 admixture hydrated at 3, 7 and 28 days

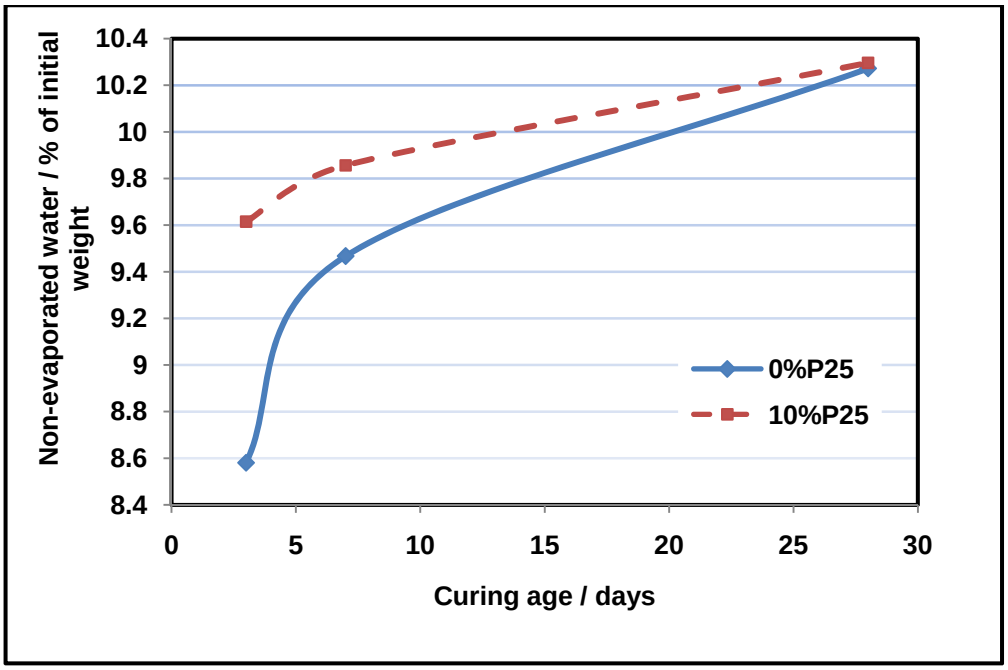

Figure 6.4 Comparison of the content of non-evaporable water in pure cement paste and P25 blended cement paste at different curing age

6.2.3 TiO_2 particle distribution in cement paste

To further investigate the physical form of the nano-TiO_2 in the hydrated cement pastes, a microstructure analysis (SEM together with EDX) was carried out. Fig. 6.5 shows the elemental distribution of Ti in the cement paste obtained by SEM-EDX. It can be observed that the nano-TiO_2 particles were not homogeneously dispersed in the cement matrix and some segregations or aggregations of TiO_2 particles were found. This finding is in agreement with another research study [Li et al., 2004] which concluded that a large quantity of nano-particles are prone to aggregate and cannot be uniformly dispersed in cement-based materials due to their high surface energy. It was suggested that the use of surfactants or ultrasonic treatment could improve the dispersion.

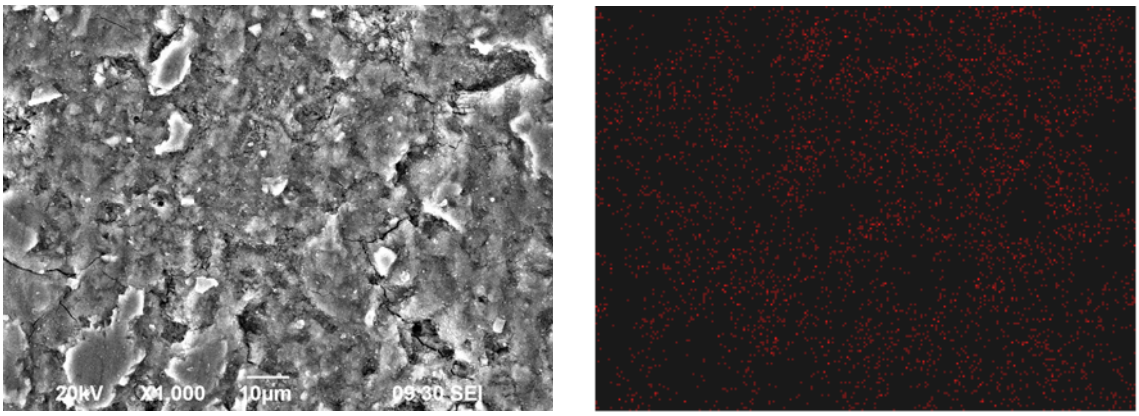

Figure 6.5 Elemental distribution of Titanium in 10% w/w P25 blended cement paste hydrated at 28 days: left, SEM observation; right, corresponding Ti (red spots) mapping

6.3 Physical and mechanical properties of nano-TiO_2 blended cements

6.3.1 Porosity

The results of porosity test for the reference sample, P25 and Anatase blended samples after different curing ages has been shown in Table 5.4. It is clear that dosing nano-TiO_2 into cement pastes decreased the porosity. As shown in Fig. 6.6, the pore size distribution and the total pore volume were also modified. The fine TiO_2 particles seemed to act as the filler of the voids. However, there is a more possible explanation for the denser microstructure formed, which is described as follows. During the hydration process, cement hydration products precipitated and grew on the nano-particles which were dispersed in the cement paste. With hydration continued, the conglomerations containing the nano-particles as nucleus expanded and filled up the pore space around them gradually. As discussed in the previous

section, the presence of "nucleus" significantly accelerated the hydration reaction rate. Therefore, the hydrates accumulated rapidly and grew outwards into the water filled voids, resulting in the decrease in porosity. Moreover, it should be noticed that the reduction of porosity mainly occurred within the capillary pore range. Capillary pores are considered to be remnants of the water-filled space between hydrated cement grains [Gartner et al., 2002]. This observation further proves that the nano-TiO_2 particles acted as nucleation sites for hydration products rather than just acted as common pore fillers. Increasing the dosage of nano-TiO_2 from 5% to 10% did not lead to significant lower cumulative pore volumes after 28 days curing (Fig. 6.6). It is possible that the production of hydrates was so greatly stimulated, even by a small quantity of inert nano-particles that most of the capillary pores were filled up and the growth was confined by limited space after 28 days hydration.

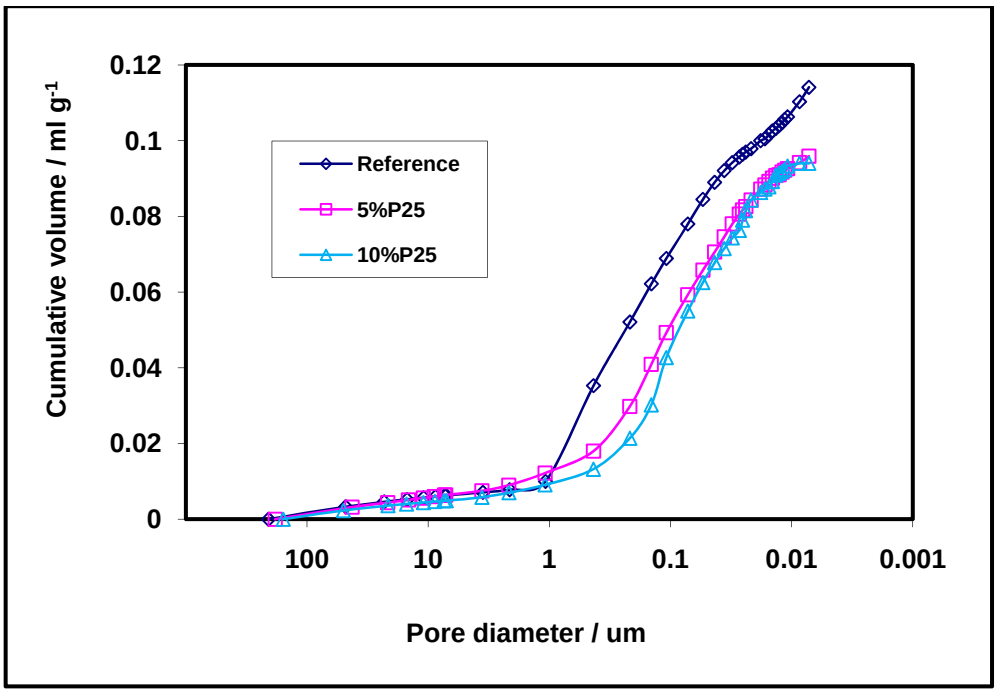

(a)

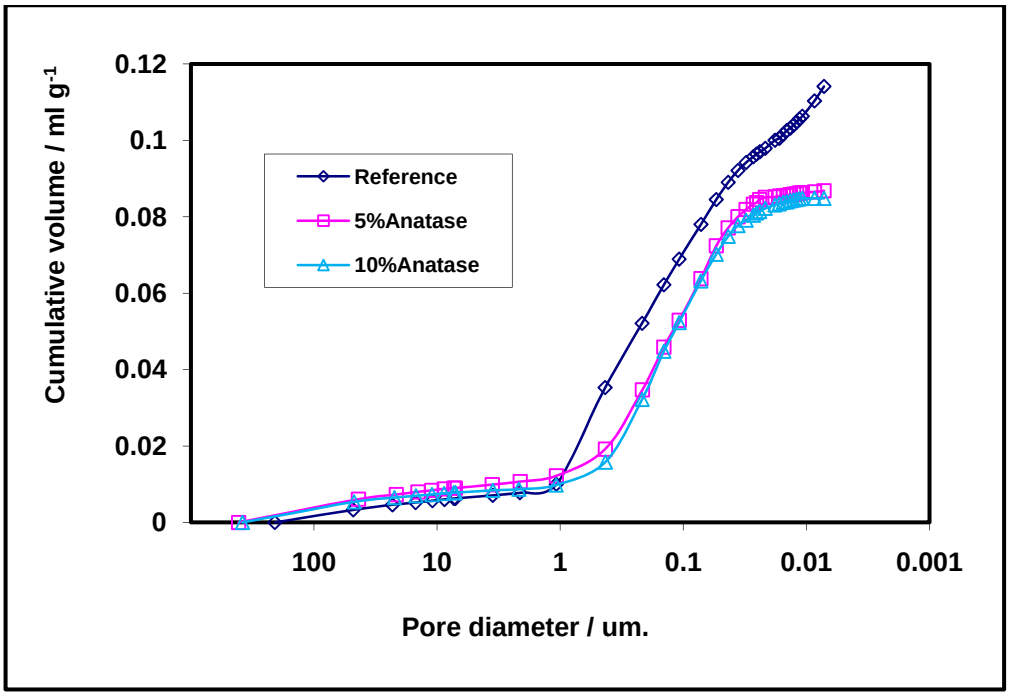

(b)

Figure 6.6 Pore size distribution of TiO_2 blended cement paste hydrated at 28days:

(a) P25, (b) Anatase

6.3.2 Standard consistence and setting time

Table 6.1 presents the summary of the cement water demand and the setting time for different samples. The "water demand" represents the amount of water required to prepare a cement paste with standard consistency, which is specified in BS EN 196-3. As expected, the nano-TiO_2 blended samples demanded more water than the pure cement sample. The higher the dosage of TiO_2, the more water was needed. The increase in water demand can be attributed to the increase in available surface area of the nano-TiO_2 particles. To maintain a standard consistence, more water is required. The setting time of the samples decreased with the increase in nano-TiO_2 content. This is because of the accelerated hydration reaction and, as a result, the viscosity increased faster and the final solidification occurred earlier. In addition, particles

with larger surface area caused a higher water demand and shorter setting time, which was consistent with the observations in the heat of hydration measurement.

Table 6.1 Physical properties of the nano-TiO_2 blended cement

Sample	Water demand / %, weight of water / weight of total materials	Setting time / min	
		Initial	Final
Reference	26.0	160	240
5% P25	31.0	110	155
10% P25	36.0	100	145
5% Anatase	28.0	130	195
10% Anatase	30.0	125	185

6.3.3 Compressive strength

The results of compressive strength development in relation to nano-TiO_2 addition levels are shown in Fig. 6.7. The compressive strength of the mortars was significantly improved at all ages due to the addition of the nano-TiO_2. Using nano-TiO_2 with larger surface area and increasing their dosage further enhanced the strength. However, the amount of superplasticizer used had to be increased with the amount of TiO_2 to keep the workability. Otherwise, additional amount of nano-TiO_2 could actually lower the strength rather than improving it. Other studies have reported mortars containing nano-SiO_2 particles showed higher compressive strength than pure cement mortars due to the pozzolanic activity of SiO_2 and their pore filler

effects [Jo et al., 2007; Lin et al., 2008b]. As discussed before, TiO_2 is not a pozzolanic material. The mechanisms for the improvement of compressive strength should be different from the SiO_2 containing mortar. Fig. 6.8 presents the comparison of relative strength. It can be seen that all the ratios decrease with curing ages. The rate of strength development mainly depends on the degree of hydration. At early ages, the hydration rate of the TiO_2 containing samples was accelerated. After a longer age of curing, the accelerating effect gradually resulting in a decreasing trend of relative strength ratio. Therefore, nano-TiO_2 mainly affected the early strength development.

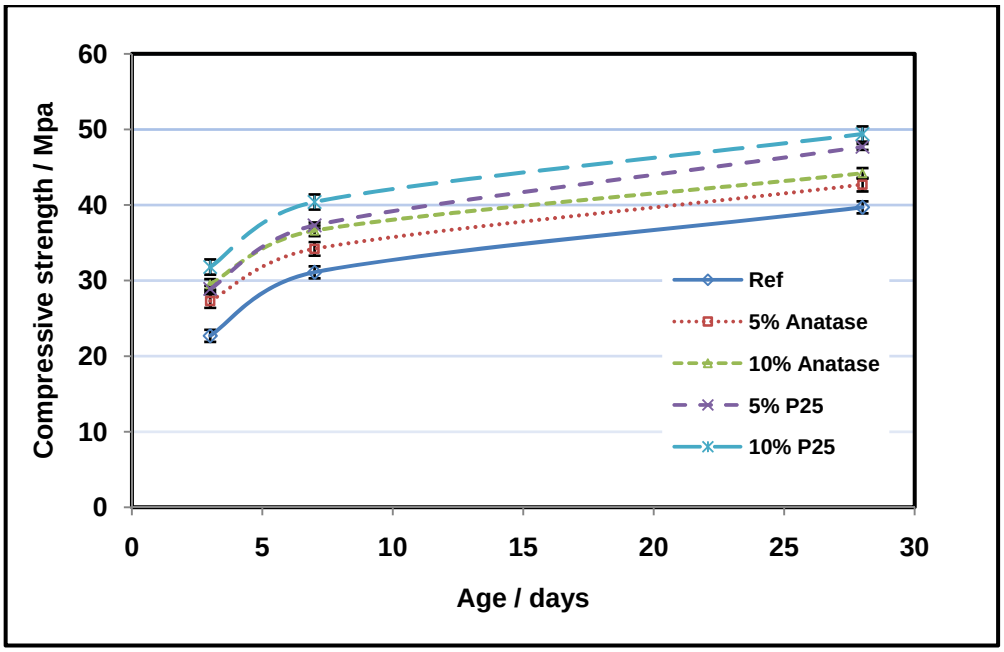

Figure 6.7 Compressive strength development

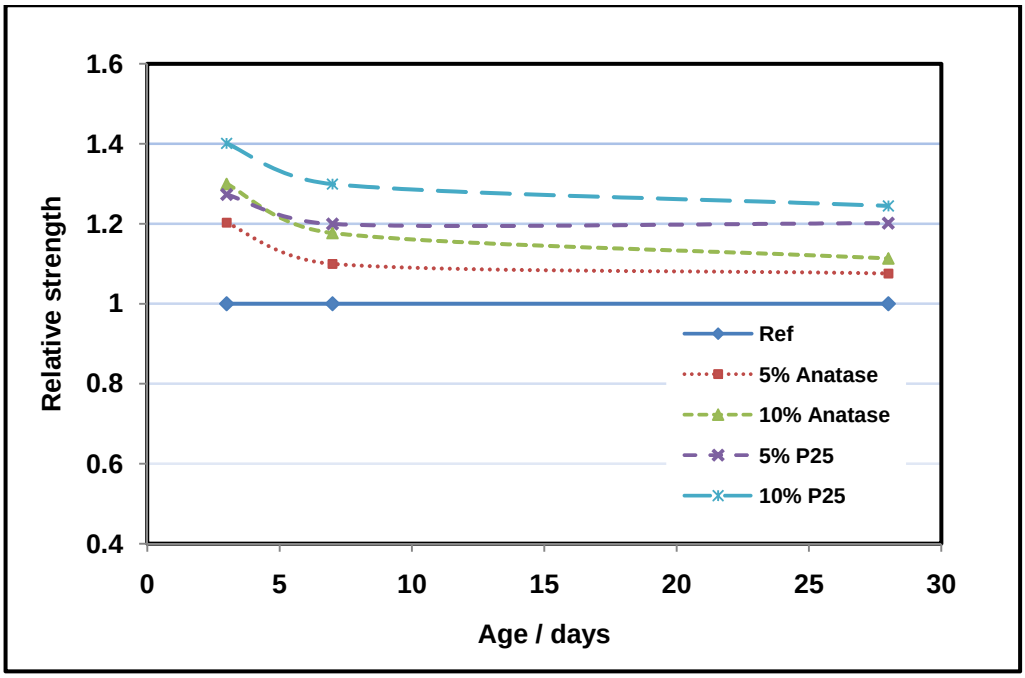

Figure 6.8 Relative strength (with respect to the compressive strength of the reference sample at specified curing age)

6.4 Summary

As a new functional construction material, the basic properties of the photocatalytic cement-based material were investigated in this study. The effects of adding nano-TiO_2 on the inherent properties of hardened cement paste were also examined. The nano-TiO_2 powders significantly accelerated the hydration rate and increased the degree of hydration at early ages. It was demonstrated that the distribution of TiO_2 in cement pastes is not homogeneous. The total porosity of the paste decreased and the pore size distribution was also altered. The acceleration of hydration rate and the change of microstructure affected the physical and mechanical properties of the cement-based material. The initial and final setting time was shortened and more water was required to maintain a standard consistence due to the addition of nano-TiO_2. The compressive strength of the mortar was enhanced, practically at early ages.

Chapter 7 Field Trial Evaluation of the NO_x Removal Efficiency of Photocatalytic Paving Blocks

7.1 Introduction

To demonstrate the effectiveness of using photocatalytic paving blocks to remove common air pollutants, two pilot field trials were carried out. This chapter presents the field trial monitoring results of those two projects. The results of durability test and statistical analysis are illustrated. The sampling problems found during monitoring campaign are discussed.

7.2 NO_x Concentration Monitoring

7.2.1 Durability test

After one year in service, a number of the laid blocks were removed from the paved area and their surfaces were cleaned by different methods, including distilled water washing, detergent washing and 1 mm surface polishing. The laboratory testing results are shown in Table 7.1. It can be seen that the photocatalytic activity of the blocks dropped significantly after one year's exposure in the real environment. Washing the block surface with distilled water did not recover the photocatalytic activity significantly. These results are not consistent with those of the previous study [Beeldens, 2007] which stated that the air pollutant removal efficiency could be maintained by washing the paving blocks with water. However, when the block

surfaces were washed by detergent or grinded, marked improvement in recovery of the NO removal ability was found. It seems possible that the deactivation of the photocatalytic paving blocks were mainly due to the accumulation of contaminants and other deposits. The precipitation of atmospheric aerosol pollutants which bounded on the surface of the blocks was difficult to be washed away by pure water. This could reduce the catalytic surface area, preventing gaseous pollutants to get in contact with the photocatalysts. Therefore, periodic servicing (by washing with detergent) of the photocatalytic blocks may be necessary to maintain the pollution removal effect.

Table 7.1 NO_x removal performance of photocatalytic paving blocks

	New blocks	Blocks after in service for one year		
		Washed by distilled water	Washed by detergent	1 mm surface polished
NO removal / μmol h^{-1} m^{-2}	75.77	20.23	44.75	60.60

7.2.2 Statistic analysis of air monitoring results

The air monitoring results and the environmental parameters recorded at the sampling points are shown in Table 7.2.

Table 7.2 NO_x concentration monitored from sampling points

Date	Temp / °C	RH / %	Photocatalytic paving block zone			Normal paving block zone		
			UV intensity / μw cm^{-2}	Breathing Zone NO_x Conc / ppb	Ground Level NO_x Conc / ppb	UV intensity / μw cm^{-2}	Breathing Zone NO_x Conc / ppb	Ground Level NO_x Conc / ppb
19/03/2007	20.8	79.4	493.3	373.7	292.7	430.0	280.4	233.2
16/04/2007	32.5	64.1	1040.0	355.3	343.3	773.3	157.4	152.4
07/05/2007	32.3	29.2	1563.3	304.7	285.0	1656.7	244.8	250.1
25/05/2007	30.2	78.3	770.0	427.7	406.0	446.7	281.0	295.0
11/06/2007	28.5	73.3	576.7	322.8	300.1	433.3	379.0	369.0
21/06/2007	32.2	54.5	830.0	264.7	236.3	1246.7	158.6	166.9
09/07/2007	33.2	72.5	423.3	243.8	216.8	333.3	155.7	147.8
25/07/2007	33.3	62.1	953.3	208.6	201.1	600.0	159.4	157.0
15/08/2007	29.7	75.1	240.0	411.7	381.3	213.3	282.3	276.3
30/08/2007	35.4	48.9	1290.0	284.0	259.3	336.7	221.1	211.4
10/09/2007	29.8	41.2	823.3	241.7	216.2	573.3	173.3	168.7
27/09/2007	33.4	52.8	1533.3	146.5	143.9	1456.7	144.8	141.3
08/10/2007	32.6	49.3	336.7	363.0	332.3	333.3	179.0	226.7
26/10/2007	35.3	52.4	876.7	388.3	373.3	896.7	207.0	187.8
14/11/2007	25.7	64.3	806.7	252.9	245.4	973.3	109.8	104.2
30/11/2007	19.3	58.3	623.3	200.7	173.1	683.3	110.6	100.2
06/12/2007	21.6	63.1	420.0	371.2	348.5	456.7	157.0	147.9
04/01/2008	18.2	61.5	713.3	188.2	161.6	810.0	77.5	77.6
23/01/2008	18.8	61.2	416.7	382.7	368.0	490.0	298.3	262.2
13/02/2008	15.3	40.0	490.0	265.1	264.5	380.0	80.9	104.2
29/02/2008	18.1	48.7	346.7	300.0	281.4	316.7	230.7	226.0
14/03/2008	20.3	54.8	506.7	302.3	293.1	290.0	177.1	162.5

Paired-samples T-test was carried out by using SPSS software to determine whether

there were nitrogen oxides (NO_x) concentration differences between air samples collected at the breathing zone and ground level at the sampling locations. For the photocatalytic paving block zone, based on the results shown in Table 3, the H_0 hypothesis that there was no difference in NO_x concentration between the samples collected at the breathing zone (ambient air) and the ground levels was rejected at a significant level of 0.05. In other words, it was 95% confident that there were differences of NO_x concentrations between the ambient air and the ground level air. The mean value shows that the NO_x concentration at ground level was 7.2% lower than that of the ambient air. A recent study by Guerrini and Peccati (2007a) also reported similar findings, showing that the NO_x concentration at a 180 cm high sampling point was about 10% higher than that of the ground level on a road paved by photocatalytic blocks.

Table 7.3 Results of paired-samples T-test for the NO_x concentration difference between ambient air and ground air for photocatalytic paving block zone

Null hypothesis (H_0): No difference of NO_x concentration between ambient air and ground air		
	Ambient air	Ground air
Mean concentration / ppb	299.98	278.33
Significance level	0.05	
T-value	6.333	
P-value	0.000 (two-tailed)	
Decision for H_0	Reject	

For the normal block paved road, the NO_x concentration difference was very little.

The H_0 hypothesis is not rejected by the paired-samples T-test analysis (Table 7.4). According to the statistical analysis of NO_x concentration for both the photocatalytic paving block zone and the non-photocatalytic paving block zone, the results suggest that photocatalytic blocks are effective in removing air pollutant such as NO_x in practical environmental conditions.

Table 7.4 Results of paired-samples T-test for the NO_x concentration difference between ambient air and ground air for normal paving block zone

Null hypothesis (H_0): No difference of NO_x concentration between ambient air and ground air		
	Ambient air	Ground air
Mean concentration / ppb	193.9	189.5
Significance level	0.05	
T value	1.105	
P value	0.281(two-tailed)	
Decision for H_0	Not reject	

Although the statistical analysis of the air monitoring data demonstrated the effectiveness of photocatalytic paving blocks in removing ground level air pollutants, the variation of wind direction, wind speed, weather conditions and traffic flow may influence the accuracy of the monitoring data. It also should be noticed that the NO_x concentrations in both ambient air and ground air sampled from the normal block road were lower than that sampled from the photocatalytic block road. The reason for this result may be related to the ventilation and dispersion of pollutants around the sampling sites. The normal block paved road was about 2 to 3 meters lower than the

traffic lane, while the photocatalytic paved road was completely parallel to the traffic lane. The dispersion of vehicle emission might have been hindered by the elevated road. Therefore, great caution should be taken for the interpretation of the monitoring data. Due to the fluctuation of meteorological factors, it is not suggested to use the air sampling to demonstrate the pollutant removal effectiveness of photocatalytic products in widely open space.

7.3 Sampling Box Monitoring

Fig. 7.1 shows the amount of nitrogen deposited in photocatalytic paving blocks over the exposure time. Compared with the results of the normal blocks (Fig. 7.2), the build-up of nitrate and nitrite with time well demonstrated the NO_x removal ability of the photocatalytic blocks in real application. It is noted that photocatalytic blocks which were put at the school located in Kowloon City trapped the highest amount of NO_x, followed by blocks monitored at MongKok and Tseung Kwan O. This trend is consistent with the NO_x concentration monitoring data obtained from the passive air samplers. This indicates that it is better to pave the photocatalytic blocks in areas with high air pollution level to fully utilize their air pollution conversion ability. To some extent, the amount of nitrogen eluted is a direct indicator of the air pollution level at the sampling sites. In addition, the accumulation of nitrate and nitrite ions in the photocatalytic blocks over three months was not equal to the sum of those deposited in each month. This can be attributed to the build-up of pollutants trapped in the block matrix, which might have covered the active surface of TiO_2, reducing the photocatalytic activity. Therefore, as pointed out in Section 7.2, the photocatalytic paving blocks should be washed (either by rain or manual cleaning)

periodically to restore the air pollutant conversion capability.

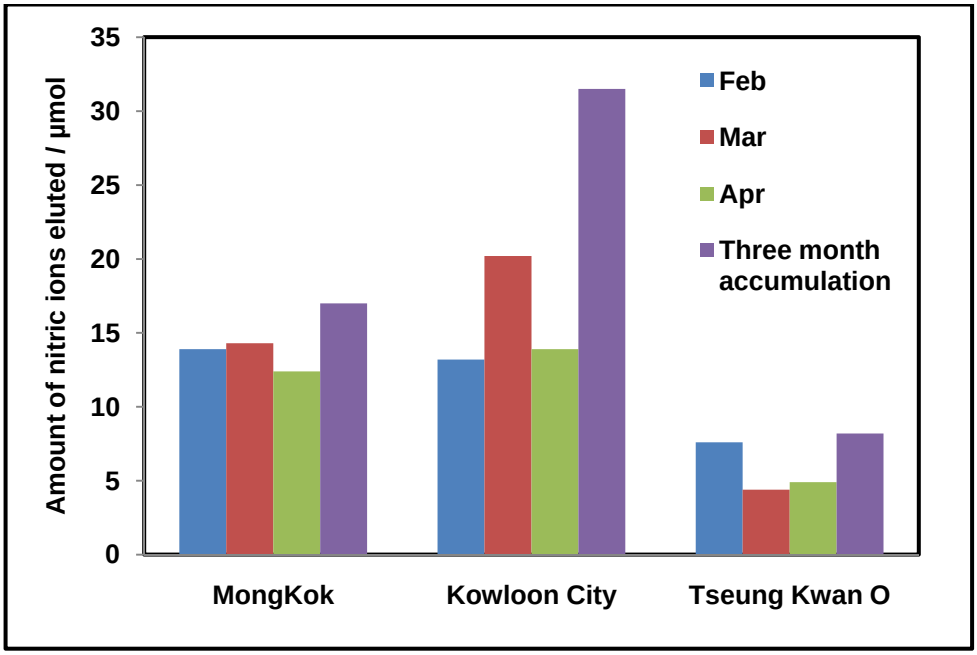

Figure 7.1 Amount of nitrogen eluted from photocatalytic blocks

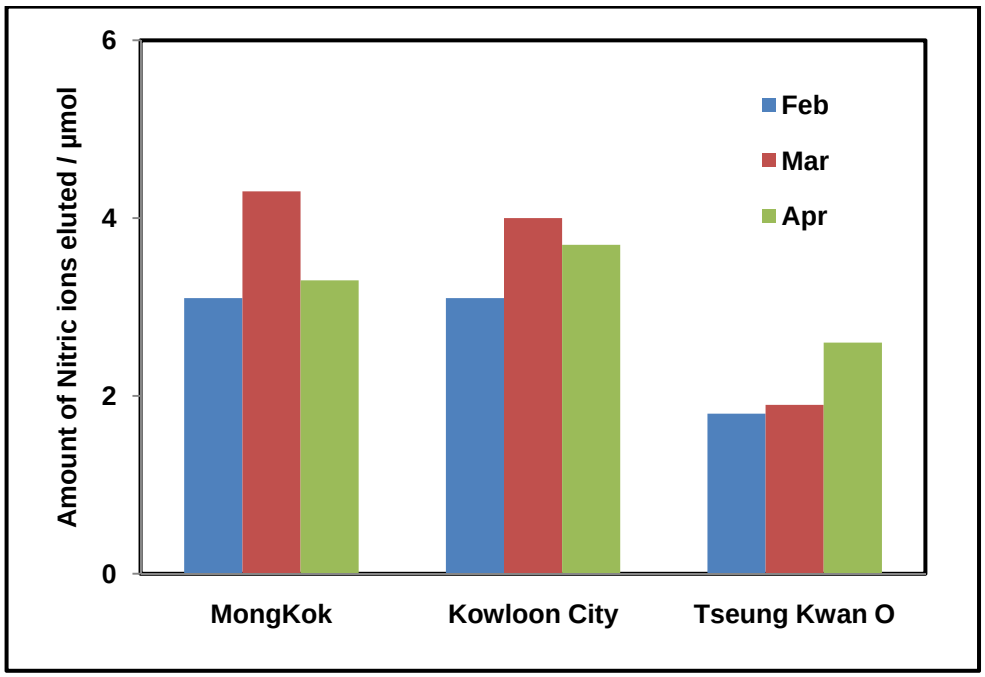

Figure 7.2 Amount of nitrogen eluted from normal blocks

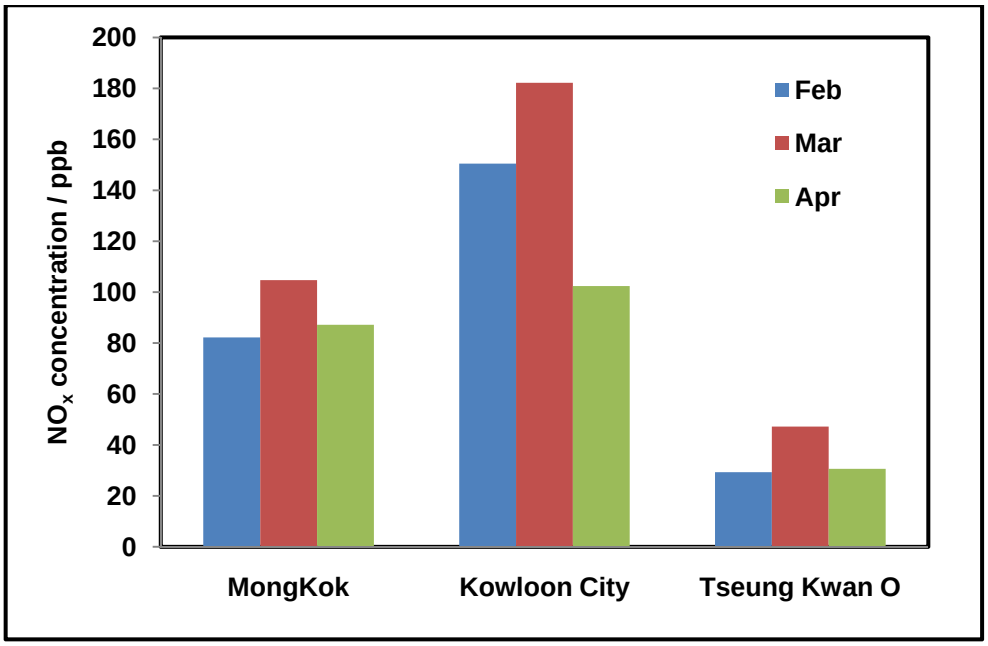

Figure 7.3 NO_x concentration at sampling sites

7.4 Summary

To evaluate the performance of the photocatalytic paving blocks used in complex ambient air conditions, two field trials were conducted. One was carried out at the campus of Hong Kong Polytechnic University, and another one was carried out at three primary schools in different districts. It was found that the NO_x removal efficiency of the paving blocks decreased with time. Washing the block surface with detergent or polishing the surface can regenerate the pollution removal ability. The statistic analysis of the monitoring data showed that 7.2 % NO_x was reduced at ground level compared with the NO_x concentration in the breathing zone in the one year monitoring period. However, it was found that it is difficult to determine the depollution effect of photocatalytic paving blocks in widely open area through simple air quality measurements. Compared with the air monitoring method, the sampling box method is more accurate in demonstrating the NO_x removal

performance. It is suggested that the photocatalytic blocks should be washed periodically and applied in heavily polluted area to maximize their pollutant removal function.

Chapter 8 Conclusions

8.1 Introduction

The aim of this study is to develop a multi-function environmentally friendly paving block which use solid wastes as construction material and can be applied to combat urban air pollution problems. Based on the research objectives, the potential of using recycled glass as aggregates in photocatalytic paving blocks was investigated (Chapter 4); the microstructure of hardened photocatalytic cement pastes and its influence on photocatalytic pollution degradation was examined (Chapter 5); the impact of adding nano-TiO_2 on the properties and hydration of cement-based materials was identified (Chapter 6); finally, monitoring frameworks for the measurement of air pollutant removal efficiency of the photocatalytic blocks in real application was developed and the long term air pollution removal performance was evaluated (Chapter 7). In this chapter, the conclusions of the above mentioned studies are drawn. Recommendations and suggestions for further research in photocatalytic paving blocks are proposed.

8.2 Conclusions

8.2.1 Influence of Utilizing Recycled Glass Cullets as Aggregates in Photocatalytic Concrete Surface Layer

The photocatalytic activity of concrete surface layers can be significantly improved when glass cullets are used as a replacement of aggregates. The incorporated glass cullets enable the TiO_2 within the inner part of the surface layer to play an active role in a photocatalytic reaction. The light transmittance property of glass cullets is a key factor for the efficiency enhancement of photocatalytic reactions. The color of glass has a significant impact on the photocatalytic performance of concrete surface layers. Lightly/mildly colored glass or clear glass performs better than the strongly colored ones. The particle size of aggregates may not be an important factor when compaction is a necessary procedure in the fabrication process of concrete surface layers. Nevertheless, high porosity of concrete structure which could be favorable to the internal dispersion of pollutants is still believed to be beneficial for pollutant removal. A significant loss of the photocatalytic activity of TiO_2 modified cementitious materials was observed during the curing process. This may be attributed to the decrease of pollutant adsorption capacity caused by the change of the pore structure in concrete.

8.2.2 Influence of the Microstructure of Cement Paste on Photocatalytic Pollution Degradation

The photocatalytic activity of cement pastes containing P25 is higher than those containing Anatase due to the difference of catalysts' surface area. With higher surface area P25 can provide more active sites which facilitate the surface reactions. White cement samples have higher photocatalytic activities than those prepared with OPC probably because the different light absorption characteristics. The descending trend of NO_x removal ability with the increment in curing age is not caused by the pozzolanic activity of TiO_2. TiO_2 is inert and chemically stable in the cement hydration reactions. It is likely that the hydration products (e.g. CSH gel) precipitate and accumulate with time, form diffusion barriers to both reactants and photons resulting in the observed decrease of NO_x removal during the cement hydration process. In general, the continuous accumulation of cement hydration products which covers the active sites of TiO_2 blocking the adsorption of reactants and the transport of photons should be the major factor leading to the loss of photocatalytic activity. The photocatalytic pollution removal capability of the composite cementitious materials not only depends on the activity of TiO_2 but also the properties of the components of cement paste and their spatial relationship. It is concluded that hydration and carbonation of TiO_2 modified cement paste has a negative effect on the efficiency of photocatalytic pollution degradation.

8.2.3 Hydration and Properties of Nano-TiO_2 Blended Cements

The influence of addition of nano-TiO_2 on cement-based materials was identified through experimental studies. The degree of hydration of at early hydration period is significantly enhanced by low dosages of nano-TiO_2 powder. TiO_2 is confirmed to be a non-reactive fine filler and is not well-dispersed in the cement matrix. They act as potential nucleation sites for the accumulation of hydration products. The total porosity of TiO_2 blended pastes is decreased and the reduction of pore volume mainly occurs within the capillary pore range. The acceleration of hydration rate and the change in microstructure also affects the physical and mechanical properties of the cementitious materials. The smaller the particle size of nano-TiO_2, the shorter the setting time and more water is required to maintain a standard consistence and workability. The compressive strength of the mortars is significantly improved, practically at early ages. In conclusion, nano-TiO_2 is not only a photocatalyst, it also has a catalytic effect in cement hydration reaction when it is mixed into cement-based materials.

8.2.4 Evaluation of the Air Pollutants Removal Performance of Photocatalytic Paving Blocks in Ambient Air Environment

When photocatalytic paving blocks are used in real environments, their pollution conversion efficiency decreases with time due to the accumulation of atmospheric aerosol pollutants on the surface of the blocks. Washing the block surface with detergent or polishing the surface can partly regenerate the pollutant removal ability. Although statistical analyses of air monitoring data can demonstrate the NO_x concentration difference in the air of the breathing zone and near the ground, it is difficult to determine the depollution efficiency of photocatalytic paving blocks in widely open areas through simple air quality measurements. The variation of wind direction, wind speed, weather conditions and traffic flow may influence the accuracy of the monitoring data. Compared with the air monitoring method, monitoring the build-up of nitrate and nitrite ions with time in blocks is much reliable in demonstrating the NO_x removal performance of the photocatalytic blocks in real applications. It is suggested that the photocatalytic blocks should be washed periodically and applied in heavily polluted area to maximize their pollutant removal function.

8.3 Suggestions

The followings suggestions are recommended for further studies in future:

- ▲ The photocatalytic activity of nano-TiO_2 is significantly reduced when they are mixed in cement-based materials. More research is needed to explore the possibility of controlling the pore structure of cement-based materials to increase the photocatalytic activity.

- ▲ It has been demonstrated that white cement samples containing TiO_2 have higher photocatalytic activities than those samples prepared with OPC. Several hypotheses are proposed to explain this phenomenon. Further work is needed to clarify this issue and find out the detailed mechanisms.

- ▲ The addition of nano-TiO_2 powders in to cement significantly accelerates the hydration rate resulting in rapid hydration heat release and the lost of workability. The content of TiO_2 in the composite must be carefully selected to avoid the undesirable effects and the amount of superplasticizer should be adjusted in accordance with the TiO_2 ratio to maintain workability and avoid cracking.

- ▲ Nano-particles are easy to aggregate and cannot be uniformly dispersed in cement-based materials. It is suggested that using surfactants or ultrasonic treatment to improve the dispersion.

- ▲ A large scale field trial project using the sampling box method should be carried out. The influence of environmental parameters, such as temperature, relative humidity, UV intensity, wind speed and direction on the performance

of photocatalytic paving blocks need to be identified.

▲ A life cycle analysis from both the environmental and economic viewpoint is suggested to be carried out to evaluate the cost-effectiveness of this technology.

▲ The self-cleaning and self-disinfecting functions of photocatalytic cement-based materials should be examined and explored.

APPENDIX A: Analytical Equipment and Procedures for IC Tests

Ion Chromatography (IC) was used to determine the concentrations of the nitrate and nitrite ions eluted from the block surface. The elution was first filtered through a 0.45 μm filter to avoid clogging the column. It was then analyzed by a Dionex DX500 ion chromatography with a conductivity detector, which was calibrated every time before analysis (Fig. A1). An AG11 guard column and an AS11 analytical column were used to separate the analytes. A Dionex ASRS ultra anion self regenerating suppressor ensured the lowest background noise levels and detection limits. A sampling loop of 50 μL was chosen. The eluent used in the IC analysis was a solution containing 0.0027 mol L^{-1} of Na_2CO_3 and 0.001 mol L^{-1} of $NaHCO_3$. Its flowrate during the analysis was kept 2 mL min^{-1}.

The mass concentrations of anions in the elution were calculated using the peak areas according to the calibration function used (Fig. A2). The concentrations of the anions in the calibration function are: 1.0 mg L^{-1}, 5.0 mg L^{-1}, 10.0 mg L^{-1}, 15.0 mg L^{-1} and 20.0 mg L^{-1} respectively.

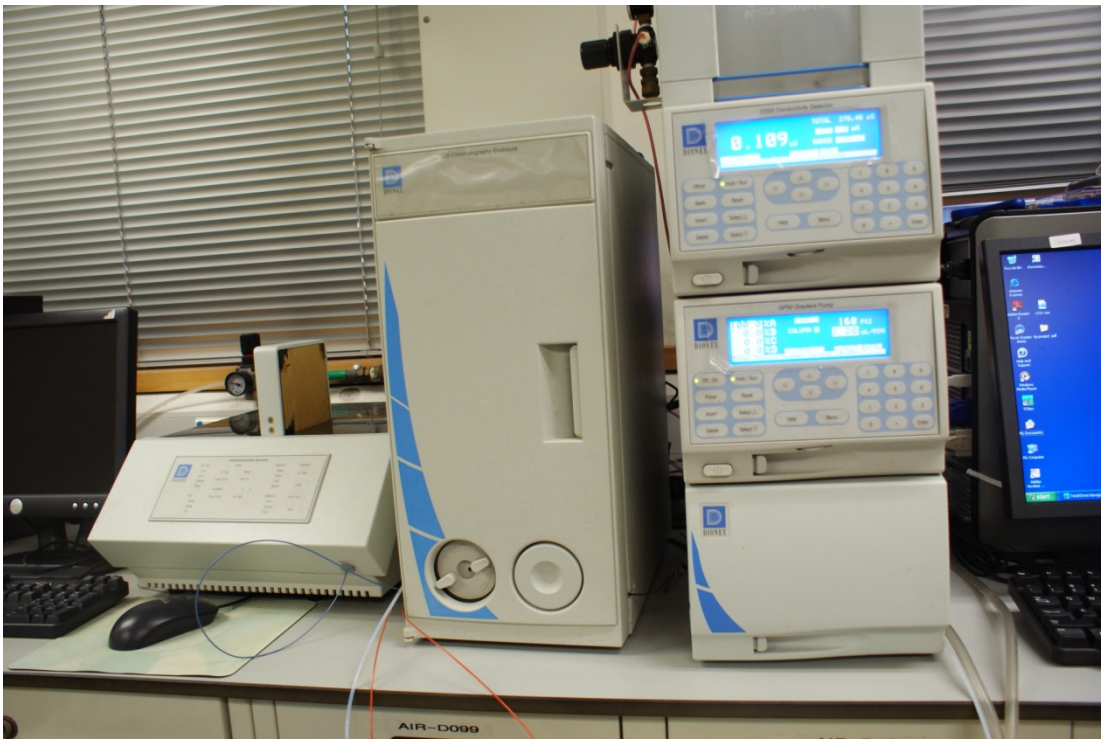

Figure A1 Dionex DX500 ion chromatography

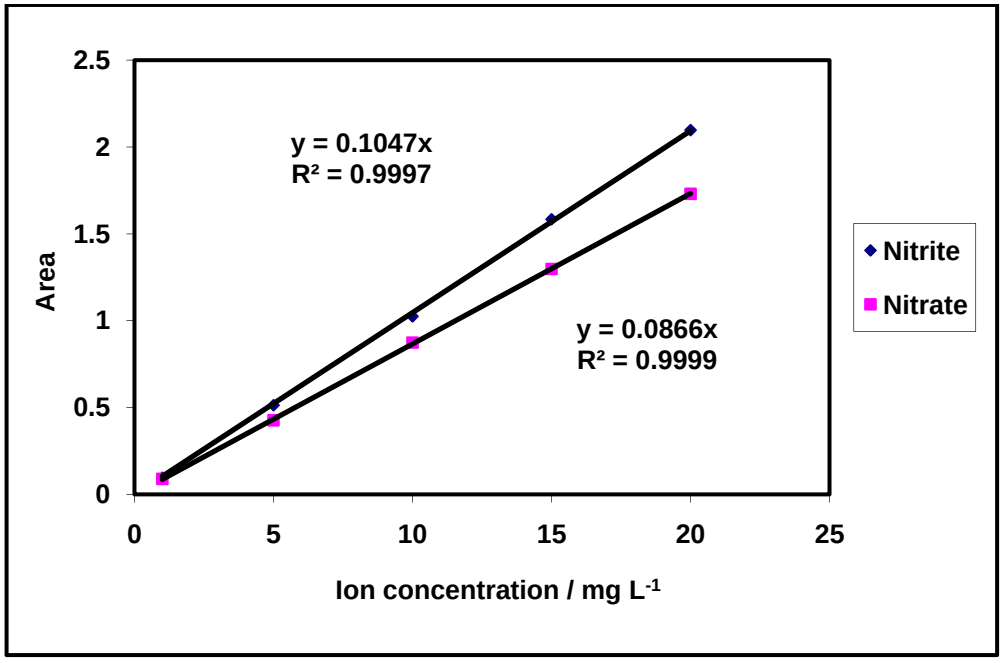

Figure A2 IC calibration function

APPENDIX B: XRD Patterns

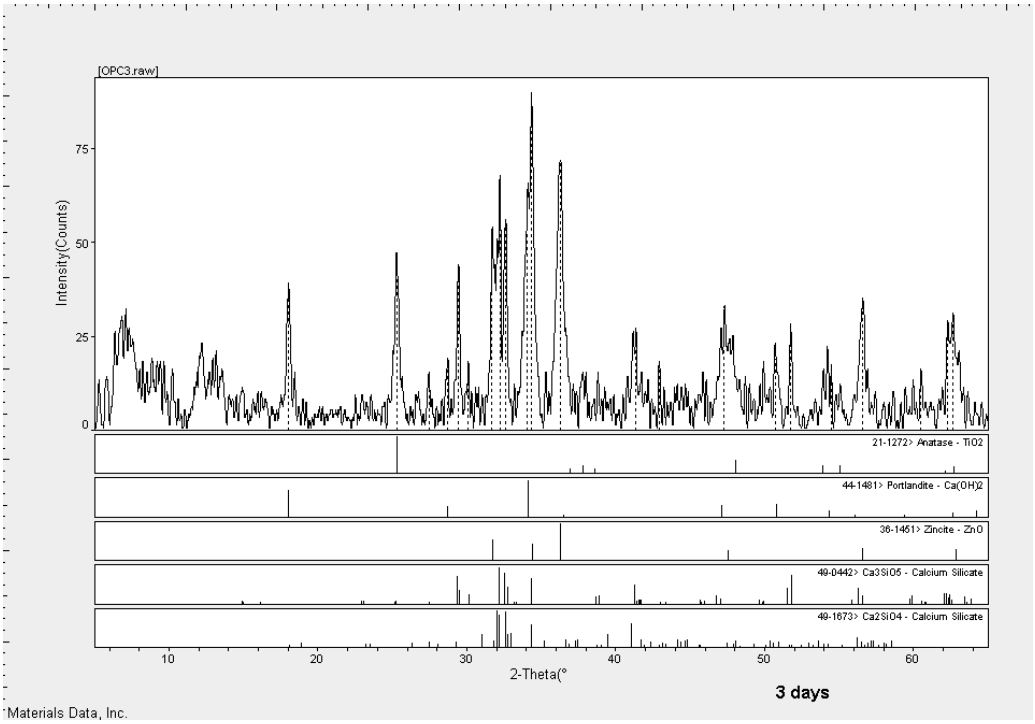

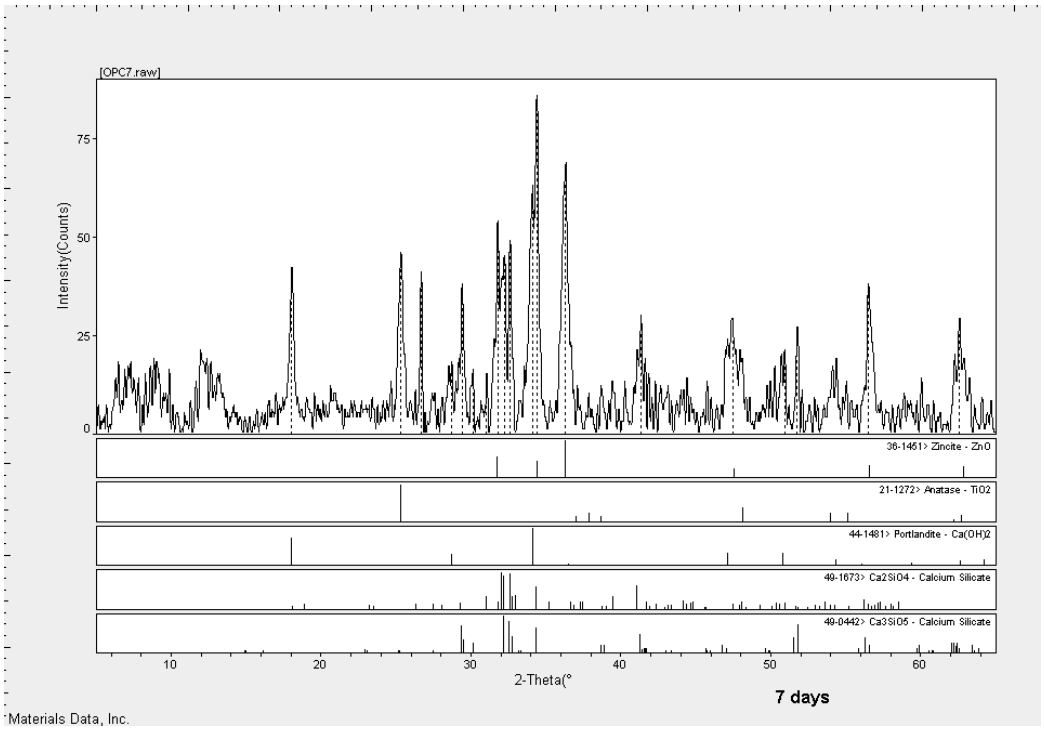

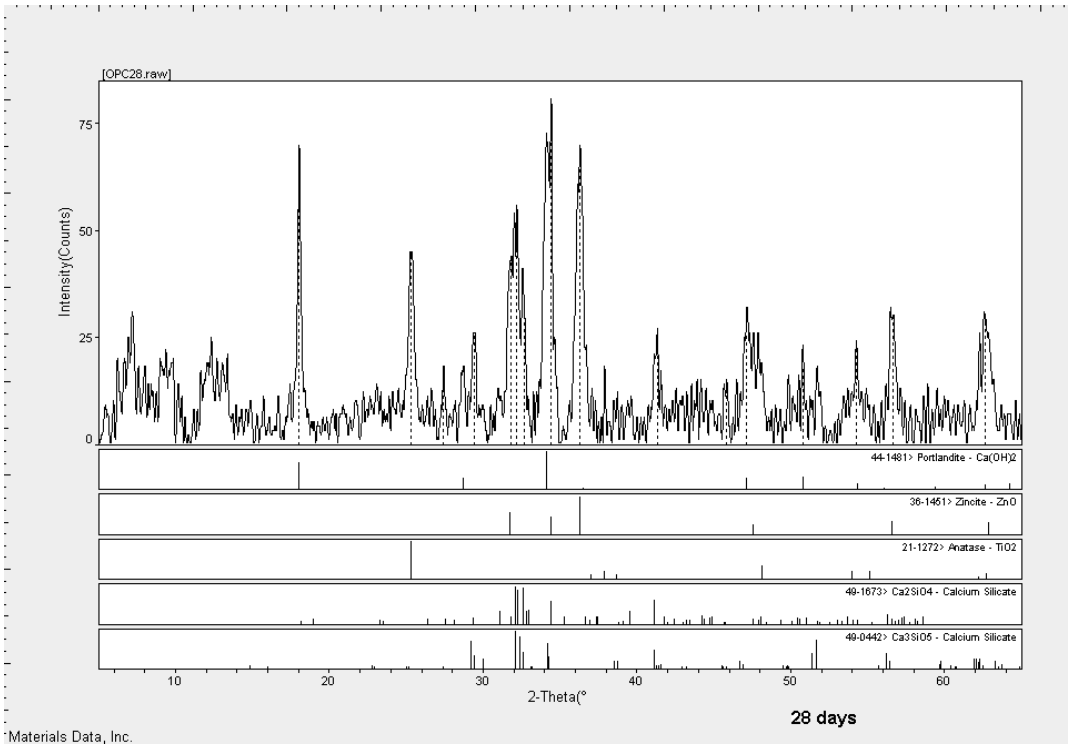

Figure B1 XRD patterns of 10% w/w P25 blended pastes hydrated at 3, 7 and 28 days

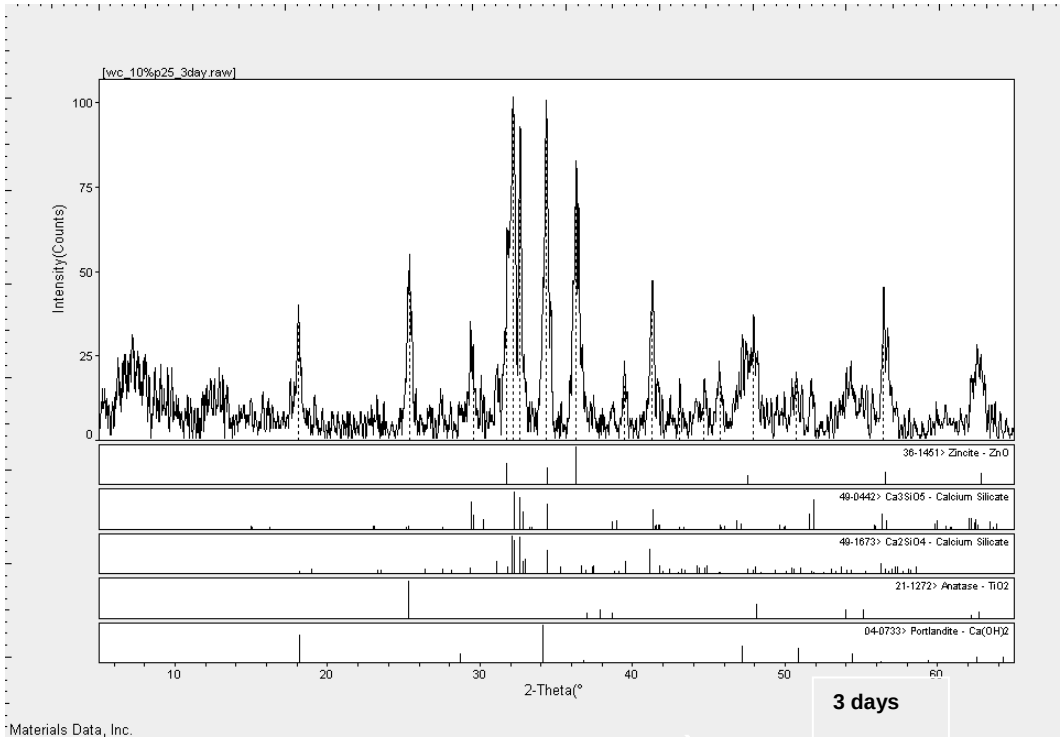

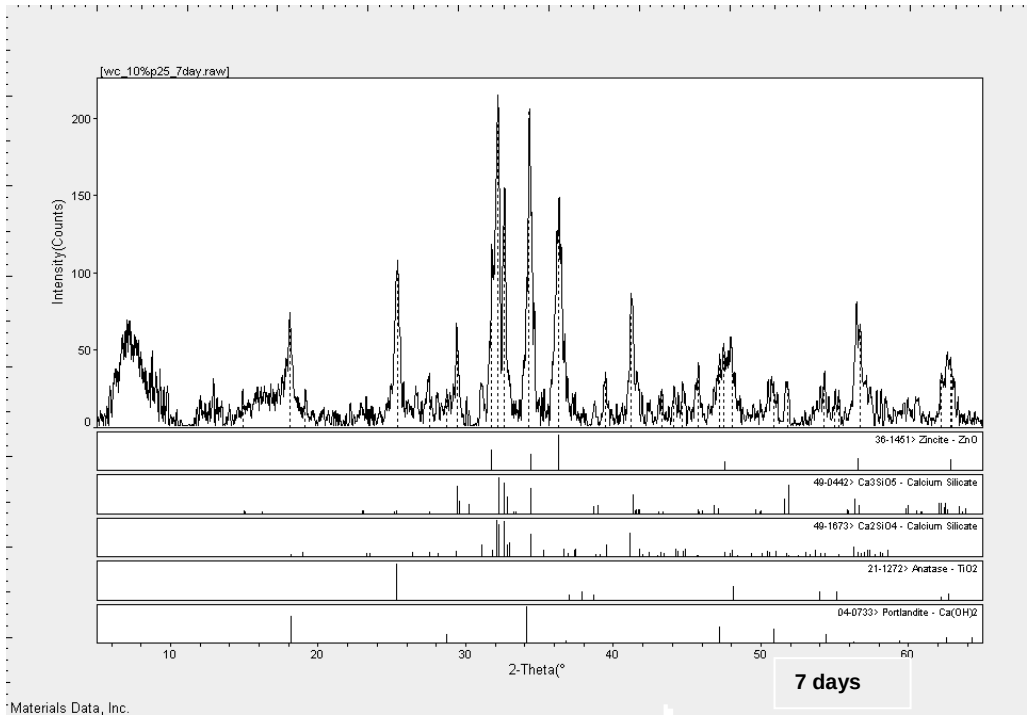

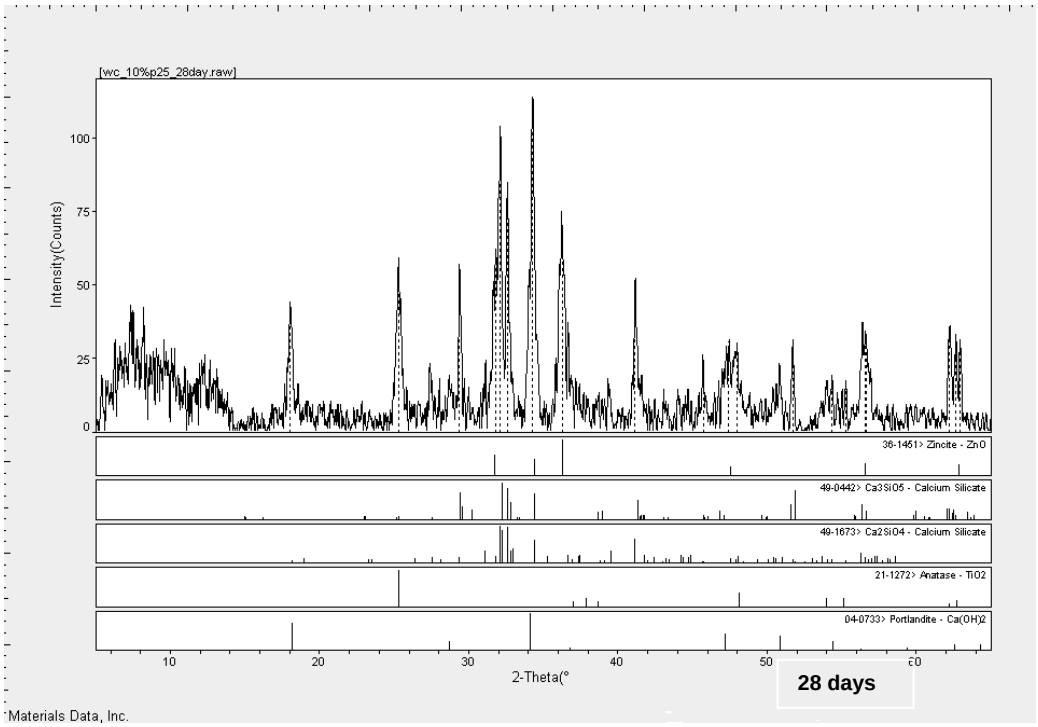

Figure B2 XRD patterns of WC_10%P25 paste hydrated at 3, 7 and 28 days

APPENDIX C: Carbonation Treatment

70 mm length cubic samples were produced using a batch of OPC and P25 mixture (10% addition of P25 by the weight of cement) with a w/c ratio of 0.35. For the samples subjected to accelerated carbonation, the two ends of each cube were coated with epoxy resin in order to ensure that carbon dioxide could diffuse into the cubes in a two-dimensional mode. After 28 days curing, the samples were transferred to a sealed chamber with a CO_2 concentration of 4% by volume to accelerate the carbonation process. The temperature and relative humidity in the chamber was kept at 20 °C and 50%. The normal samples were kept in an environmental chamber with the same temperature and humidity conditions as the carbonation chamber.

The carbonated and normal samples were tested for NO_x removal after the 56, 90 and 120 days of curing using the same experimental set-up described in section 3.4.1.3. In order to eliminate the influence of environmental factors, a strong UV irradiation provided by two 8W UV–A fluorescent lamps (TL 8W/08 BLB, Philips, Holland, Fig. C1) were used in this experiment. The wavelength of the lamps ranged from 300 to 400 nm with a maximum intensity at 365 nm. The UV intensity was 10 W m^{-2} at the center of the reactor.

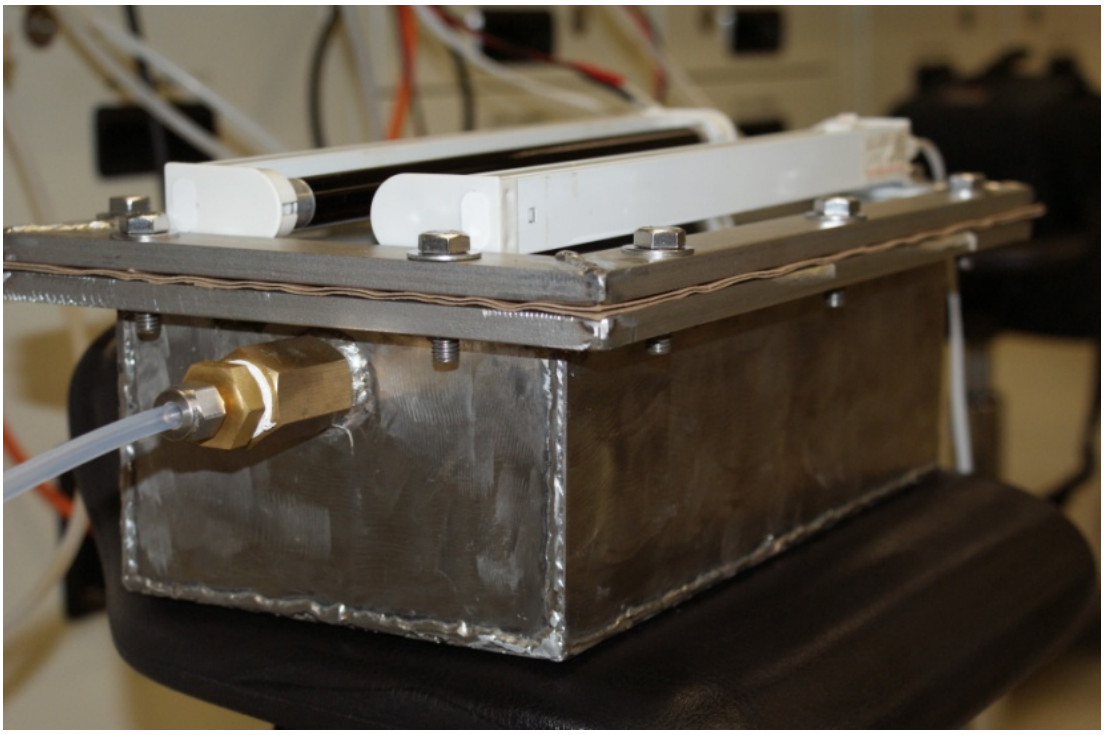

Figure C1 Reactor used for NOx removal test (samples subjected to accelerated carbonation)

The determination of carbonation depth followed the instruction of a standard method, BS EN 14630. The hydrated cement cubes were split after photocatalytic NO_x removal test. The freshly split surface was cleaned and then sprayed with a solution of the phenolphthalein pH indicator. The solution of phenolphthalein indicator was made by dissolving 1 g phenolphthalein in 70 ml ethyl alcohol (99.0%, V/V) and diluted to 100 ml with distilled water. In the noncarbonated part of the sample, where the cement paste was still highly alkaline, a purple-red color was obtained. In the carbonated part of the specimen where the alkalinity of paste is reduced, no coloration occurred. Immediately after spraying the indicator, the average depth of the colorless phenolphthalein area was measured from three points, perpendicular to the two edges of the split face.

REFERENCES

Agrios, A.G. and Pichat, P. State of the art and perspectives on materials and applications of photocatalysis over TiO_2. *Applied Electrochemistry* **2005**, 35 (7), 655-663.

Alarcon-Ruiz, L., Platret, G., Massieu, E. and Ehrlacher, A. The use of thermal analysis in assessing the effect of temperature on a cement paste. *Cement and Concrete Research* **2005**, 35 (3), 609-613.

Alberici, R.M. and Jardim, W.F. Photocatalytic destruction of VOCs in the gas-phase using titanium dioxide. *Applied Catalysis B: Environmental* **1997**, 14 (1-2), 55-68.

Aligizaki, K.K. *Pore structure of cement-based materials: testing, interpretation and requirements;* Taylor&Francis: Oxon, 2006; pp 5-21.

Allen, N.S., Edge, M., Verran, J., Straatton, J., Maltby, J. and Bygott, C. Photocatalytic titania based surfaces: Environmental benefits. *Polymer Degradation and Stability* **2008**, 93 (9), 1632-1646.

Amama, P.B., Itoh, K. and Murabayashi, M. Photocatalytic degradation of trichloroethylene in dry and humid atmospheres: role of gas-phase reactions. *Journal of Molecular Catalysis A: Chemical* **2004**, 217 (1-2), 109-115.

Ameen, M.M. and Raupp, G.B. Reversible catalyst deactivation in the photocatalytic oxidation of dilute o-xylene in air. *Journal of Catalysis* **1999**, 184 (1), 112-122.

Amézaga-Marid, P., Nevárez-Moorillón, G.V., Orrantia-Borunda, E. and Miki-Yoshida, M. Photoinduced bactericidal activity against Pseudomonas

aeruginosa by TiO_2 based thin films. *FEMS Microbiology Letters* **2002**, 211 (2), 183-188.

Arandigoyen, M., Bicer-Simsir, B., Alvarez, J.I. and Lange, D.A. Variation of microstructure with carbonation in lime and blended pastes. *Applied Surface Science* **2006**, 252 (20), 7562-7571.

ASTM C109. *Standard Test Method for Compressive Strength of Hydraulic Cement Mortars (Using 2-in. or [50-mm] Cube Specimens)*; ASTM International, 2008.

ASTM C 125-07. *Standard terminology relating to concrete and concrete aggregates*; ASTM International, 2007.

Auvinen, J. and Wirtanen, L. The influence of photocatalytic interior paints on indoor air quality. *Atmospheric Environment* **2008**, 42 (18), 4101-4112.

Beeldens, A. Air purification by road materials: results of the test project in Antwerp. In *Photocatalysis, Environment and Construction materials*, Proceedings of the International RILEM Symposium, Italy, 2007; Baglioni, P. and Cassar, L., Eds.; RILEM: Bagneux, 2007.

Bekbolet, M. Photocatalytic bactericidal activity of TiO_2 in aqueous suspensions of E. coli. *Water Science and Technology* **1997**, 35 (11-12), 95-100.

Benoit-Marquie, F., Wilkenhoner, U., Simon, V., Braun, A., Oliveros, E. and Maurette, M.T. VOC photodegradation at the gas-solid interface of a TiO_2 photocatalyst part I: 1-butanol and 1-butylamine. *Journal of Photochemistry and Photobiology A: Chemistry* **2000**, 132 (3), 225-232.

Betioli, A.M., Filho, J.H., Cincotto, M.A., Gleize, P.J.P. and Pileggi, R.G. Chemical interaction between EVA and Portland cement hydration at early-age. *Construction and Building Materials* **2009**, 23 (11), 3332-3336.

Boonstra, A.H. and Mutsares, C.A.H.A. Relation between the photoadsorption of oxygen and the number of hydroxyl groups on a titanium dioxide surface. *Journal of Physical Chemistry* **1975**, 79, 1694-1698.

Brandt, A.M. *Cement-based composites: Materials, mechanical properties and performance,* 2nd ed.; Taylor&Francis: Oxon, 2009; p 145.

BS EN 14630. *Products and systems for the protection and repair of concrete structures — Test methods — Determination of carbonation depth in hardened concrete by the phenolphthalein method*; European Committee for Standardization, 2006.

BS EN 196-3. *Methods of testing cements — Part 3: Determination of setting times and soundness*; European Committee for Standardization, 2005.

Bygott, C.E., Maltby, J.E., Stratton, J.L. and McIntyre, R. Photocatalytic coatings for the construction industry. In *Photocatalysis, Environment and Construction materials*, Proceedings of the International RILEM Symposium, Italy, 2007; Baglioni, P. and Cassar, L., Eds.; RILEM: Bagneux, 2007.

Cabrera, J.G. and Lynsdale, C.J. A new gas permeameter for measuring the permeability of mortar and concrete. *Magazine of Concrete Research* **1988**, 40 (144), 177-182.

Camera, R.G. and Santarelli, F. Optimization of the thickness of a photocatalytic film on the basis of the effectiveness factor. *Catalysis Today* **2007**, 129 (1-2), 161-168.

Cao, L., Gao, Z., Suib, S.L., Obee, T.N., Hay, S.O., and Freihauty, J.D. Photocatalytic oxidation of toluene on nanoscale TiO_2 catalysts: studies of deactivation and regeneration. *Journal of Catalysis* **2000**, 196 (2), 253-261.

Cassar, L. Photocatalysis of cementitious materials: clean buildings and clear air. *MRS Bulletin* **2004**, 29 (5), 328-331.

De Ceukelaire, L. and Van Nieuwenburg, D. Accelerated carbonation of a blast-furnace cement concrete. *Cement and Concrete Research* **1993**, 23 (2), 442-452.

Chen, C.H., Huang, R., Wu, J.K. and Yang, C.C. Waste E-glass particles used in cementitious mixtures. *Cement and Concrete Research* **2006**, 36 (3), 449-456.

Chen, D., Li, F. and Ray, A.K. External and internal mass transfer effect on photocatalytic degradation. *Catalysis Today* **2001**, 66 (3-4), 475-485.

Cho, K.C., Hwang, K.C., Sano, T., Takeuchi, K. and Matsuzawa, S. Photocatalytic performance of Pt-loaded TiO_2 in the decomposition of gaseous ozone. *Journal of Photochemistry and Photobiology A: Chemistry* **2004**, 161 (2-3), 155-161.

Chung, D. *Multifunctional cement-based materials*; Marcel Dekker: New York, 2003.

Copeland, L.E., and Bragg, R.H. Quantitative X-ray diffraction analysis. *Analytical Chemistry* **1958**, 30, 196–201.

Dadjour, M.F., Ogino, C., Matsumura, S. and Shimizu, N. Kinetics of disinfection of Escherichia coli by catalytic ultrasonic irradiation with TiO_2. *Biochemical Engineering Journal* **2005**, 25 (3), 243-248.

Dalton, J.S., Janes, P.A., Jones, N.G., Nicholson, J.A., Hallam, K.R. and Allen, G.C. Photocatalytic oxidation of NO_x gases using TiO_2: a surface spectroscopic approach. *Environmental Pollution* **2002**, 120 (2), 415-422.

Demeestere, K., Dewulf, J., De Witte, B., Beeldens, A. and Van Langenhove, H. Heterogeneous photocatalytic removal of toluene from air on building materials enriched with TiO_2. *Building and Environment* **2008**, 43 (4), 406-414.

Demeestere, K., Dewluf, J., De Witte, B. and Van Langenhove, H. Titanium dioxide mediated heterogeneous photocatalytic degradation of gaseous dimethyl sufide: parameter study and reaction pathways. *Applied Catalysis B: Environmental* **2005**, 60 (1-2), 93-106.

Duan, X., Su, D., Zhu, Z., Chen, X. and Shi, P. Photocatalytic decomposition of toluene by TiO_2 film as photocatalyst. *Journal of Environmental Science & Health Part A-Toxic/Hazardous Substances & Environmental Engineering* **2002**, 37, 679-692.

Dubosc, A., Escadeillas, G. and Blanc, P.J. Characterization of biological stains on external concrete walls and influence of concrete as underlying material. *Cement and Concrete Research* **2001**, 31 (11), 1613-1617.

Ducman, V., Mladenovic, A. and Suput, J.S. Lightweight aggregate based on waste glass and its alkali-silica reactivity. *Cement and Concrete Research* **2002**, 32 (2), 223-226.

Escalante-Garcia, J.I. Nonevaporable water from neat OPC and replacement materials in composite cements hydrated at different temperatures. *Cement and Concrete Research* **2003**, 33 (11), 1883-1888.

Espinosa, R.M. and Franke, L. Influence of the age and drying process on pore structure and sorption isotherms of hardened cement paste. *Cement and Concrete Research* **2006**, 36 (10), 1969-1984.

Fox, M.A. and Dulay, M.T. Heterogeneous photocatalysis. *Chemical Reviews* **1993**, 93 (1), 341-357.

Frank, S.N. and Bard, A.J. Heterogeneous photocatalytic oxidation of cyanide ion in aqueous solution at TiO_2 powder. *Journal of American Chemical Society* **1977**, 99, 303-304.

Fujishima, A. and Honda, K. Electrochemical photolysis of water at a semiconductor electrode. *Nature* **1972**, 238, 37-38.

Fujishima, A., Hashimoto, K. and Watanabe, T. *TiO_2 photocatalysis: fundamentals and applications*; BKC: Japan, 1999.

Fujishima, A., Rao, T.N. and Tryk, D.A. Titanium dioxide photocatalysis. *Journal of Photochemistry and Photobiology C: Photochemistry Reviews* **2000**, 1 (1), 1-21.

Fujishima, A. and Zhang, X.T. Titanium dioxide photocatalysis: present situation and future approaches. *Comptes Rendus Chimie* **2006**, 9 (5-6), 750-760.

Fujishima, A., Zhang, X.T. and Tryk, D.A. TiO_2 photocatalysis and related surface phenomena. *Surface Science Reports* **2008**, 63 (12), 515-582.

Gartner, E.M., Young, J.F., Damidot, D.A. and Jawed, I. Hydration of Portland cement. In *Structure and Performance of cements*; Bensted, J. and Barnes, P. Eds.; Spon Press: London, 2002.

Gonen, T. and Yazicioglu, S. The influence of compaction pores on sorptivity and carbonation of concrete. *Construction and Building Materials* **2006**, 21 (5), 1040-1045.

Goodeve, C.F. and Kitchener, J.A. The mechanism of photosensitization by solids. *Transaction of the Faraday Society* **1938**, 34, 902-908.

Guan, K. Relationship between photocatalytic activity, hydrophilicity and self-cleaning effect of TiO_2/SiO_2 films. *Surface and Coatings Technology* **2005**, 191 (2-3), 155-160.

Guarino, M., Costa, A. and Porro, M. Photocatalytic TiO_2 coating – to reduce ammonia and greenhouse gases concentration and emission from animal husbandries. *Bioresource Technology* **2008**, 99 (7), 2650-2658.

Guerrini, G.L. and Peccati, E. Photocatalytic cementitious roads for depollution. In *Photocatalysis, Environment and Construction materials*, Proceedings of the International RILEM Symposium, Italy, 2007a; Baglioni, P. and Cassar, L., Eds.; RILEM: Bagneux, 2007.

Guerrini, G.L., Plassais, A., Pepe, C. and Cassar, L. Use of photocatalytic cementitious materials for self-cleaning applications. In *Photocatalysis, Environment and Construction materials*, Proceedings of the International RILEM Symposium, Italy, 2007b; Baglioni, P. and Cassar, L., Eds.; RILEM: Bagneux, 2007.

Gutteridge, W.A. and Dalziel, J.A. Filler cement the effect of the secondary component on the hydration of Portland cement. *Cement and Concrete Research* **1990**, 20 (6), 778-782.

Hager, S. and Bauer, R. Heterogeneous photocatalytic oxidation of organics for air purification by near UV irradiated titanium dioxide. *Chemosphere* **1999**, 38 (7), 1549-1559.

Herz, R.K. Intrinsic kinetics of first-order reactions in photocatalytic membranes and layers. *Chemical Engineering Journal* **2004**, 99 (3), 237-245.

Hobbs, D.W. *Alkali-silica reaction in concrete*; Thomas Telford: London, 1988.

Huang, Z., Maness, P.C., Blake, D.M., Wolfrum, E.J., Smolinski, S.L. and Jacoby, W.A. Bactericidal mode of titanium dioxide photocatalysis. *Journal of Photochemistry and Photobiology A: Chemistry* **2000**, 130 (2-3), 163-170.

Hüsken, G., Hunger, M. and Brouwers, H. Comparative study on cementitious products containing titanium dioxide as photo-catalyst. In *Photocatalysis, Environment and Construction materials*, Proceedings of the International RILEM Symposium, Italy, 2007; Baglioni, P. and Cassar, L., Eds.; RILEM: Bagneux, 2007.

Ichiura, H., Kitaoka, T., and Tanaka, H. Removal of indoor pollutants under UV irradiation by a composite TiO_2-zeolite sheet prepared using a papermaking technique. *Chemosphere* **2003**, 50 (1), 79-83.

Ismail, Z.Z. and AL-Hashmia, E.A. Recycling of waste glass as a partial replacement for fine aggregate in concrete. *Waste Management* **2009**, 29 (2), 655-659.

Jacoby, W.A., Maness, P.C., Wolfrum, E.J., Blake, D.M. and Fennell, J.A. Mineralization of bacterial cell mass on a photocatalytic surface in Air. *Environmental Science and Technology* **1998**, 32 (17), 2650-2653.

JIS R 1701-1. *Fine ceramics (advanced ceramics, advanced technical ceramics) – Test method for air purification performance of photocatalytic materials - Part I: Removal of nitric oxide*; Japanese Standard Association, 2004.

Jo, B.W., Kim, C.H., Tae, G.H., and Park, J.B. Characteristics of cement mortar with nano-SiO_2 particles. *Construction and Building Materials* **2007**, 21 (6), 1351-1355.

Kadri, E.H. and Duval, R. Hydration heat kinetics of concrete with silica fume. *Construction and Building Materials* **2009**, 23 (11), 3388-3392.

Kaneko, M. and Okura, I. *Photocatalysis: science and technology*; Kodansha: Tokyo, 2002.

Kim, S.B., Hwang, H.T. and Hong, S.C. Photocatalytic degradation of volatile organic compounds at the gas-solid interface of a TiO_2 photocatalyst. *Chemosphere* **2002**, 48 (4), 437-444.

Kim, S.B. and Hong, S.C. Kinetic study for photocatalytic degradation of volatile organic compounds in air using thin film TiO_2 photocatalyst. *Applied Catalysis B: Environmental* **2002**, 35 (4), 305-315.

Kisch, H. What is photocatalysis? In *Photocatalysis: Fundamentals and applications*; Serpone, N. and Pelizzetti, E. Eds; John Willy & Sons: New York, 1989.

Kou S.C. and Poon, C.S. Properties of self-compacting concrete prepared with recycled glass aggregate. *Cement and Concrete Composites* **2009**, 31 (2), 107-113.

Kurth, J.C., Giannantonio, D.J., Allain, F., Sobecky, P.A. and Kurtis, K.E. Mitigating biofilm growth through the modification of concrete design and practice. In *Photocatalysis, Environment and Construction materials*, Proceedings of the International RILEM Symposium, Italy, 2007; Baglioni, P. and Cassar, L., Eds.; RILEM: Bagneux, 2007.

Lackhoff, M., Prieto, X., Nestle, N., Dehn, F. and Niessner, R. Photocatalytic activity of semiconductor-modified cement—influence of semiconductor type and cement ageing. *Applied Catalysis B: Environmental* **2003**, 43 (3), 205-216.

Lam, C.S., Poon, C.S. and Chan D. Enhancing the performance of pre-cast concrete blocks by incorporating waste glass – ASR consideration. *Cement and Concrete Composites* **2007**, 29 (8), 616-625

Li, G. Properties of high-volume fly ash concrete incorporating nano-SiO_2. *Cement and Concrete Research* **2004**, 34 (6), 1043-1049.

Li, H., Xiao, H.G., Yuan, J. and Ou, J. Microstructure of cement mortar with nano-particles. *Composites Part B: Engineering* **2004**, 35 (2), 185-189.

Li, K., Liu, S.Y., Khetarpal, S. and Chen D.H. TiO_2 photocatalytic oxidation of toluene and PCE vapor in the air. *Journal of Advanced Oxidation Technology* **1998**, 3, 311-314.

Lim, T.H., Jeong, S.M., Kim, S.D. and Gyenis, J. Photocatalytic decomposition of NO by TiO_2 particles. *Journal of Photochemistry and Photobiology* **2000**, 134 (3), 209-217.

Lin, D.F., Lin, K.L., Chang, W.C., Luo, H.L. and Cai, M.Q. Improvements of nano-SiO_2 on sludge/fly ash mortar. *Waste Management* **2008a**, 28 (6), 1081-1087.

Lin, K.L., Chang, W.C., Lin, D.F., Luo, H.L. and Tsai, M.C. Effects of nano-SiO_2 and different ash particle sizes on sludge ash–cement mortar. *Journal of Environmental Management* **2008b**, 88 (4), 708-714.

Linkous, C.A., Carter, G.J., Locuson, D.B., Ouellette, A.J., Slattery, D.K. and Smitha, L.A. Photocatalytic inhibition of algae growth using TiO_2, WO_3, and cocatalyst modifications. *Environmental Science and Technology* **2000**, 34 (22), 4754 -4758.

Maggos, T., Plassais, A., Bartzis, J.G., Vasilakos, C., Moussiopoulos, N. and Bonafous, L. Photocatalytic degradation of NO_x in a pilot street canyon configuration using TiO_2-mortar panels. *Environmental Monitoring and Assessment* **2008**, 1369 (1-3), 35-44.

Maggos, T., Bartzis, J.G., Liakou, M. and Gobin, C. Photocatalytic degradation of NO_x gases using TiO_2-containing paint: a real scale study. *Journal of Hazardous Materials* **2007**, 146 (3), 668-673.

Matsunaga, T., Tomoda, R., Nakajima, T. and Wake, H. Photoelectrochemical sterilization of microbial cells by semiconductor powders. *FEMS Microbiology Letters* **1985**, 29 (1-2), 211-214.

Mills, A. and Hunte, S.L. An overview of semiconductor photocatalysis. *Journal of Photochemistry and Photobiology A: Chemistry* **1997,** 108 (1), 1-35.

Mills, A. and Lee, S.K. A web-based overview of semiconductor photochemistry-based current commercial applications. *Journal of Photochemistry and Photobiology A: Chemistry* **2002**, 152 (1-3), 233-247.

Mindess, S., Young J.F. and Darwin D. *Concrete*; Pearson: New Jersey, 2003.

Mohseni, M. and David, A. Gas phase vinyl chloride (VC) oxidation using TiO_2-based photocatalysis. *Applied Catalysis B: Environmental* **2003**, 46 (2), 219-228.

Motohashi, K. and Inukai, T. Self-cleaning performance evaluation of commercial photocatalyst coating materials through 5 years outdoor exposure. In *Photocatalysis, Environment and Construction materials*, Proceedings of the International RILEM Symposium, Italy, 2007; Baglioni, P. and Cassar, L., Eds.; RILEM: Bagneux, 2007.

Newman, J. and Choo B.S. *Advanced concrete technology: constituent materials*; Elsevier: Oxford, 2003.

Noguchi, T., Fujishima, A., Sawunytama, P. and Hashimoto, K. Photocatalytic degradation of gaseous formaldehyde using TiO_2 film. *Environmental Science and Technology* **1998**, 32 (23), 3831-3833.

Obee, T.N. Photooxidation of sub-parts-million toluene and formaldehyde levels on titania using a glass-plate reactor. *Environmental Science and Technology* **1996**, 30 (12), 3578-3584.

Obee, T.N. and Brown, R.T. TiO_2 photocatalysis for indoor air applications: effects of humidity and trace contaminant levels on the oxidation rates of formaldehyde, toluene, and 1,3-butadiène. *Environmental Science and Technology* **1995**, 29 (5) 1223-1231.

Obee, T.N. and Hay, S.O. Effects of moisture and temperature on the photooxidation of ethylene on titania. *Environmental Science and Technology* **1997**, 31 (7), 2034-2038.

Ohko, Y., Hashimoto, K. and Fujishima, A. Kinetics of photocatalytic reactions under extremely low-intensity UV illumination on titanium dioxide thin films. *Journal of Physical Chemistry A* **1997**, 101 (43), 8057-8062.

Ollis, D.F., Pelizzetti, E. and Serpone, N. Photocatalyzed destruction of water contaminants. *Environmental Science and Technology* **1991**, 25 (9), 1523-1529.

Oua, H.H. and Lo, S.L. Photocatalysis of gaseous trichloroethylene (TCE) over TiO_2: The effect of oxygen and relative humidity on the generation of dichloroacetyl chloride (DCAC) and phosgene. *Journal of Hazardous Materials* **2007**, 146 (1-2), 302-308.

Parmon, V.N. Photocatalysis as a phenomenon: aspects of terminology. *Catalysis Today* **1997**, 39 (3), 137-144.

Peral, J. and Ollis, D.F. Heterogeneous photocatalytic oxidation of gas-phase organics for air purification - acetone, 1-butanol, butyraldehyde, formaldehyde, and meta-xylene oxidation. *Journal of Catalysis* **1992**, 136 (2), 554-565.

Peruchon, L., Puzenat, E., Girard-Egrot, A., Bium, L., Herrmann, J.M. and Guillard, C. Characterization of self-cleaning glasses using Langmuir-Blodgett technique to control thickness of stearic acid multilayers - Importance of spectral emission to define standard test. *Journal of Photochemistry and Photobiology A: Chemistry* **2008**, 197 (2-3), 170-176.

Pfaender, H.G. *Schott Guide to Glass,* 2nd ed.; Chapman & Hall: London, 1996.

Pichat, P. and Herrmann, J.M. Adsorption-desorption, related mobility and reactivity in photocatalysis. In *Photocatalysis: Fundamentals and applications*; Serpone, N. and Pelizzetti, E. Eds; John Willy & Sons: New York, 1989.

Poon, C.S. and Cheung, E. NO removal efficiency of photocatalytic paving blocks prepared with recycled materials. *Construction and Building materials* **2006**, 21 (8), 1746-1753.

Poppe, A.M. and De Schutter, G. Cement hydration in the presence of high filler contents. *Cement and Concrete Research* **2005**, 35 (12), 2290-2299.

Puddu, V., Choi, H., Dionysiou, D.D. and Puma, G.L. TiO_2 photocatalyst for indoor air remediation: Influence of crystallinity, crystal phase, and UV radiation intensity on trichloroethylene degradation. *Applied Catalysis B: Environmental* **2009**, In Press, Corrected Proof.

Rachel, A., Subrahmanyam, V. and Boule, P. Comparison of photocatalytic efficiencies of TiO_2 in suspended and immobilized form for the photocatalytic degradation of nitrobenzenesulfonic acids. *Applied Catalysis B: Environmental* **2002**, 37 (4), 301-308.

Rincon, A.G. and Pulgarin, C. Absence of E. coli regrowth after Fe^{3+} and TiO_2 solar photoassisted disinfection of water in CPC solar photoreactor. *Catalysis Today* **2007**, 124 (3-4), 204-214.

Saito, T., Iwase, T., Horie, J. and Morioka, T. Mode of photocatalytic bactericidal action of powdered semiconductor TiO_2 on mutans streptococcl. *Journal of Photochemistry and Photobiology B: Biology* **1992**, 14 (4), 369-379.

Sakai, N., Fujishima, A., Watanabe, T. and Hashimoto, K. Quantitative evaluation of the photoinduced hydrophilic conversion properties of TiO_2 thin film surfaces by the reciprocal of contact angle. *Journal of Physical Chemistry B* **2003**, 107 (4), 1028 -1035.

Sano, T., Negishi, N., Takeuchi, K. and Matsuzawa, S. Degradation of toluene and acetaldehyde with Pt-loaded TiO_2 catalyst and parabolic trough concentrator. *Solar Energy* **2004**, 77 (5), 543-552.

Sanchez, B., Cardona, A.I., Romero, M., Avila, P. and Bahamonde, A. Influence of temperature on gas-phase photo-assisted mineralization of TCE using tubular and monolithic catalysts. *Catalysis Today* **1999**, 54 (2-3), 369-377.

Sanderson, K., Buschow, K.H., Cahn, R.W., Flemings, M.C., Ischner, B., Kramer, E.J., Mahajanm, S. and Veyssiere, P. *Glass, self-cleaning*; Elsevier: Oxford, 2001.

Schwarz, P.F., Turro, N.J., Bossmann, S.H., Braun, A.M., Wahab, A.A. and Dürr, H. A new method to determine the generation of hydroxyl radicals in illuminated TiO_2 suspensions. *Journal of Physical Chemistry B* **1997**, 101 (36), 7127-7134.

Senff, L., Labrincha, J.A., Ferreira, V.M., Hotza D. and Repette, W.L. Effect of nano-silica on rheology and fresh properties of cement pastes and mortars. *Construction and Building Materials* **2009**, 23 (7), 2487-2491.

Shelby, J.E. *Introduction to Glass Science and Technology*; The Royal Society of Chemistry: Cambridge, 1997.

Shi, C., Wu, Y., Riefler, C. and Wang, H. Characteristics and pozzolanic reactivity of glass powders. *Cement and Concrete Research* **2005**, 35 (5), 987-993.

Shi, C. and Zheng, K. A review on the use of waste glasses in the production of cement and concrete. *Resources, Conservation and Recycling* **2007**, 52 (2), 234-247.

Shimohigoshi, M. and Saeki, Y. Research and application of photocatalyst tiles. In *Photocatalysis, Environment and Construction materials*, Proceedings of the International RILEM Symposium, Italy, 2007; Baglioni, P. and Cassar, L., Eds.; RILEM: Bagneux, 2007.

Sleiman, M., Ferronato, C. and Chovelon, J.M. Photocatalytic removal of pesticide dichlorvos from indoor air: a study of reaction parameters, intermediates and mineralization. *Environmental Science and Technology* **2008**, 42 (8), 3018-3024.

Sunada, K., Watanabe, T. and Hashimoto, K. Bactericidal activity of copper-deposited TiO_2 thin film under weak UV light illumination. *Environmental Science and Technology* **2003**, 37 (20), 4785-4789.

Stathatos, E., Lianos, P., Delmonte, F., Levy, D. and Tsoourvas, D. Formation of TiO_2 nanoparticles in reverse micelles and their deposition as thin film on glass substrates. *Langmuir* **1997**, 13 (16), 4295-4300.

Stokke, J.M. and Mazyck, D.W. Photocatalytic degradation of methanol Using silica–titania composite pellets: effect of pore size on mass transfer and reaction kinetics. *Environmental Science and Technology* **2008**, 42 (10), 3808-3813.

Strini, A., Cassese, S. and Schiavi, L. Measurement of benzene, toluene, ethylbenzene and o-xylene gas phase photodegradation by titanium dioxide dispersed in cementitious materials using a mixed flow reactor. *Applied Catalysis B: Environmental* **2005**, 61 (1-2), 90-97.

Taoda, H., Fukaya, M. and Watanabe, E. VOC decomposition by photocatalytic wall paper. *Materials Science Forum* **2006**, Eco-material Processing & Design VII **(**510-511), 22-25.

Tao, J. Preliminary study on the water permeability and microstructure of concrete incorporating nano-SiO_2. *Cement and Concrete Research* **2005**, 35 (10), 1943-1947.

Tyagi, M.S. *Introduction to semiconductor materials and devices*; John Wiley & Sons: New York, 1991.

Vallee, F., Ruot, B., Bonafous, L., Guillot, L., Pimpinelli, N., Cassar, L., Strini, A., Mapelli, E., Schiavi, L., Gobin, C., Andre, H., Moussiopoulos, N., Papadopoulos, A., Bartzis, J., Maggos, T., Mclntyre, R., Lehaut-Burnouf, C., Henrichsen, A., Laugesen, P., Amadelli, R., Kotzias, D. and Pichat, P. Cementitious materials for self-cleaning and depolluting facade surfaces. In *Environment-Conscious Materials and Systems for Sustainable Development*, Proceedings of the International RILEM Symposium, Japan, 2004; Kashino, N. and Ohama, Y. Eds.; RILEM: Japan, 2004.

Wang, J.X., Chen, C.Y., Liu, Y., Jiao, F., Li, W., Lao, F., Li, Y.F., Li ,B., Ge, C.C., Zhou, G.Q., Gao, Y.X., Zhao, Y.L. and Chai, Z,F. Potential neurological lesion after nasal instillation of TiO_2 nanoparticles in the anatase and rutile crystal phases. *Toxicology Letters* **2008**, 183 (1-3), 72-80.

Wang, K., Tsai, H. and Hsieh, Y. A study of photocatalytic degradation of trichloroethylene in vapor phase on TiO_2 photocatalyst. *Chemosphere* **1998a**, 36 (13) 2763-2773.

Wang, R., Hashimoto, K., Fujishima, A., Chikuni, M., Kojima, E., Kitamura, A., Shimohigoshi, M. and Watanabe, T. Light-induced amphiphilic surfaces. *Nature* **1997**, 388, 431-432.

Wang, R., Hashimoto, K., Fujishima, A., Chikuni, M., Kojima, E., Kitamura, A., Shimohigoshi, M. and Watanabe. T. Photogeneration of highly amphiphilic TiO_2. *Surfaces Advanced Materials* **1998b**, 10 (2), 135-138.

Wang, S., Ang, H.M. and Tade, M.O. Volatile organic compounds in indoor environment and photocatalytic oxidation: State of the art. *Environment International* **2007**, 33 (5), 694-705.

Wu, J.F., Hung, C.H. and Yuan, C.S. Kinetic modeling of promotion and inhibition of temperature on photocatalytic degradation of benzene vapour. *Journal of Photochemistry and Photobiology A: Chemistry* **2005**, 170 (3), 299-306.

Yacobi, B.G. *Semiconductor materials: an introduction to basic principles*; Kluwer Academic/Plenum Publishers: New York, 2003.

Yamazaki, S., Tanaka, S. and Tsukamoto, H. Kinetic studies of oxidation of ethylene over a TiO_2 photocatalyst. *Journal of Photochemistry and Photobiology A: Chemistry* **1999**, 121 (1), 55-61.

Ye, Q., Zhang, Z., Kong, D. and Chen, R. Influence of nano-SiO_2 addition on properties of hardened cement paste as compared with silica fume. *Construction and Building Materials* **2007**, 21 (3), 539-545.

Yu, C.M. *Deactivation and regeneration of environmentally exposed Titanium Dioxide (TiO_2) based products.* Departmental Order Ref. No.: E183413;

Environmental Protection Department, HKSAR: Hong Kong, 2003.

Zhao, J. and Yang, X. Photocatalytic oxidation for indoor air purification: a literature review. *Building and Environment* **2003**, 38 (5), 645-654.

Zhang, L., Anderson, W.A., Sawell, S. and Moralejo, C. Mechanistic analysis on the influence of humidity on photocatalytic decomposition of gas-phase chlorobenzene. *Chemosphere* **2007**, 68 (3), 546-553.

Zhang, Y., Crittenden, J.C., Hang, D.W. and Perram, D.L. Fixed-Bed Photocatalysts for Solar Decontamination of Water. *Environmental Science and Technology* **1994**, 28 (3), 435-442.

Zhu, H. and Byars, E. Post-Consumer glass in concrete: Alkali–silica reaction and case studies, Glass Waste. In *Sustainable Waste Management and Recycling*, Proceedings of the International Conference organized by the Concrete and Masonry Research Group, UK, 2004; Limbachiya M.C. and Roberts J.J., Eds.; RILEM, London, 2004.

Zorn, M.E., Tompkins, D.T., Zeltner, W.A. and Anderson, M.A. Photocatalytic oxidation of acetone vapor on TiO_2/ZrO_2 thin films. *Applied Catalysis B: Environmental* **1999**, 23 (1), 1-8.